Targeting aberrant dendritic integration
to treat cognitive comorbidities of epilepsy

Dissertation

zur

Erlangung des Doktorgrades (Dr. rer. nat.)

der Mathematisch-Naturwissenschaftlichen Fakultät

der

Rheinischen Friedrich-Wilhelms-Universität Bonn

Vorgelegt von

Nicola Masala

Aus Oristano, Italien

Bonn, 2022

Angefertigt mit Genehmigung der
Mathematisch-Naturwissenschaftlichen Fakultät der
Rheinischen Friedrich-Wilhelms-Universität

1. Gutachter: Prof. Dr. Heinz Beck
2. Gutachter: Prof. Dr. Walter Witke

Tag der Promotion: 23.02.2022
Erscheinungsjahr: 2022

Abstract

Memory deficits are one of the most debilitating and common symptoms of temporal lobe epilepsy. However, so far, little is known about mechanisms underlying cognitive deficits and how pharmacologically target them. In most CNS pyramidal neurons, dendrites generate local spikes initiated by dendritic voltage-gated Na+ channels activation. Dendritic spikes are elicited by precisely spatiotemporally clustered inputs that only arise if specific ensembles of presynaptic neurons are synchronously active. They have been proposed to endow neurons with the capability to act as input feature detectors. Indeed, dendritic spikes are relevant for triggering place-related firing in CA1 neurons and are strongly implicated in spatial navigation. They thus constitute a key mechanism for dendritic integration and neuronal input-output computations.

Dendritic spikes rely on the targeted expression of voltage-gated ion channels in dendritic branches. In epilepsy and numerous other CNS disorders, the expression and function of ion channels are profoundly altered in CA1 neuron dendrites. In chronic epilepsy models, many channelopathies such as changes in K^+ channels, T-type Ca^{2+} channels, HCN channels, or Na^+ channels have been identified. However, these studies have mainly focused on larger caliber, apical dendrites of pyramidal neurons, while the integrative properties of thin, higher-order dendrites and how they change in chronic epilepsy have not been investigated so far.

In this study, I describe a channel-dependent $Na_v1.3$ mechanism. This is based on a changed dendritic integration of the hippocampus and deteriorated location coding in vivo and spatial memory deficits in experimental chronic temporal lobe epilepsy.

Two-photon glutamate uncaging experiments in vitro revealed that the mechanisms constraining the generation of dendritic spikes in first-order hippocampal pyramidal cell dendrites are profoundly degraded in experimental epilepsy. This phenomenon was reversed by selectively blocking $Na_v1.3$ sodium channels.

In-vivo two-photon imaging in awake mice revealed that spatial representations in hippocampal neurons were significantly less precise in epileptic animals. The blocking of $Na_v1.3$ channels significantly improved the precision of spatial coding and reversed hippocampal memory deficits in epileptic animals.

Thus, a proximal dendritic channelopathy that can be pharmacologically targeted may underlie cognitive deficits in epilepsy and constitute a new avenue to enhance cognition in chronic epilepsy.

Contents

Chapter 1

Introduction

1.1. Epilepsy

Epilepsy is a chronic disorder of the central nervous system (CNS) in which neuronal activity becomes abnormal, resulting in epileptic seizures. An epileptic seizure is defined as a sudden, uncontrolled aberrant electrical signaling in the brain characterized by hyperactive or synchronous neuronal activation with transient periods of unusual behavior, disturbed sensory perception, motor function, and sometimes loss of awareness that interferes with mnemonic and cognitive processes (Fisher et al., 2005; Fisher et al., 2014; Engel, 2006; Engel & Padley, 2008).

Epilepsy is one of the world's oldest described diseases, documented with written records dating back to 4000 BC. The term epilepsy refers to the Greek word *epilambanem*, which means "to possess, to seize", and it was believed as a supernatural phenomenon in different cultures for a long time.

In 1870, starting with Dr. John Hughlings Jackson's magnificent contribution, epilepsy, and epileptic seizures were systematically investigated and defined as brain disorders. Following the event of new medical advances and techniques, particularly the development of electroencephalogram recordings in 1930 by Hans Berger, the scientific community's interest in epilepsy research grew steadily.

Today, epilepsy is known as one of the most common health disorders, globally affecting over 70 million people worldwide (World Health Organization 2020; Thijs et al., 2019).

In chronic epilepsy, the brain shows multiple heterogeneous physiopathological alterations correlated with the generation of spontaneous seizures. The cause of the numerous alterations described that occur during epilepsy can be found in situations of injured brain trauma, metabolic abnormalities, and genetic disorders with ion channels, neurotransmitters, and proteins mutations (Engel, 2001a; Shneker & Fountain, 2003; Engel, 1996; Johnson & Sandler, 2001; Beck & Elger, 2008). However, in many cases, the reason underlying the evolution of epilepsy disease is unknown.

To diagnose epilepsy, at least two or more unprovoked seizures in a period greater than 24h apart are required (Fisher et al., 2005; 2014). Some patients suffering from epilepsy have generalized seizures affecting all brain structures, while others have focal seizures, so-called

partial seizures, that affect only part of the brain. In other cases, they have both generalized and focal seizures (Devinsky et al., 2018). Seizures can result in motor or nonmotor onset characteristics (Fisher et al., 2017), and their frequency can vary from less than one per year to several per day (Gasparini et al., 2016).

1.1.1. Mesial temporal lobe epilepsy

One of the most common forms of focal epilepsy is the Mesial Temporal Lobe Epilepsy (MTLE) (Engel, 2001b), characterized by seizures that originate from the limbic areas of the temporal lobe, in particular from the amygdala and hippocampal formation (Schmidt & Löscher, 2005; Sendrowski & Sobaniec, 2013).

One of the more prominent associated causes of MTLE is brain insult during early life associated with genetic predisposition (Blümcke, 2002). In 40% of cases, epilepsy develops after abnormal situations like a febrile seizure, head injuries, birth trauma, and infections that affect the central nervous system (Banerjee et al., 2009). Reported brain insults are considered a potential starting point that leads to physiopathological changes where a healthy brain develops a chronic epileptic state. This process is known as epileptogenesis (Wieser, 2004; Beck & Elger, 2008; Kasperaviciute et al., 2013; Cendes et al., 2014). Epileptogenesis in temporal lobe epilepsy is also characterized by pathological changes in expression and distribution of ion channels and neurotransmitters in the hippocampus (Blumcke et al., 2000; Pathak et al., 2007; Bernard et al., 2004; Becker et al., 2008; Cendes et al., 2014). It is essential to state that epileptogenesis processes can also occur without a clear brain insult, and however, it is still unknown whether the MTLE is usually caused by hippocampal physiopathology or whether the hippocampus is damaged by recurrent seizures (Sloviter, 2005).

Patients with a reported initial insult can take several years before experience spontaneous seizures. This asymptomatic phase is known as the latent period (Mathern et al., 1995; Wieser, 2004), which anticipates the chronic epilepsy state characterized by spontaneous recurrent seizures.

MTLE is most commonly associated with a neurodegenerative process and structural change known as hippocampal sclerosis (HS) encountered in the majority (60-80 %) of patients diagnosed with this condition (Margerison & Corsellis, 1966; Taylor, 1989; Davies et al., 1996; Blümcke et al., 2007; Blumcke & Wiestler, 2002; Blümcke et al., 2013). HS is associated with a characteristic pattern of selective and extensive loss of excitatory and inhibitory neurons and astrogliosis processes, resulting in proliferation and hypertrophy of

glial cells (Engel, 1996; Blümcke et al., 2013) and aberrant mossy fiber sprouting (Wozny et al., 2005). In particular, a loss of excitatory neurons has been described in the entire hippocampal structure: 80% of pyramidal cells (PCs) within CA1, 30-50% in CA2, 30–90% in CA3 (Blümcke et al., 2012), and 50-60% of granule cells in the dentate gyrus (Bratz, 1899; Margerison & Corsellis, 1966) (**Fig. 1.1**).
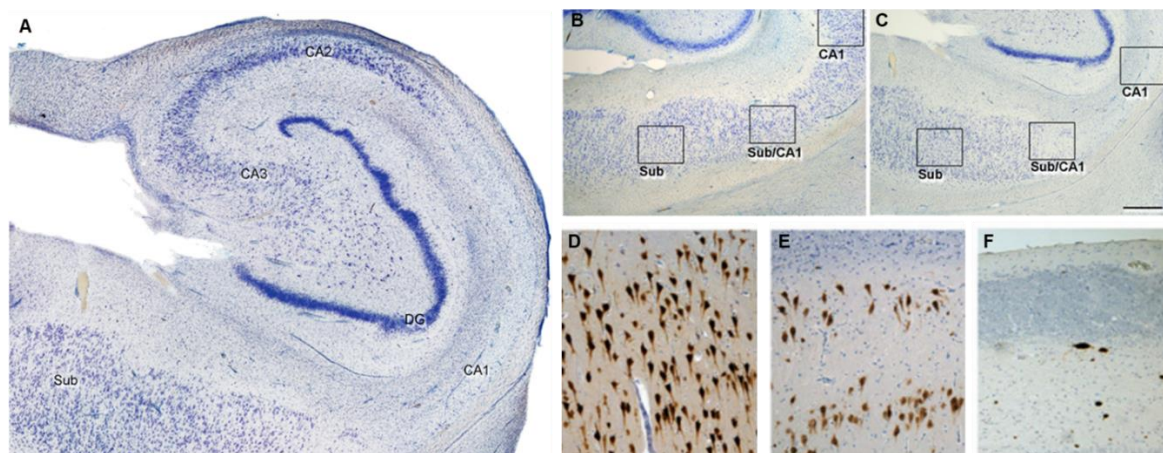
Fig. 1.1, Typical pathological features of human hippocampal sclerosis in MTLE. a, Low-power photomicrograph of a Nissl-stained section to illustrate a sclerotic hippocampus at the level of the medial hippocampal formation. **b,** Photomicrographs of Nissl-stained sections of non-sclerotic and **c,** sclerotic hippocampal formation. **d,** CA1 pyramidal cell layer in a patient with MTLE but no evidence of neuronal loss. **e,** CA1 with evidence of partial neuronal loss and **f,** CA1 with severe neuronal depletion and collapse of the layer. (Adapted from Alonso-Nanclares et al. 2011; Thom M. et al. 2014)

A wide variety of well-characterized animal models have been developed for the study of MTLE (Sarkisian, 2001). Despite the fact that no single model can precisely mimic the human condition, they recapitulate distinctive phenotypes of the disease, including HS (Curia et al., 2014; Kuwabara et al., 2010; Polli et al., 2014; Schmied et al., 2008; Wagner et al., 2014). However, neuropathological alterations, temporal profile, and magnitude can differ between experimental animal models (Covolan and Mello, 2000; Kandratavicius et al., 2014). The kainic acid (KA) model (Lévesque & Avoli, 2013) and the pilocarpine model are among the most commonly investigated models for MTLE.

In rodents, intracerebral injection of KA, a glutamate analog, rapidly induces a characteristic pattern of severe intense limbic seizures typically culminating in status epilepticus (SE), followed by a quiescent period of usually several weeks.

During this latent period, the brain undergoes physiological, structural, and metabolic changes, developing at the end a chronic state of epilepsy characterized by recurrent spontaneous seizures (McNamara et al., 2006). In addition, the KA model displays a similar pathological HS observed in MTLE patients (**Fig. 1.2**). These changes typically include pyramidal cell loss within CA3 and CA1 pyramidal layers of the hippocampus and GABAergic interneurons death in the dentate hilus (Curia et al., 2008; Sutula et al., 1994). Moreover, as observed in the human epileptic hippocampus (Magloczky, 2010; Sutula et al., 1989), mossy fiber sprouting in the dentate gyrus is also observed in the KA model (Cavazos et al., 2003). Together, these changes indicate a pathological reorganization of the hippocampal synaptic circuit.

These features make the KA model a suitable tool to investigate the basic mechanisms underlying seizures, aberrant synaptic and neuronal network properties, and long-term behavioral changes associated with epilepsy. Indeed, the KA model displays behavioral impairments which mimic those observed in human MTLE (Liu et al., 2020; Kim et al., 2020). Therefore, the KA model offers many advantages for studying cognitive dysfunction associated with epilepsy, identifying potential mechanisms underlying these comorbidities, and preclinical testing of therapeutic strategies (Brooks-Kayal et al., 2013).
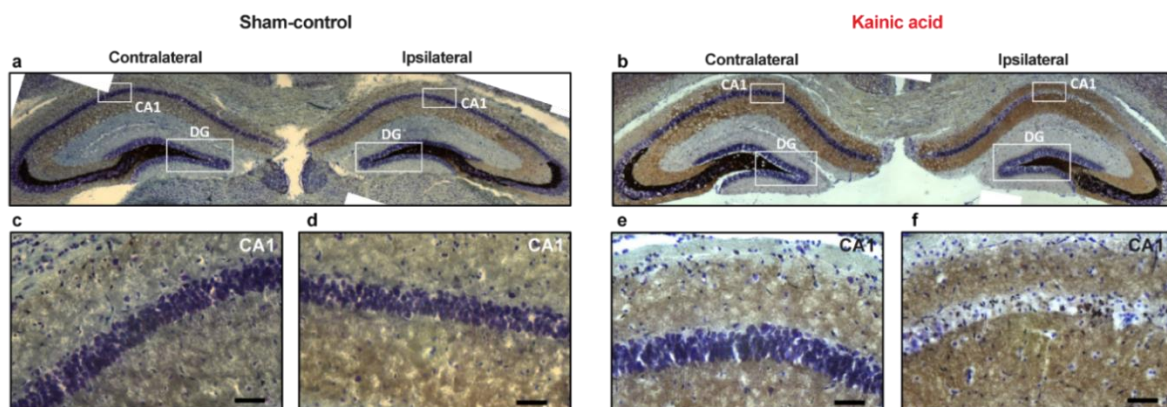
Fig. 1.2, Neuropathological changes in the Kainic Acid TLE model. The hippocampal slices in (**a**) and (**b**) were obtained from mice 4 weeks after NaCl or Kainic Acid supra-hippocampal injection, respectively. Zinc-containing axon terminals (brown) were stained using Timm staining, and cell bodies (blue) were counterstained with Toluidine blue. Only Kainic acid-treated mice (**b**) reveal pathological changes known to occur in human TLE patients and other chronic epilepsy animal models. Comparing the Kainic Acid treated mice with their intact contralateral hippocampus or sham control mice injected with NaCl, a loss of the hippocampal CA1 cells (c-f) can be observed.

1.1.2. Cognitive impairment in MTLE

In addition to the disabling consequences of spontaneous recurrent seizures, many people affected by epilepsy suffer from a wide range of comorbidities, including psychological and behavioral abnormalities (Sillanpää, 2004; Whatley et al., 2010; Kerr, 2012; Fisher et al., 2018; Scheffer et al., 2018). In particular, memory function is impaired in more than 40% of epilepsy patients (McAuley et al., 2010), especially in individuals suffering from MTLE (Davidson et al., 2007), where memory-related mesial temporal lobe structures are compromised. Thus, impairments in storing, retaining, and recalling information are commonly observed in these patients (Dodrill, 2002; Elger et al., 2004; Williams, 2003; Wilkinson et al., 2012; Helmstaedter & Kockelmann, 2006). However, the magnitude of memory deficits that a person may develop can differ depending on many variables, such as the severity (Cheung et a., 2006), the underlying cause (Tassi et al., 2009), the frequency, and the type of seizures (Pullianen et al., 2000). In addition, antiepileptic drugs (AEDs) can also contribute to memory impairment (Lévesque et al., 2018; Meador et al., 2006; Hermann et al., 2010).

The nature of these memory impairments has been the focus of many studies. It is now generally recognized that MTLE patients present with deficits in declarative memory: our knowledge of places, people, events (Hermann et al., 1997 Höttinget al., 2010). Indeed, a loss of information about the autobiographical history and inability to maintain new memory over a period of time have been observed in many cases (Helmstaedter, 2002; Tramoni et al., 2011; Hoppe et al., 2007). In addition, spatial learning and spatial navigation impairment have been described in MTLE, with degraded abilities in route learning, visual imagery, scene recognition, or topographical memory (Amlerova et al., 2013; Brown et al., 2015; Grewe et al., 2013; Rosas et al., 2013). This is not surprising considering that hippocampal structures, fundamental in spatial memory processes, undergo pathological sclerosis in MTLE. Spatial memory is a cognitive ability with a particular impact on everyday life. The egocentric and allocentric strategies have been proposed as the basis of spatial navigation (Iaria et al., 2003). Through the egocentric strategy, we define the position of targets present in the environment according to our location, independently of distant landmarks. In contrast, allocentric memory relies on a cognitive map of the environment using landmarks and their spatial relationship to the targets (O'Keefe & Dostrovsky, 1971). While egocentric navigation relies on the parietal cortex (Weniger et al., 2009), allocentric navigation involves mesial temporal lobe structures, particularly the hippocampus (Bohbot et al., 2004). Many tasks based on a human equivalent to the Morris water maze (Hort et al., 2007; Amlerova 2012)

and a virtual reality version of the hole board (Rosa Cánovas 2011) have been used to investigate spatial memory in MTLE patients. These studies have revealed poor spatial navigation and impaired allocentric spatial navigation in epilepsy.

In addition to long-term and spatial memory, working memory deficits have also been described in many patients (Nair & Szaflarski, 2020; Rzezak et al., 2017; Van Geldorp et al., 2014). Working memory, also known as the "everyday tasks memory", is used to temporarily hold a limited amount of information at the ready for immediate use, and it is particularly relevant in decision-making and behavior. Notably, working memory does not exclusively involve hippocampal-dependent process but requires the participation of other CNS areas, including the septum, basal forebrain, and prefrontal cortex.

Even though memory impairments are extremely debilitating, the mechanisms underlying these comorbidities are not well understood. Nevertheless, since these processes require the integrity of the temporal lobe structure that is preferentially affected in MTLE, many studies have investigated the cellular morpho-functional changes in the hippocampus, leading to the general idea that a hyperexcitable 'epileptic circuit' underlies memory abnormalities.

Indeed, the epileptic hippocampus from patients and experimental models presents a largely imbalanced excitatory-inhibitory transmission (Bonansco et al., 2016) and remarkably impaired synaptic plasticity (Beck et al., 2000; Butler et al., 2008). Both overexcitability and dysfunctional plasticity lead to degraded memory processes (Barry et al., 2012). In addition, spontaneous recurrent seizures and interictal epileptiform discharges per se cause temporary memory impairment (Horak et al., 2017). Epileptic seizure occurrence directly impacts synaptic transmission, neuronal firing patterns, and temporal coding of information (Zhou et al., 2007; Žiburkus et al., 2013; Liu et al., 2003; Lenck-Santini et al., 2008), all contributing to aberrant processing of information and memory function.

Moreover, network alterations in MTLE patients have been shown to alter the pattern of brain activations during memory encoding (Kalitzin et al., 2019; Sidhu et al., 2015). There are three major network oscillatory patterns in the hippocampus: gamma waves (25-140 Hz), theta (4-7 Hz) waves, and sharp waves ripples (SPW-Rs) (140-250 Hz). Gamma oscillations are widespread in all brain structures, whereas theta and sharp waves are specific to the hippocampus. All of them play an essential role in memory formation processes. New memories are first formed during the acquisition phase and then strengthened during the replay phase. Theta oscillations modulate specific hippocampal neuronal pathways activated during the acquisition phase. Indeed, local field potential recordings in awake animals showed how the activity in the hippocampus during exploration is dominated by theta waves

(Vanderwolf, 1969). Subsequently, new memories are reinforced by a replay of similar population patterns during SPW-Rs (Buzsáki., 1989). These types of activity are particularly prevalent during immobility, drinking, and resting behaviors (Buzsáki et al., 1983).

Importantly, abnormal high-frequency SPW-Rs (250–600 Hz), termed fast ripples, have been observed in patients and animal models of epilepsy (Bragin et al., 1999). These fast ripples reflect the hypersynchronous bursting of excitatory pyramidal cells, and they can be exploited as a biomarker of epileptogenicity in diagnostic (Jacobs et al., 2009). Thus, aberrant SPW-Rs have been considered a correlate of a consolidation deficit associated with cognitive impairment in MTLE (Zhen et al., 2021; Marchioni et al., 2019).

Notably, all these studies are greatly supported by the availability of animal models, which mimic most of the characteristic features of MTLE, including spatial learning and working memory deficits (Leite et al., 1990; Stafstrom et al., 1993; Letty et al., 1995; Nissinen et al., 2000; Yang et al., 2000; Van Den Herrewegen, 2019).

1.2. Hippocampal circuits

The hippocampus is a structure of the limbic system, located in the mammalian temporal lobe (Amaral & Witter 1989; Amaral et al., 2007; Squire et al., 2004), consisting of the dentate gyrus (DG), the cornu ammonis (CA) and the subiculum. The CA field of pyramidal cells is subdivided into four subregions (CA1–CA4) (Lorente de Nò, 1934; Amaral, 1993; Lavenex et al., 2007).

The entorhinal cortex (EC) represents a relay station for most cortical inputs conveyed to the hippocampus. Inputs from the lateral entorhinal cortex (LEC) and medial entorhinal cortex (MEC) convey nonspatial sensory information (Wang et al., 2018) and spatial information (Fyhn et al., 2004), respectively. These inputs are then processed within the hippocampus and sent back to the EC through CA1 (Van Strien et al., 2009). Information is propagated from EC through the hippocampal circuitry in many different pathways. The most well-characterized route is the indirect pathway that streams the information through the trisynaptic loop (**Fig.1.3**).

In this excitatory circuit, EC layers II and III project to the DG via the perforant pathway (PP) (Steward & Scoville, 1976; Amaral & Witter, 1989; Witter et al., 1989; Witter, 1993), providing the primary input to the hippocampus (first synapse) (Witter & Amaral, 1991).

From then, the information is passed into CA3 via DG axonal projections called mossy fibers (second synapse) (Amaral & Witter, 1989). CA3 axons termed Schaffer collaterals (SC) then project into CA1 (third synapse). Axons from CA1 then project both to the subiculum and

back to layer V and IV of the EC (Amaral, 1993; Amaral & Lavenex, 2007; Witter et al., 1989; Witter, 1993). In addition to the trisynaptic pathway, CA1 receives a direct excitatory projection from layer III of EC through the temporoammonic pathway (TA), which forms synapses on the very distal apical dendrites of CA1 neurons (Witter et al., 1988).

Modern tracing studies revealed more complex hippocampal connectivity, contrasting the idea that the hippocampal circuit is only unidirectional. Indeed, CA1 neurons also receive strong excitatory input from the CA2 region (Chevaleyre & Siegelbaum, 2010). Similar to CA1 neurons, CA2 receives direct input from EC onto their distal dendrites (Hitti & Siegelbaum, 2014) and indirect input from CA3 onto their proximal dendrites (Chevaleyre & Siegelbaum 2010).
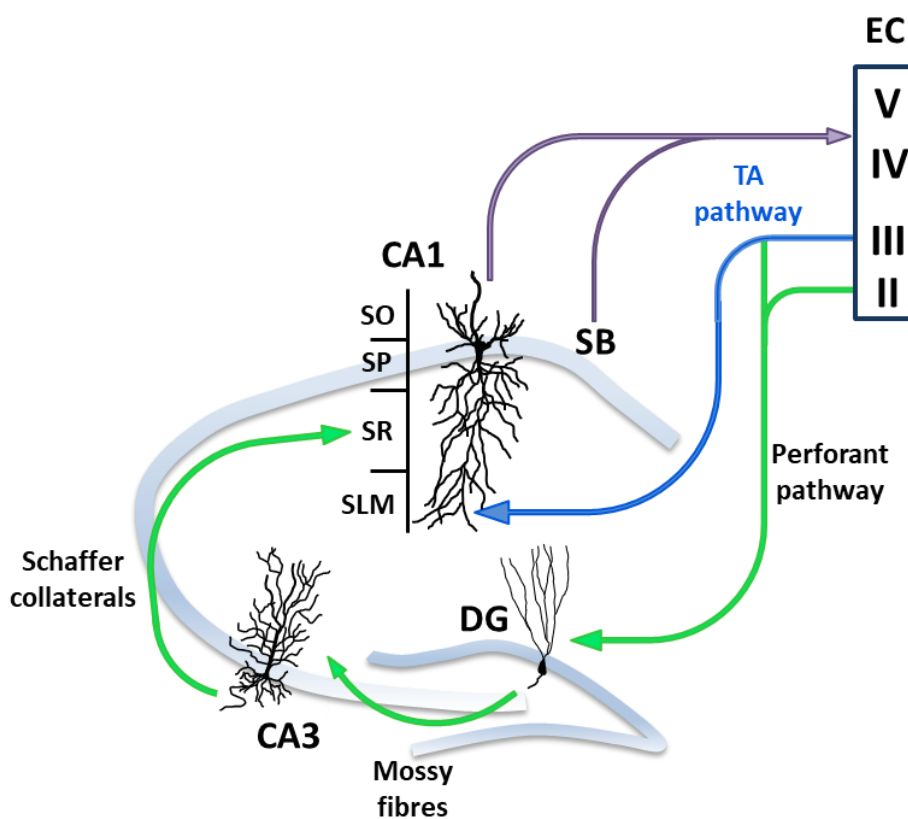
Fig. 1.3, Representative scheme of intrahippocampal excitatory circuitry. EC: entorhinal cortex, DG: dentate gyrus, SB: subiculum, TA: temporoammonic pathway, SO: stratum oriens, SP: stratum pyramidale, SR: stratum radiatum, SLM: stratum lacunosum-moleculare. Blue arrow showing the temporoammonic pathway, and the green arrow showing the trisynptic circuitry.

1.2.1. The CA1 region

CA1 is one of the most intensely studied brain regions in MTLE patients and animal models. It is known that selective damage of this hippocampal area leads to extensive memory loss and cognition impairments (Zola-Morgan et al., 1986a; 1986b; Bartsch et al., 2011), which are one of the most common comorbidities associated with MTLE.

Somata of excitatory pyramidal cells in CA1 are tightly packed in a dense layer and form the stratum pyramidale. Within CA1, there are circa 220.000 pyramidal cells (Bonthius et al. 2004), and each cell receives input from 15.000 to 30.000 CA3 neurons (Li et al., 1994).

The dendritic arborization of the CA1 pyramidal neuron has two distinct domains: the basal and the apical dendrites. Basal dendrites rising from the somata spread their arborization into the stratum oriens. Axonal segments also cross the stratum oriens and then project to the subiculum and layer V of the EC (Bannister & Larkmmann, 1995a; Pyapali et al., 1998).

A large apical dendrite, termed apical trunk, emanates from the soma and bifurcates in small-caliber apical oblique dendrites before giving rise to the apical tuft. These latter apical dendrites spread into the stratum radiatum (Bannister & Larkmmann, 1995a), and they receive inputs through the indirect pathway via the SC from CA3. The tuft of the dendritic tree, located in the stratum lacunosum moleculare, receives afferent input from the direct PP inputs from the EC.

Due to distinct dendritic locations, axonal projections from CA3 and EC provide a different magnitude of excitatory inputs, mainly as a consequence of the dendritic cable properties. PP synapses on distal dendrites are more attenuated and provide a weak excitation at the soma. However, these distal inputs have an essential role in providing precisely timed signals and modulating input-timing-dependent plasticity at the proximal dendrites (Dudman et al., 2007). In contrast, SC inputs on more proximal dendrites are less attenuated and provide strong excitation.

Both basal and apical dendrites are branched in small-caliber processes covered with dendritic spines, forming synapses with the presynaptic neurons. These synapses located in these thin dendrites represent the communication point for neuronal circuits, receiving the 80% of excitatory glutamatergic inputs (Ramon y Cajal, 1893; Lorente de No, 1934; Bannister & Larkman, 1995b).

1.2.2. The role of the hippocampus in memory processes and spatial coding

The first evidence that the hippocampus is an essential structure for memory formation in humans was provided by the clinical case of Henry Gustav Molaison (Scoville & Milner, 1957). Indeed, after a surgically bilateral resection of two-thirds of his hippocampi, he was utterly unable to form new memories. Following the case of Molaison, other similar clinical cases contributed to the general understanding of the hippocampal role in memory processes. Thus, hippocampal lesions often result in anterograde amnesia and degraded acquisition, retention, and recall of episodic memory.

CA1 plays an essential role for most, if not all, forms of hippocampal-dependent memory. Indeed, fMRI studies in humans have shown that memory recall of a prior experience is associated with the engagement of a general network centered on the hippocampus, including CA1 (Rugg & Vilberg 2013). CA1 lesion in both patients and animal models leads to severe memory impairment (Zola-Morgan et al. 1986; Squire 2004), and optogenetic transient inactivation of CA1 neurons in rodents markedly impairs memory recall (Goshen et al. 2011). Apart from the evidence of the hippocampus involved in the generation and consolidation of explicit memories (Martin & Morris, 2002; Bird & Burgess, 2008), today, we have a more intriguing view of the hippocampal function.

Together with other neocortical regions, the EC streams the 'Where' and 'What' experience-dependent sensory information into the hippocampus. Thus, spatial and temporal inputs flow into the hippocampus and are integrated to form specific associations and representations (Moscovitch et al., 2016). Moreover, the hippocampus constantly receives and send information from and to widespread many other brain regions highly interconnected like the amygdala, which is involved in emotional processing (Ikegaya et al., 1994; Maren & Fanselow, 1995; Vazdarjanova & McGaugh, 1999; Girardeau et al., 2017) and the nucleus accumbens, which is an essential station in the reward system (LeGates et al., 2018; Sjulson et al., 2018).

Therefore, the complex flow of spatiotemporal information through the hippocampus is integrated and associated with objects, scenes, environment representations, emotional components (Suzuki et al., 1997; Knierim et al., 2006) and finally stored in the cortex for eventual retrieval and recall of memories.

Our understanding of the neurophysiological basis of hippocampal function as a map of space that can be used for spatial memory processes was promoted by the breakthrough discovery of hippocampal place cells by O'Keefe and Dostrovsky. Place cells have been described for the first time in the hippocampal CA1 region of rats during exploration. These pyramidal

neurons have the peculiarity to respond precisely at a particular spatial location (place field) when an animal it (O'Keefe & Dostrovsky, 1971). Indeed, place cells show low or absent activity outside the place field, making these particular cells highly predictable (**Fig. 1.4**). Moreover, a pivotal feature for place cells is how they change their firing behavior depending on the spatial context, a phenomenon termed "remapping". If any change is introduced in the environment (visual cues, novel objects, object location, shape of the experimental arena), place cells can alter their place-related firing behavior (O'Keefe, 1976; Muller & Kubie 1989; Muller & Kubie, 1987; Kubie et al., 2020 Gothard et al., 1996a; 1996b; O'Keefe & Burgess, 1996). Thus, the hippocampus has been proposed to constitute a cognitive map, in which place cells integrate the spatial representation of the environment (O'Keefe,1976) during spatial navigation (Hartley et al., 2014; Marr, 1971; Morris, 2007).
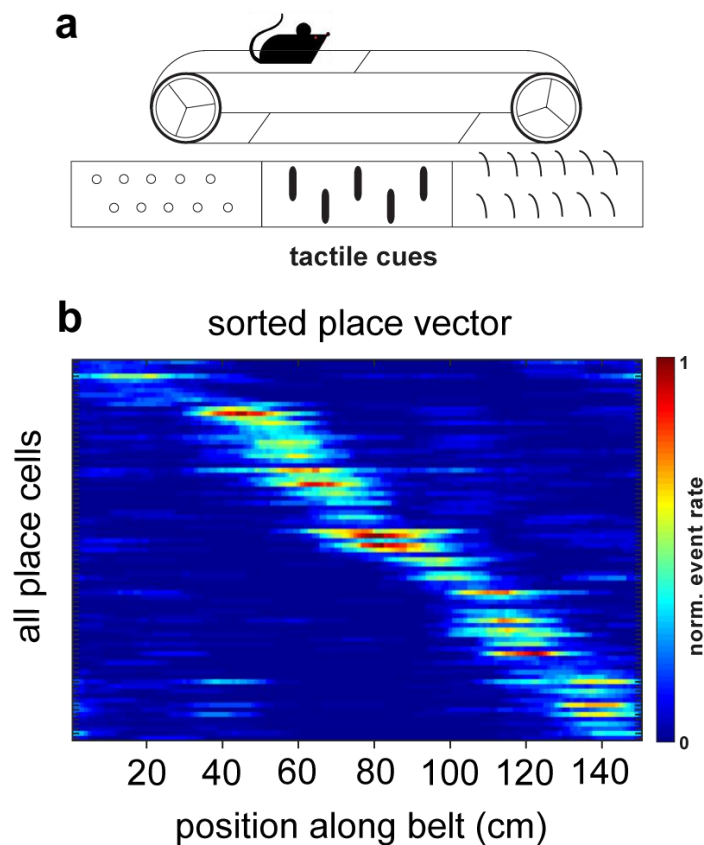
Fig. 1.4, Investigating place cell spatial coding via 2-photon Ca^{2+} imaging. Ca^{2+} imaging in hippocampal CA1 area from (a) a mouse running on a linear track equipped with spatial cues shows how place cells respond specifically to precise place field. (b) Place cells are spatially tuned, and the corresponding heatmap of their normalized fluorescence calcium events shows the activity restricted to a specific place of the belt (red color scale) and almost absent outside their place field (blue color scale).

The discovery of place cells and their unique role in spatial memory processes has been an essential foundation to investigate memory and behavioral deficits in MTLE. Spatial learning impairments and degraded long-term retention of information have been extensively studied in many animal models of MTLE through behavioral task and direct neuronal activity recordings (O'Keefe & Nadel 1978; Morris et al., 1982; Sutherland et al., 1982; Chiu et al., 2004; Liu X et al., 2003). Moreover, the event of modern techniques such as in-vivo electrophysiological and calcium imaging recordings from place cells contribute to the understanding of dysfunctional place coding in epilepsy (**Fig. 1.5**). The quality of spatial information is generally reduced in epileptic models, with place cells that show a significant broadening of place representations with degraded precision and less stability (Shuman et al., 2020; Lenck-Santini & Holmes, 2008; Liu X et al., 2003). Nevertheless, despite the association between cognitive impairment and MTLE or other CNS disorders, the mechanism underlying the dysfunction in the place coding and the degraded integration of spatial inputs is still unclear.
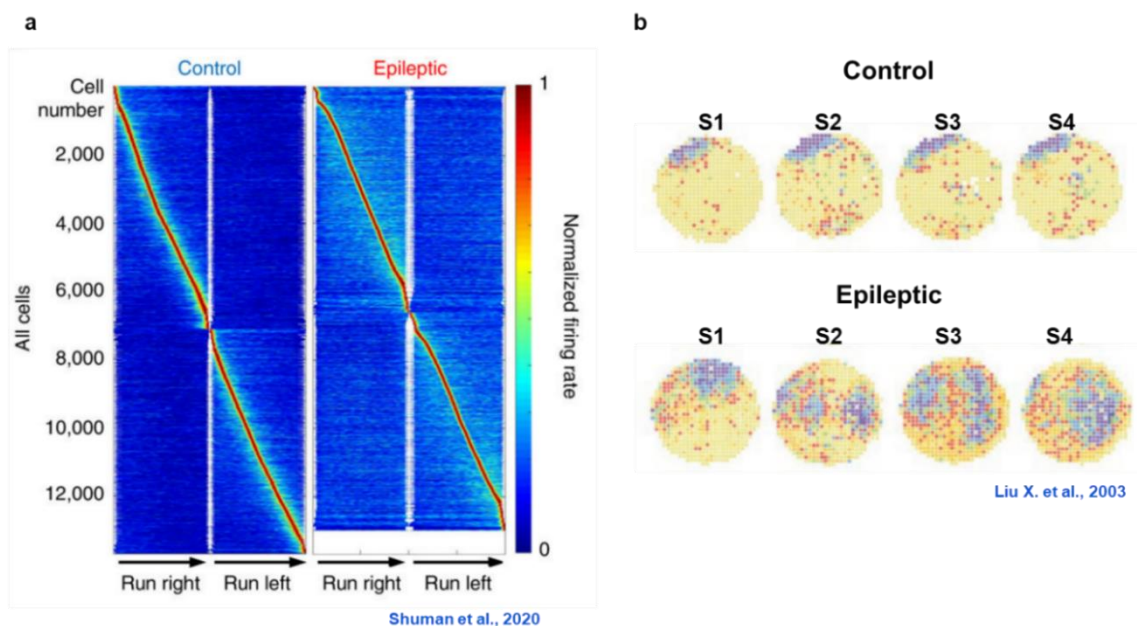
Fig. 1.5, Impaired spatial coding in chronic epilepsy. a, Normalized spatial firing rates from hippocampal CA1 pyramidal cells in control and epileptic mice. Both showed spatially tuned firing patterns. However, the quality of spatial information is substantially reduced in epileptic mice (Shuman et al., 2020). **b,** Place cell firing patterns showed by rate maps from four successive recording sessions for a single place cell in control and epileptic rat. The intervals between sessions 1 and 2 and between sessions 3 and 4 were 3 min; the interval between sessions 2 and 3 was 4-6 hr. Epileptic rats showed fields that vary considerably from session to session resulting in strong impaired place cells stability (Adapted from Shuman et al. 2020 and Liu X et al., 2003).

1.2.3. The cellular mechanism of learning and memory

The cellular mechanism of information storage and memory formation is thought to involves synaptic plasticity processes that enable the formation of preferentially connected neuronal assemblies. Indeed, one of the striking features of synapses in the central nervous system, especially those in the hippocampal circuit, is the extent to which their synaptic strength can be persistently modulated. The strength of synaptic connections is regulated by processes such as long-term potentiation (LTP), long-term depression (LTD), and spike-timing-dependent plasticity (STDP).

LTP represents the signature of the Hebbian synaptic learning theory, in which a potentiation in the synaptic transmission arises when a robust presynaptic activity repetitively and persistently stimulates a postsynaptic neuron. As a result, a specific strengthened pathway of inputs is facilitated to drive postsynaptic neuronal firing (Bliss & Collingridge, 1993). The mechanism underlying hippocampal activity-dependent LTP is underpinned by the NMDA receptors (Collingridge et al., 1983). NMDARs are high permeable to Ca^{2+}, which acts as a second messenger to activate several downstream signaling cascades. Thus, NMDARs recruitment causes a rise in intracellular Ca^{2+} levels, which leads to activation of Ca^{2+} calmodulin-dependent protein kinase II (CaMKII), critical for the induction of LTP (Malenka et al. 1989; Malinow et al. 1989). The LTP mechanism raises the scenario that synapses may become saturated during life, thus no longer capable of storing new information. However, an activity-dependent reduction in the synaptic strength is engaged through LTD (Bear & Abraham, 1996). Similar to LTP, LTD requires activation of NMDARs and the influx of postsynaptic Ca^{2+} (Bear and Abraham 1996). During LTP, a large influx of Ca^{2+} flows through NMDARs; in contrast, during LTD, the flow results lower but more long-lasting (Neveu & Zucker, 1996). The different Ca^{2+} activity results in two distinct molecular mechanisms. LTP recruits the activation of protein kinases, LTD recruits calcium-dependent phosphatases that dephosphorylate target postsynaptic proteins reducing the receptor density and the sensitivity to glutamate (Mulkey et al., 1994).

Despite Hebbian synaptic plasticity is conceptually an attractive mechanism underlying learning, the general utility of such mechanisms has been debated, primarily because of the non-physiological prolonged high-frequency activity required. Nonetheless, it has been shown that more physiological stimulation patterns can also induce long-lasting synaptic potentiation via STDP, a plasticity mechanism based on the relative spiking timing between pre- and postsynaptic neuron.

At the postsynaptic neuron, the backpropagation of an action potential could recruit the NMDARs located in the spines shortly after synaptic activation. Thus, the convergent spines membrane depolarization induced by the presynaptic activity and the increased dendritic Ca^{2+} influx through NMDRs will lead to transduction cascades that result in LTP or LTD at active synapses (Yuste & Denk, 1995).

Altogether, this evidence points out that activity-dependent synaptic plasticity presents feature consistent with the hypothesis of a cellular mechanism underlying memory storage.

A large body of data demonstrates how long-term plasticity is the cellular substrate for learning and memory, and much of this evidence has been obtained through pharmacologic or genetic approaches. The first evidence that LTP is required to form new memories in vivo is that the pharmacological block of NMDRs activity via intrahippocampal APV injection induces spatial memory deficits in animals performing behavioral tasks such as the Morris water maze (Morris et al., 1986). In a different study, NMDARs were genetically impaired in the CA1 area from mice. Silencing the NMDARs activity results in animals with very poor spatial navigation and disrupted precision of hippocampal place coding, further supporting the role of LTP in spatial learning (McHugh et al., 1996).

In addition, other studies demonstrated how exposure to a stimulus-enriched environment or learning training to a particular task, for example, radial arm maze, water maze, and eyeblink conditioning lead to a potentiated synaptic strength (Martin & Morris, 2002).

Although information storage in the hippocampus is thought to be primarily mediated by various forms of synaptic plasticity, it has been discovered that not only synapses are plastic but also the dendritic tree itself. Indeed, the dendritic membrane excitability can change in an activity-dependent manner, which means there exist dendritic as well as synaptic learning rules. Recent experimental data (Losonczy et al., 2008) show that the coupling between dendritic branches and the soma via active dendritic electrogenesis is adapted through a mechanism termed "branch-strength potentiation" (BSP), and evidence exists that BSP is relevant in vivo (Makara et al., 2009).

1.3. Hippocampal dendritic integration

Acquiring new memory requires the association of information during sensory experiences or the reprocessing of internal representations. These associations result in synaptic plasticity that enables the formation of preferentially connected neuronal assemblies. At the single-cell level, this occurs through integration and association of inputs that coincide in time or space

to influence neuronal activity. Thus, investigating how individual neurons integrate thousands of synaptic inputs they receive is fundamental to understand the mechanism underlying memory formation.

The process in which neurons receive and compute the signaling from other cells delivered via synapses on dendrites is termed "dendritic integration". The presynaptic site is located on the axonal segment, and the postsynaptic site is on the dendritic spines.

As a result of their activation, presynaptic cells release neurotransmitters in the synaptic cleft onto the postsynaptic neuronal dendrites. In the CNS, the primary excitatory neurotransmitter is the amino acid glutamate, which binds to ionotropic receptors located on the dendritic spines. These receptors contain a permeable channel capable of flowing positively charged ions either into or out of the neuron. At excitatory synapses, the ion channels typically allow Na^+ into the neuron, generating excitatory postsynaptic currents. This depolarizing current leads to an increase in membrane potential, the excitatory postsynaptic potential (EPSP). The EPSP generated in a single synapse from a dendritic spine is termed unitary EPSP (uEPSP). Multiple uEPSPs on different synaptic sites can be generated with different temporal patterns in different dendritic locations. Thus, according to their spatiotemporal characteristics, uEPSPs sum up their responses, generating larger EPSPs (Tamás et al., 2002).

This dendritic summation of inputs is termed linear integration. In this process, the voltage deflection generated by simultaneously activated synapses reflects the arithmetic summation of all the uEPSPs. Thus, EPSPs grow linearly with the number of inputs (**Fig. 1.6**).

In addition, the dendritic structure plays a fundamental role in shaping the integration of the input. EPSPs generated in the dendrites travel hundreds of micrometers before arriving at the soma and the axonal segment, and during their passive propagation, they are filtered. Thus, the EPSP amplitude will decrease as it propagates along the dendrite (Rall, 1967; Rall & Rinzel, 1973; Spruston, 2008). Therefore, EPSPs generated in a distal dendritic site in passive dendrites provide less contribution to the neuronal output than EPSPs evoked in proximal sites. However, the attenuation of excitatory inputs along the dendrite can be partially compensated by a mechanism called synaptic scaling (Magee & Cook, 2000). Thus, distal oblique dendrites in CA1 compensate for distance-dependent attenuation by increasing the amount of ionotropic receptors in the synapses (Andrasfalvy & Magee, 2001).

In general, the attenuation of linearly integrated EPSPs is determined by the dendritic cable properties, depending on the membrane resistance, intracellular resistance, and membrane capacitance. The membrane resistance is a function of the amount of ion channels open at rest. A reduced membrane resistance results in a loss in charge across the membrane and,

thus, more pronounced EPSP attenuation (Stuart et al., 2008). The intracellular resistance determines how efficiently the EPSPs propagate along dendrites with different caliber. Thick dendrites have low intracellular resistance; thus, the EPSP propagation is facilitated (Koch, 1999). The capacitive property of the dendrites depends on their morphology. Indeed, the size and shape of the membrane affect how fast a membrane can be charged. More extensive dendritic arborization results in higher membrane capacitance, the membrane is slowly charged, and thus fast EPSPs are strongly filtered (Migliore and Shepherd, 2002; Stuart et al., 2008).

Altogether, these passive dendritic properties shape the time-course and amplitude of synaptic signals and how different dendritic synapses inputs are integrated.
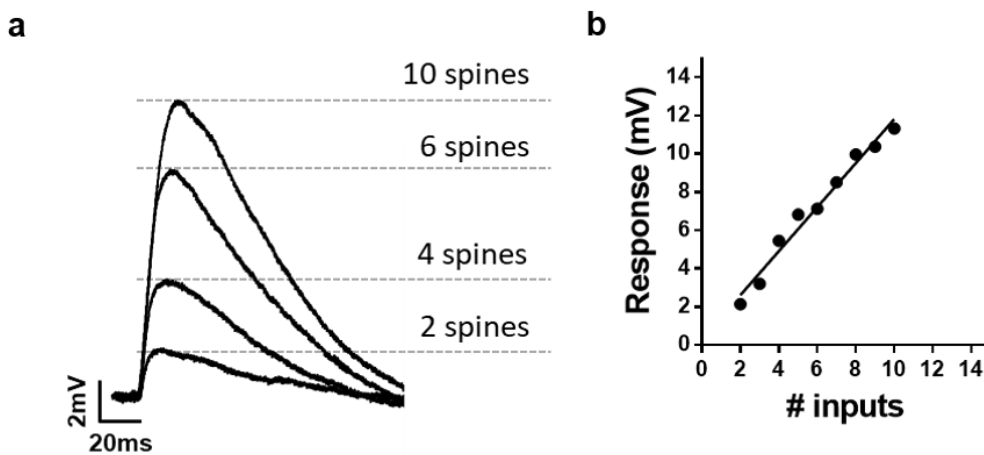
Fig. 1.6, Linear integration. (a) Representative somatic recordings of compound linear EPSPs evoked by an increasing number of activated spines. (b) The amplitude of EPSPs is proportional to the number of activated synapses.

However, dendrites are not passive in most neurons. A large body of studies has demonstrated that neurons can perform a plethora of different forms of synaptic integration due to active, voltage-dependent properties of their dendrites (Poirazi & Mel, 2001; Poirazi et al., 2003; Yuste, 2011; Häusser et al., 2000; Gulledge et al., 2005; Sjöström et al., 2008).

Indeed, the presence of voltage-gated ion channels along the dendrites makes the integration of synaptic inputs much more intriguing and complex than a passive cable (Häusser et al., 2000; Gulledge et al., 2005; Sjöström et al., 2008). There are many ways how active conductances could shape the dendritic integration. One of them is the capability of local

regenerative dendritic events in response to excitatory synaptic input, a process termed supralinear dendritic integration (Schiller et al., 1997; Hausser et al., 2000; Nevian et al., 2007; Yuste, 2011).
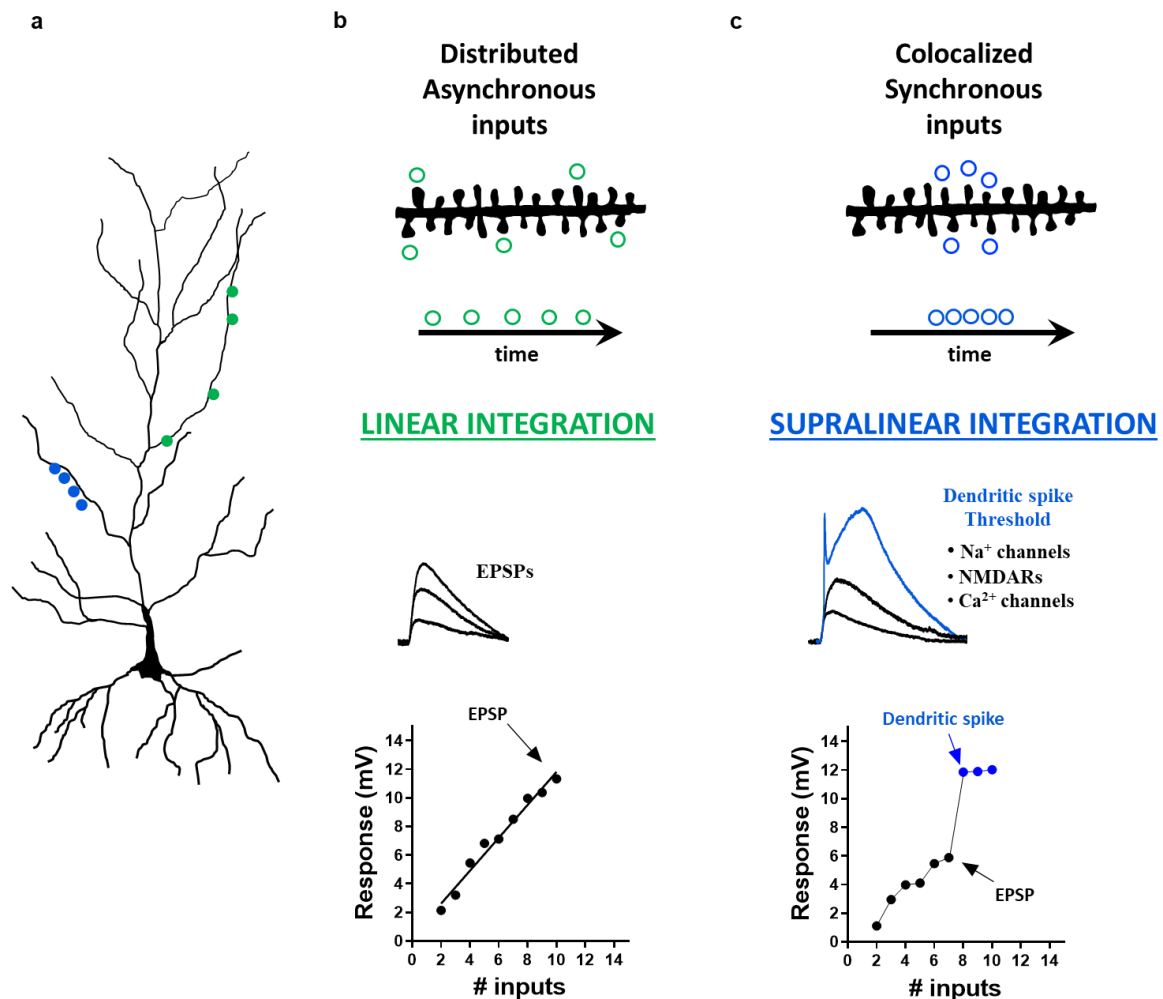
Fig. 1.7, Model of dendritic integration. a, Representation of a CA1 pyramidal neuron with sparse (blue dots) and cluster (red dots) synaptic inputs site along apical oblique dendrites. **b,** When excitatory inputs onto single dendritic spines are spatiotemporally distributed and asynchronous, they are summed up in a linear fashion with EPSPs amplitude that is growing in relation to the increasing number of synaptic inputs. **c,** When neighboring synapses are active simultaneously, and a certain threshold is reached, an additional non-linear step takes place. Na$^+$ voltage-gated channel and NMDAr activation lead to a supralinear response that deviates from the linear arithmetic summation, resulting in dendritic spike generation with a larger influence on somatic firing than the classic EPSP.

Spencer and Kandel provided the first evidence of additional dendritic features for integrating excitatory inputs in the early 1960s. Following in‑vitro, in‑vivo, and computational studies

have demonstrated how many pyramidal neurons in the cortex and hippocampus are capable of generating additional non-linear steps termed dendritic spikes (Schiller et al., 2000; Larkum et al., 2001, 2009; Wei et al., 2001; Ariav et al., 2003; Gasparini et al., 2004; Jarsky et al., 2005; Milojkovic et al., 2005; Nevian et al., 2007; Major et al., 2008). One of the most important requirements for generating supralinear integration via dendritic spikes is that inputs have to be synchronous in time and clustered in space (**Fig.1.7**) (Shepherd & Brayton, 1987; Mel, 1993; Mel et al., 1998; Ariav et al., 2003; Poirazi et al., 2003a-b; Polsky et al., 2004; Losonczy & Magee, 2006; Katz et al., 2009; Gómez González et al., 2001). In different types of neurons, the voltage-gated mechanisms that generate dendritic spikes can differ. Dendritic spikes can be mediated by different voltage-gated ion channels, such as voltage-gated Ca^{2+} channels (Ca^{2+} spikes), voltage-gated Na^+ channels (Na^+ spike), and NMDA receptors (NMDA spike plateau) (Larkum & Nevian, 2008; Antic et al., 2010; Major et al., 2013).

Basal and apical oblique dendrites from CA1 pyramidal neurons mainly generate fast transient Na^+ spikes, which shape and amplitude largely differ from the EPSPs (**Fig. 1.8a,b**) (Losonczy et al., 2008; Losonczy & Magee, 2006; Remy et al., 2009).

Dendritic Na^+ spikes are threshold responses characterized by a fast spikelet initial component, driven by Na^+ channels. Subsequently, this fast initial depolarization indirectly facilitates the activation of NMDA receptors and calcium channels, which together drive the slow component of this variant of dendritic spikes (**Fig. 1.8c**) (Ariav et al., 2003; Losonczy & Magee, 2006; Schiller et al., 2000). The dependence of voltage-gated Na^+ channels to generate dendritic spikes in CA1 dendrites can be easily confirmed by blocking the Na^+ channels with tetrodotoxin, which completely abolishes the supralinearity (**Fig.1.8d-f**) (Gasparini et al., 2004; Losonczy & Magee, 2006).
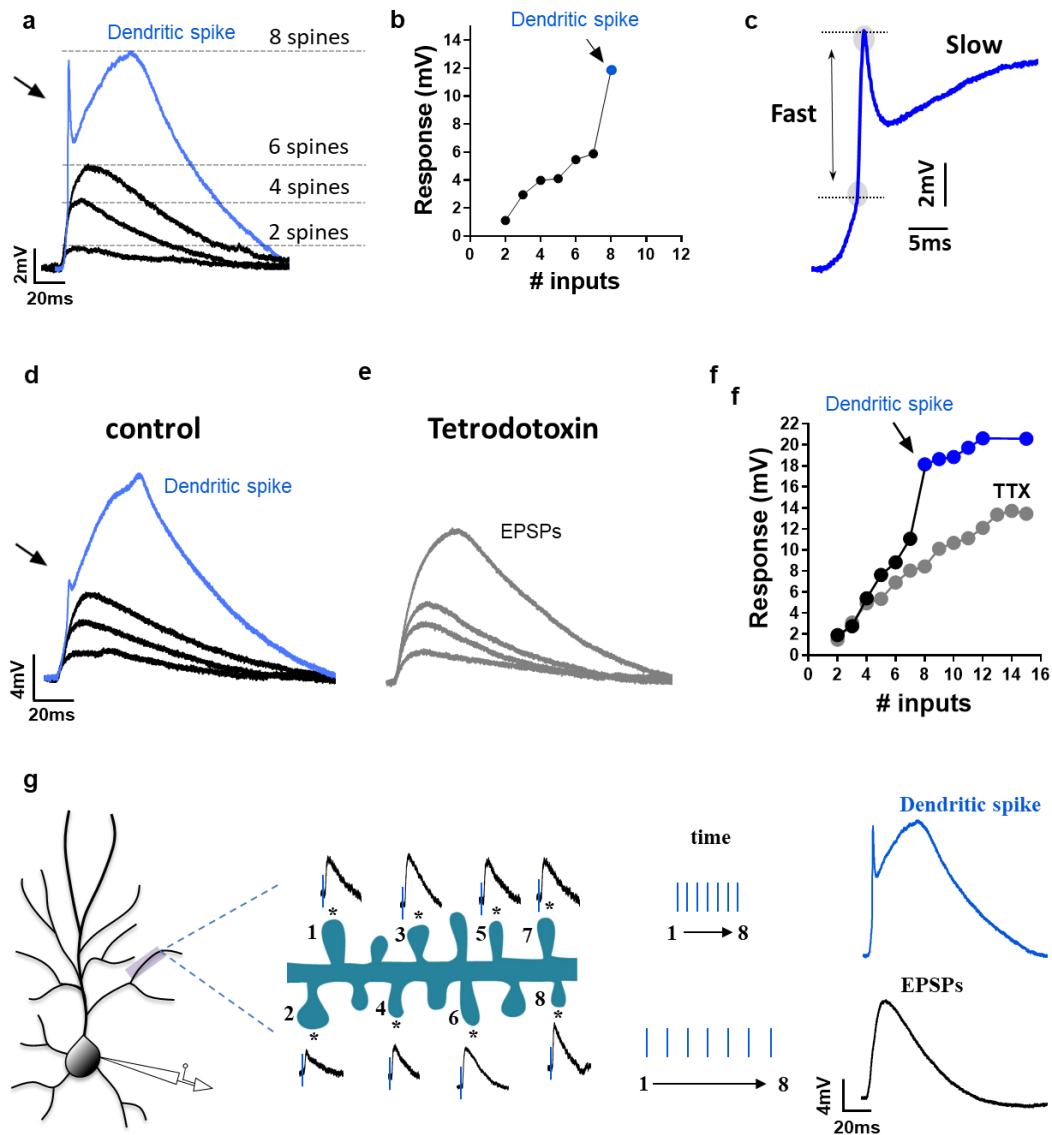
Fig. 1.8, Supralinear integration. a,b, if a certain threshold is reached as the result of spatiotemporally clustered synapses activation, some dendrites are capable of generating supralinear dendritic spikes (blue traces). The measured dendritic spike magnitude is larger compared to EPSP responses that would be obtained from the activation of the same number of spines, resulting in a deviation from the linearity. **c,** Dendritic spikes are generated by the fast activation of Na^+ voltage-gated channel, which subsequently facilitates the opening of NMDA receptors and calcium channels that drive the slow phase component. **Dendritic spikes rely on the activation of voltage-gated Na^+ channels. d,e,f,** Tetrodotoxin (0.5 µM), a non-selective Na^+ channel blocker, completely abolished the dendritic spike generation, and the supralinearity became linearity. **Input synchrony dependence of dendritic spikes. g,** quasi synchronous activation of dendritic synapses results in supralinear integration, while increasing the interval time between the same inputs fails to generate supralinear responses.

In contrast to a linear summation of EPSPs, the generation of dendritic spikes results in a stronger depolarization than it would be expected by the simple arithmetic summation of uEPSPs, with a concurrently larger influence on somatic firing. Indeed, dendritic spikes have been shown to drive temporally precise somatic action potential firing. This can occur with very few synchronously active inputs, resulting in a greater specificity of spiking.

The strong synchrony requirement, as well as the requirement for inputs to be colocalized on the same dendritic branch, implies that dendritic spikes can be generated only in response to very precise inputs with quasi-synchronous timing from specific presynaptic neuronal ensembles (Losonczy & Magee, 2006). Thus, dendritic spike generation reflects the synchronous recruitment of presynaptic neuronal ensembles. In contrast, even a slight uEPSPs desynchronization prevents the initiation of dendritic spikes, and their summation results in a linear integration (**Fig.1.8g**) (Gasparini & Magee, 2006; Losonczi & Magee, 2006). Thus, this form of dendritic computation, acting as a simple coincidence detector, allows neurons to respond with extremely high temporal precision to particular features of the input ensemble (Ariav et al., 2003; Golding & Spruston, 1998; Losonczy & Magee, 2006; Losonczy et al., 2008; Milojkovic et al., 2004). The implementation of dendritic spikes is also relevant since the capability for such integration increases the neuronal information storage capacity (Hausser &Mel, 2003; Govindarajan et al., 2006; Larkum & Nevian, 2008). Thus, the supralinear integration represents a concrete biophysical mechanism, which adds to the neurons the capability to perform different tasks and compute input-output signals that would typically require multiple neurons connected in a network (Poirazi & Mel, 2001; Wu & Mel, 2009).

Dendritic spikes have been proposed to provide the conditions for the synaptic plasticity required to store complex spatio-temporal input features. They can drive a large calcium influx into the dendrites providing the postsynaptic depolarization necessary for the synaptic plasticity essential for storing new information (Golding et al., 2002; Basu et al., 2016; Takahashi et al., 2016; Bittner et al., 2017). Dendritic spikes are also involved in spike-timing-dependent plasticity (STDP), which depends on the precise timing of presynaptic inputs and postsynaptic firing (Kampa et al., 2006), and in forms of synaptic plasticity that are thought to be independent of postsynaptic action potentials (Remy & Spruston, 2007; Golding et al., 2002).

In addition, they have been shown to undergo intrinsic plasticity through activity and experience-dependent mechanisms in a process termed branch-strength potentiation (BSP) (Losonczy et al., 2008).

Several features of dendritic spikes, such as the mechanisms underlying their generation and contribution to computational processes, have been extensively investigated in single neuron and neural circuits. However, little is known about dendritic spike's contribution to sensory perception and cognition, which was one of the first questions raised when the existence of active dendrites was proposed. Only recently, with the event of new cutting-edge technologies, it is possible to investigate dendritic dynamics in conjunction with animal behavior.

Indeed, many studies have started to explore the role of dendritic spikes in sensory processing, cognition, and in the spatial representation of the environment, including their role in hippocampal place coding (Sheffield & Dombeck, 2015; Schmidt-Hieber et al. 2017; Bittner et al., 2015; Hill et al. 2013).

In the hippocampus, spatial information is likely encoded by dendritic spikes in place cells. During spatial exploration, in these neurons, dendritic spikes contribute to the generation of complex spike burst activity in the soma. These complex spikes are a signature of place cells, and they drive a large influx of Ca^{2+} which acts as a second messenger promoting synaptic plasticity (Bittner et al., 2015; Cohen et al., 2017).

Furthermore, multi-planar two-photon Ca^{2+} imaging from dendrites and somata of CA1 place cells in behaving animals has shown dendritic spikes participation in the spatial representation. Indeed, it has been demonstrated how the higher prevalence of dendritic spikes across a place field (branch-spike prevalence) strongly correlates with increased spatial precision and stability of place cells (Sheffield & Dombeck, 2015). It has been shown that dendritic spikes often occur prior to somatic place field firing, and since they can provide the depolarization necessary for synaptic potentiation, they can likely support the formation of new CA1 place fields (Sheffield et al., 2017). In addition, the electrical properties of individual dendrites can be modified by experience. Indeed, increased propensity and strength for dendritic spikes have also been observed in-vivo following exposure of animals to an enriched environment (Makara et al., 2009).

Altogether, these studies highlight the contribution of dendritic spikes in driving specific forms of time-dependent plasticity and in increasing the computational ability of neurons during sensory processing and spatial memory.

1.4. Dendritic channelopathies in epilepsy

Because voltage-gated channels are central to mediating dendritic excitability and integration, changes in the function or expression of these channels may strongly impact neuronal input-output properties, information storage capability and plasticity.

The alteration or dysfunction of ion channels is termed channelopathy. This term was used for the first time by Louis Ptáček to describe a Na^+ channel dysfunction during hyperkalemic paralysis (Ptáček, 1997). Since then, the term channelopathy has been used for many diseases with dysfunction of ion channels at their origin, including epilepsy.

The link between channelopathy and epilepsy has been only an assumption for many years, based on the "epileptic neuron hypothesis" which describes the hyperexcitability in epilepsy as a consequence of aberrant synaptic currents and intrinsic alterations (Ward, 1961). Following, many studies have provided clear evidence that ion channel dysfunctions are a major pathophysiological mechanism underlying epilepsy (Davies, 1995; Macdonald & Kelly, 1995; Elmslie & Gardiner, 1995). CA1 pyramidal neurons are known to regulate the expression of various ion channels along with their dendrites, such as A-type K^+ channels, HCN channels, Ca^{2+} channels, and Na^+ channels (**Fig. 1.9**) (Beck & Yaari, 2008; Spruston, 2008). Patch-clamp experiments have demonstrated the fundamental role of these channels in shaping the integration of subthreshold synaptic potentials regulating the degree of voltage attenuation of EPSPs (Johnston et al., 1996; Häusser et al., 2000; Magee, 2000; Spruston, 2008) and in filtering the action potential backpropagation through the dendritic arborization (Stuart et al., 1997).

Moreover, dendritic voltage-gated channels play a crucial role during active dendritic integration driving supralinear dendritic integration via the generation of dendritic spikes (Losonczy & Magee, 2006; Remy, 2009; Golding & Spruston, 1998; Jarsky et al., 2005).

Thus, considering the relevant role of voltage-gated ion channels in regulating the dendric excitability and their recruitment in many dendritic active electrogenesis, any perturbation at these channels may result in dysfunctional feature input detection.

A large body of data has described how during epilepsy, neurotransmitter receptor and ion channel conductances such as A-type K^+ channels (Bernard et al., 2004; Singh, 2006; Lugo, 2008), HCN channels (Shah et al. 2004; Jung et al., 2007; Dyhrfjeld-Johnsen et al., 2009), T-type Ca^{2+} channels (Su et al., 2002; Yaari et al., 2007; Becker et al., 2008) and Persistent Na^+ currents (Chen et al., 2011; Royeck et al., 2015), are strongly affected in CA1 dendrites. As a result, these channelopathies increase the intrinsic neuronal excitability contributing to the abnormal firing and the aberrant dendritic integration in chronic epilepsy.

	Current/channel				
	I_h (HCN)	$I_{Ca,R}$ (Ca$_v$2.3)	K$_v$2.1	I_{Na}	I_M (K$_v$7)
	$I_{K,A}$ (K$_v$4.2)	$I_{K,DR}$ (K$_v$3)			I_{Nax}, I_{NaP}
Compartment	$I_{Ca,T}$ (Ca$_v$3.2)				$I_{K,DR}$ (K$_v$3.1)
Distal dendrite					
Apical dendrite					
Soma					
Axon initial segment					
Ranvier node					

Beck & Yaari, 2008
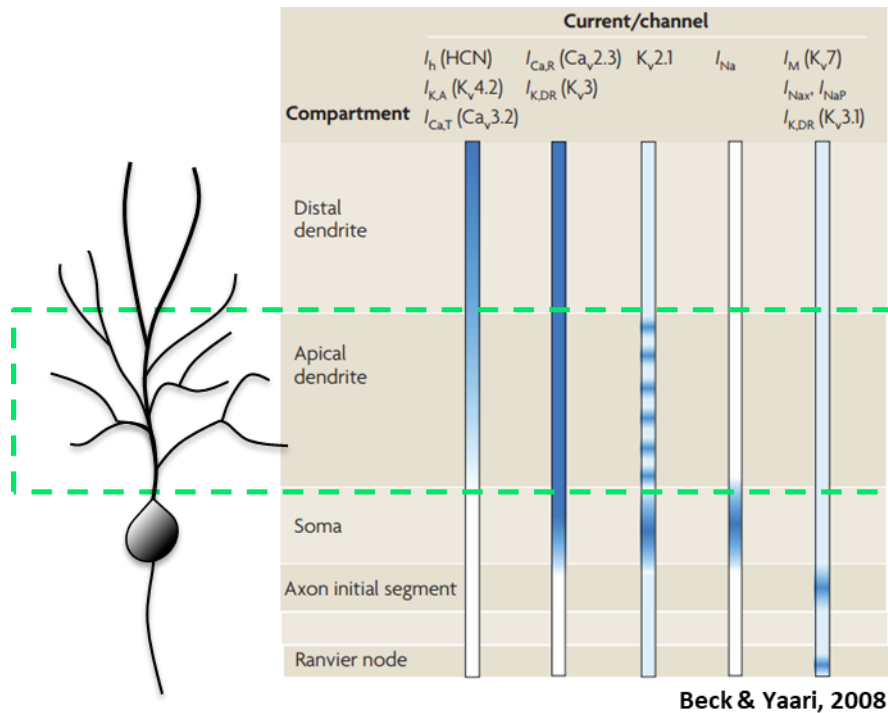
Fig. 1.9, General distribution of voltage-gated ion channels and currents in a hippocampal CA1 pyramidal neuron. Ih, $I_{K,A}$ and $I_{Ca,T}$, and their corresponding ion-channel subunits are concentrated in distal dendrites. R-type Ca^{2+} channels ($I_{Ca,R}$), as well as some K$^+$ channel subunits (K$_v$3), are distributed throughout the dendrites. Some channel types, such as K$_v$2.1, are found in clusters on the soma and proximal dendrites. Most types of high-threshold Ca^{2+} channels, as well as specific subtypes of Na$^+$ currents (I_{Na}) and delayed rectifier K$^+$ currents, are found predominantly in the perisomatic region. The initial segment of the axon and the nodes of Ranvier display a striking aggregation of K$_v$7 channels that underlie I_M, transient Na$^+$ channels with specific properties (I_{Nax}), and some types of K$^+$ channels (K$_v$3.1). Persistent Na$^+$ currents (I_{NaP}) are also found predominantly at this location. (adapted from Beck & Yaari, 2008).

1.4.1. A-type K$^+$ channels in epilepsy

A-type K$^+$ channels were the first, dendrically expressed channels that were shown to be regulated in epilepsy (Bernard et al., 2004). This study used whole-cell dendritic current-clamp recordings to examine the activity of A-type K$^+$ channels in dendrites from CA1 pyramidal neurons in chronically epileptic rats. In physiological conditions, the I_A current generated by A-type K$^+$ channels, mainly by the K$_v$4.2 isoform, increases linearly along dendrites, reaching densities about five-fold greater than that at the soma (Hoffman et al., 1997). Thus, higher I_A density levels are correlated with lower dendritic excitability due to their attenuation of backpropagated APs and EPSPs. In contrast, in epileptic animals, a

reduction of A-type K$^+$ currents along dendrites was observed, and it is caused by increased phosphorylation of K$_v$4.2 subunits with consequent downregulation of K$_v$4.2 channels (Bernard et al., 2004). This down-regulation leads to increased amplitudes of backpropagating APs, with consequently enhanced activation of voltage-gated Ca^{2+} channels and NMDARs, resulting in a pathological dendritic overexcitability.

1.4.2. HCN channels in epilepsy

A different voltage-gated ion channel highly expressed in dendrites of CA1 pyramidal neurons is the hyperpolarization-activated cyclic nucleotide-gated channel (HCN channel). HCN channels mediate I_h and are permeable to both Na$^+$ and K$^+$ ions. As the A-type K$^+$, channel density has been shown to increase linearly along the dendrites, reaching densities ten times greater than at the soma (Magee, 1998). The role of dendritic HCN channels is particularly relevant to modulate repetitive excitatory synaptic input, filtering the temporal summation of EPSPs (Magee et al., 1999; Poolos et al., 2012). Pharmacological experiments reveal that blocking the HCN channel activity results in hyperpolarizes the resting membrane potential and enhances dendritic excitability due to the interaction with other ion channels expressed along the membrane (George et al., 2009). In epilepsy, HCN channels are downregulated and undergo functional changes leading to neuronal hyperexcitability in hippocampal and entorhinal cortex (Marcelin et al., 2009; Shah et al., 2004; Jung et al., 2007).

1.4.3. Voltage-gated Ca^{2+} channels in epilepsy

Voltage-gated calcium channels (VGCCs) have also been immunolocalized along the dendritic arborization of CA1 pyramidal neurons. In particular low voltage-activated T-type channels (Ca$_v$3.2) and high voltage-activated R-type channels (Ca$_v$2.3) are expressed at higher levels in dendrites compared to the soma (Magee & Johnston, 1995). T- and R- type Ca^{2+} channel regulation has been shown to occurs in epilepsy. Indeed, hippocampal pyramidal neurons are known to switch their regular action potential firing rate (Jensen et al., 1994; 1996; Azouz et al., 1996) to burst firing during epilepsy (Sanabria et al., 2001) due to a Ca$_v$3.2 upregulation in the apical dendrites (Su et al., 2002; Yaari et al., 2007; Becker et al., 2008). Ca$_v$2.3 channels can induce plateau potentials in the CA1 region (Tai et al., 2006) and trigger hippocampal seizure activity (Hamilton et al., 1997).

In addition, VGCCs play fundamental roles in dendritic excitability and synaptic integration. Activation of these channels promotes regenerative depolarizations that generate dendritic

spikes (Golding et al., 1999). In addition, action potential backpropagation into the apical dendrites of pyramidal neurons also recruits Ca^{2+} channels, which then modulate synaptic plasticity such as STDP and LTP (Sjöström & Nelson, 2002). Thus, abnormal up-regulation of these channels could also have additional effects on calcium electrogenesis and synaptic plasticity.

1.4.4. Voltage-gated Na^+ channels in epilepsy

The Na^+ conducting pore of voltage-gated sodium channels (VGSCs) is formed by a single α subunit associated with modulatory β subunits. Nine isoforms of VGSC α subunits, termed $Na_v1.1$–$Na_v1.9$, have been identified in mammals, with $Na_v1.1$, $Na_v1.2$, $Na_v1.3$, and $Na_v1.6$ being the principal isoforms expressed in the mammalian CNS (Goldin, 2001).

These channels play a crucial role in the generation and propagation of action potentials (Wang et al., 2017; Hille, 1971; 1972; Sato et al., 2001, Catterall, 2000; Catterall, 2012).

Moreover, Na^+ channel activation along CA1 dendrites is essential for driving the fast Na^+ dendritic spikes (Gasparini et al., 2004; Losonczy & Magee, 2006).

Although there is little data on the distribution of most Na^+ channel subtypes within CA1 dendrites, Na^+ currents have been observed through the entire somatodendritic axis with homogeneous density (Magee & Johnston, 1995).

Na^+ channels in CA1 apical dendrites are known to drive persistent sodium currents (I_{NaP}), characterized by slow inactivation and a low activation threshold (Lunko et al., 2014; Fleidervish & Gutnick, 1996).

These I_{NaP} arise principally perisomatically (Yue et al., 2005) and play an important role in amplifying and boosting distal EPSPs, compensating for the electrotonic attenuation during their propagation to the soma (Lipowsky et al., 1996). Interestingly, I_{NaP} currents have been shown to increase in animal models of chronic epilepsy (Chen et al., 2011), particularly in CA1 proximal apical dendrites, with consequent abnormal enhancement in the linear integration of EPSPs (Royeck et al., 2015).

Several changes in Na_v channels have been described and associated with chronic epilepsy. These include their expression level regulation and kinetics, such as channel activation, inactivation, recovery from inactivation. Among the Na_v subtypes related to epilepsy, the $Na_v1.3$ isoform recently became of particular interest.

Scn3a encodes the channel $Na_v1.3$, which is highly expressed in the brain during embryonic and neonatal development (Cheah et al., 2013; Whitaker et al., 2000; Vacher et al., 2008),

but expressed at low or undetectable levels at postnatal stages (Beckh et al., 1989). Several studies have shown that regulation of $Na_v1.3$ channel and its encoding gene Scn3a are significantly increased in human epilepsy (Yu et al., 2012; Whitaker et al., 2001) and in experimental epilepsy models (Tan et al., 2017; Lin et al., 2017; Xu et al., 2012).

Moreover, Na^+ channels have become an intense focus of channelopathy research owing to their involvement in genetic epilepsy syndromes, with the vast majority discovered in Scn1A, Scn2A, Scn8A (Mulley et al. 2005; Striano et al. 2006; Sawyer et al. 2014) and more recently in Scn3a (Zaman et al. 2019; 2020; Lamar et al., 2017; Tan et al., 2017; Vanoye et al., 2014). In addition to being strongly regulated in acquired and genetic epilepsies, Na^+ channels are a major drug target in both types of epilepsy. The most commonly used antiepileptic drugs (AEDs) modulate VGSCs in a use-dependent manner (Macdonald & Kelly, 1995; Ragsdale & Avoli, 1998) that preferentially inhibits prolonged high-frequency activity, as it occurs during a seizure (Bragin et al., 1999).

1.5. Key questions

Despite the fact that cognitive comorbidities are extremely debilitating in MTLE patients, not much effort has been directed towards understanding the biology of these impairments.

Dendritic spikes are a cornerstone of dendritic integration, are important for spatial representations in hippocampal neurons, and underlie specific forms of plasticity. Thus, disturbed dendritic spikes could be an important mechanism of altered spatial coding and memory, but changes in chronic epilepsy have so far not been studied.

Therefore, using a multi-level approach ranging from the level of signal processing in dendrites to in-vivo imaging and behavioral approaches, this thesis addresses the following key questions:

- Is the hippocampal dendritic integration affected during chronic epilepsy?
- What is the mechanism underlying the abnormal dendritic excitability in epilepsy?
- Could a dysfunctional dendritic integration contribute to degraded memory in epilepsy?
- Could the aberrant dendritic integration be therapeutically targeted to restore impaired cognition in chronic epilepsy?

Chapter 2

# Materials and Methods

2.1. Animals

All experiments followed institutional guidelines of the Animal Care and Use Committee of the University of Bonn. All in vitro and behavioral experiments were performed on C57BL/6J male wild-type mice (Charles River, Sulzfeld). For in vivo 2-photon imaging experiments, we used Thy1-GCaMP6 (C57BL/6J-Tg(Thy1-GCaMP6s) mice, which express GCaMP6s in most hippocampal neurons (Dana et al.,2014). All efforts were made to minimize animal suffering and to reduce the number of animals used.

2.1.1. Kainate model of temporal lobe epilepsy

The kainic acid model (KA) of acquired temporal lobe epilepsy has greatly contributed to understanding the molecular, cellular, and pharmacological mechanisms underlying epileptogenesis and ictogenesis (Bedner et al., 2015). In this project, I used the KA model, which presents neuropathological and electroencephalographic features observed in patients with temporal lobe epilepsy. It consists of unilateral stereotactic injection to deliver the kainic acid just above the alveus and hippocampal CA1, which results in acute bouts of neuronal hyperactivity and seizures, leading to chronic experimental epilepsy.

For the experiments, 5 week-old mice were injected with analgesic ketoprofen (Gabrilen, Mibe; 5 mg/kg b.w.; injection volume 0.1 ml/10 g b.w., s.c.) diluted in H_2O (Ampuwa, Fresenius Kabi Deutschland) 30 minutes before injecting the anesthetic. Mice were anesthetized using a mixture of ketamine (Medistar; 80mg/kg b.w.) and medetomidine hydrochloride (Domitor, Orion Pharma; 1.2mg/kg b.w.; injection volume 0.1 mL/10 g, i.p.) and placed in a stereotaxic frame in a flat skull position. Eyes were covered with eye-ointment (Bepanthen, Bayer) to prevent drying, and body temperature was maintained at 37°C using a regulated heating plate (TCAT-2LV, Physitemp) and a rectal thermal probe. The surface was locally anesthetized with a drop of 10% lidocaine, and after 3-5 min, residual soft tissue was removed from the skull bones with a scraper and 3% H_2O_2/NaCl solution. After complete drying, the cranial sutures were clearly visible and served as orientation for the determination of the drilling and injection sites. For stereotactic injection, a hole was carefully drilled

through the skull with a dental drill, avoiding excessive heating and injury to the meninges. Any minor bleeding was stopped with a sterile pad. A stainless-steel cannula (0.5 mm outer diameter) connected to a 10 μl microsyringe (Hamilton, Bonaduz, Switzerland) was filled with a 20 mM kainic acid (KA) solution (Sigma, Lyon, France) in 0.9% sterile sodium chloride (NaCl, Fresenius Kabi Deutschland) and positioned above the right dorsal hippocampus (anteroposterior −1.9 mm; mediolateral −1.5mm; dorsoventral, −1.7 mm) with bregma as a reference. Injections of dextran-biotin (50nl) marker showed that these coordinates correspond to the upper border of the CA1 region of the dorsal hippocampus (**Fig. 2.1 a,b**).
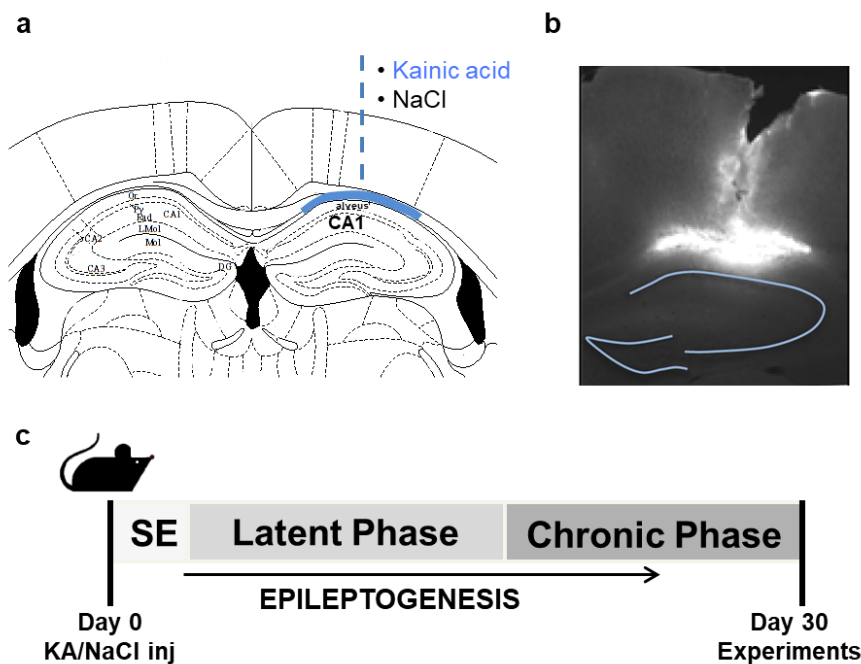
Fig. 2.1, Chronic acquired temporal lobe epilepsy in the Kainic acid model (KA). a, schematic representation of supra-hippocampal injection coordinates and **b,** dextran-biotin (50nl) marker showing the targeted area. **c,** timeline of chronic epilepsy development.

Once the cannula reached the correct depth, it was left in place for 2 minutes before beginning injection to wait for the tissue adjustment. Mice were given injections for ~2 min (20nL/min) of 50 nl of the KA solution using a micropump (Micro4 Microsyringe Pump Controller, WPI) operating the microsyringe. After injection, the cannula was left in place for additional 2 minutes to avoid reflux of the injected solution along the needle track. Sham-operated mice were given injections of 50 nl of 0.9% sterile NaCl but were otherwise treated identically. In mice intended for 2-photon in vivo imaging, an additional virus injection and placement of a head fixation were carried out (see below). Mice had their scalp incision sutured and their

anesthesia terminated with atipamezole hydrochloride (Antisedant, Orion Pharma; 2.5mg/kg b.w.; injection volume 0.1 mL/10 g, i.p.). Diazepam (Ratiopharm, injection volume 0.15 ml/20 g, s.c.) was administered to all mice 4 hours after the start of status epilepticus (SE) to terminate the convulsions. At the same time, mice were also injected with glucose monohydrate (Glucosteril, Fresenius Kabi Deutschland; injection volume 0.25 ml, s.c.). Mice were returned to their cages and kept on a heat-pad until they woke from anesthesia. After recovery from anesthesia, the animals were kept under observation, and they were injected with the analgesic ketoprofen to alleviate pain for 4 days. After surgery, mice were housed in individual cages. They were subsequently used for in vitro experiments 30 days after kainate/sham injection or for in vivo 2-photon imaging or behavioral experiments (**Fig. 2.1 c**).

2.2. *Slice preparation and patch-clamp recording*

Mice were deeply anesthetized with isoflurane and then decapitated. Brains were rapidly removed and placed in ice-cold ($<2°C$) sucrose-based artificial cerebrospinal fluid (sucrose-ACSF) containing (in mM): 60 NaCl, 100 sucrose, 2.5 KCl, 1.25 NaH2PO4, 26 NaHCO3, 1 CaCl2, 5 MgCl2, 20 glucose. Slices of 300 μm were cut with a vibratome (Leica, Wetzlar, Germany) and incubated in sucrose-ACSF at 35°C for 30 min. Subsequently, slices were transferred to a submerged holding chamber containing normal ACSF containing (in mM): 125 NaCl, 3.5 KCl, 1.25 NaH_2PO_4, 26 $NaHCO_3$, 2.6 $CaCl_2$, 1.3 $MgCl_2$, 15 glucose at room temperature. All extracellular solutions were equilibrated with 95% O2 and 5% CO2.

Selected CA1 cells were visualized with infrared oblique illumination optics and a water immersion objective (60x, 0.9 NA, Olympus) (**Fig.2.2**), and somatic whole-cell current-clamp recordings were performed with a BVC-700 amplifier (Dagan Corporation, Minneapolis MN, USA). Data were filtered at 10 kHz and sampled at 50 kHz with a Digidata 1440 interface controlled by pClamp Software (Molecular Devices, Union City, CA). Patch-pipettes were pulled from borosilicate glass (outer diameter 1.5 mm, inner diameter 0.8 mm; Science Products, Hofheim, Germany) with a Flaming/Brown P-97 Puller (Sutter Instruments, Novato, USA) to resistances of 2 to 5 MΩ in bath and series resistances ranging from 8 to 30 MΩ. The standard internal solution contained (in mM): 140 K-gluconate, 7 KCl, 5 HEPES, 0.5 $MgCl_2$, 5 phosphocreatine, 0.16 EGTA. Internal solutions were titrated to pH 7.3 with KOH, had an osmolality of 295 mOsm, and contained 100 μM Alexa Fluor 594 (Invitrogen, Eugene OR, USA). Voltages were not corrected for the calculated liquid-junction potential of +14.5 mV. Membrane potential was adjusted to -75 mV for all

recordings. To assess somatic action potential firing, current steps (800 ms) of increasing amplitudes were injected via the somatic patch pipette. The analysis of the effects of S-Lic or ICA-121431 on maximal firing rates was done by identifying the current injection at which maximal firing rates were obtained under control conditions. Effects of drugs and washout were quantified using this current injection magnitude. Passive membrane properties, action potential properties, and firing patterns were assessed throughout the entire course of the experiment. Cells with unstable input resistances or lacking overshooting action potentials were discarded as well as recordings with holding currents >-200 pA for 60 mV and access resistances > 30 MOhm.

For AMPA receptor-mediated miniature EPSC (mEPSC) recordings, the Na^+ channel blocker tetrodotoxin (1 µM) and GABAA receptor antagonist bicuculline (20 µM) were added to the extracellular ACSF at least 15 minutes before starting recordings. Cells were voltage-clamped at −60 mV, and synaptic currents were recorded with an Axopatch 200-B amplifier (Axon Instruments, Foster City, CA, USA), filtered at 2 kHz, and digitized at 5 kHz. Analysis was performed with Minianalysis.
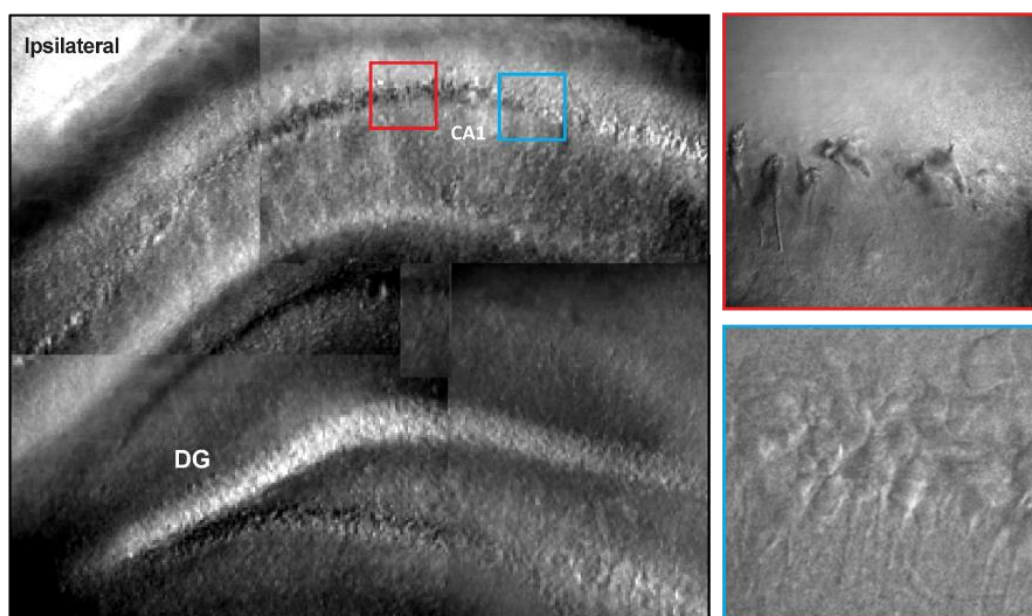
Fig. 2.2, Representative hippocampal coronal slice (300 µm) from the ipsilateral injected hemisphere in the kainic acid-treated mouse. Patch-clamp recordings were obtained from CA1 pyramidal neurons (blue inset) close to the sclerotic area (red inset).

2.2.1. In vitro two-photon uncaging

Two-photon glutamate uncaging at apical oblique dendrites of CA1 was performed using a dual galvanometer-based scanning system (Prairie Technologies, Middleton, WI, USA) to photo-release glutamate at multiple dendritic spines of CA1 neurons. MNI-caged-L-glutamate 15 mM (Tocris Cookson) was dissolved in HEPES-buffered solution (in mM as follows: 140 NaCl, 3KCl, 1.3 $MgCl_2$, 2.6 $CaCl_2$ 20 D-glucose, and 10 HEPES, pH 7.4 adjusted with NaOH, 305 mOsmol/kg) and was applied using positive pressure via glass pipettes (< 1 MΩ) placed in closed proximity to the selected apical oblique dendrites of CA1 neurons. We used two ultrafast laser beams of Ti:sapphire pulsed lasers (Chameleon Ultra, Coherent) tuned at 860 nm to excite the Alexa 594, and one tuned to 720 nm was used to photo-release at 10-15 dendritic spines (within ~ 10μm in length). The intensity of each laser beam was independently controlled with electro-optical modulators (Conoptics Model 302RM, Danbury, CT, USA). MNI-glutamate was uncaged at an increasing number of spines (2-15) with 0.5 ms exposure times, and the laser was rapidly moved from spine to spine with a transit time of ~0.1 ms. The laser power at the slice surface was kept below 22 mW to avoid photodamage. The glutamate was uncaged onto a sequence of single spines to evoke unitary excitatory postsynaptic potential (uEPSP). To quantify deviations from linearity in dendritic integration, the arithmetic summation calculated from each individual uEPSP was compared to the measured EPSP during glutamate uncaging onto the same sequence of spines. The rate of rise of the dendritic spike initial fast phase was calculated from the maximum dV/dt value from dendritic spikes generated at a similar number of spines (sham-control vs. epilepsy, 9.81±0.31 and 9.51±0.29 stimulated spines). The slow phase NMDA area was calculated from the same dendritic spikes used to quantify dV/dt. The dendritic spike threshold was calculated as the amplitude of the expected EPSP at which dendritic spikes first occurred. All data analyses were done with Clampfit 9.2 software (Molecular Devices), IGOR Pro (Wavemetrics), and GraphPad Prism (GraphPad Software).
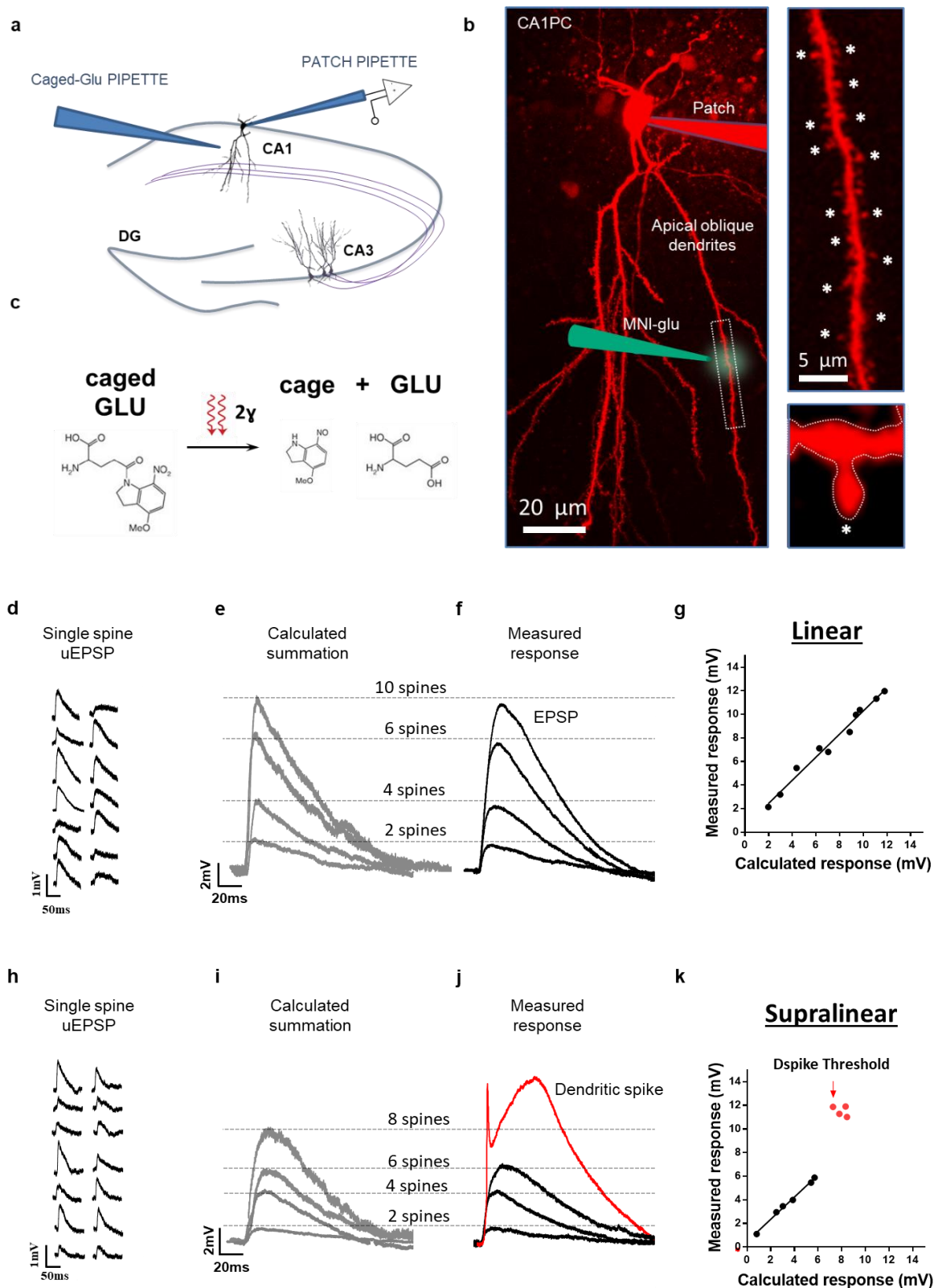
Fig. 2.3, Two-photon glutamate uncaging in apical oblique dendrites to probe linear and supralinear dendritic integration from CA1 pyramidal neurons. a, scheme representing the experimental setup. b, patch-clamp recordings from CA1 pyramidal cells (CA1PC) were performed in whole-cell mode. Neurons were filled with Alexa 594 via patch pipette to visualize their morphology with a two-photon microscope. A second patch pipette with a large aperture, filled with

15 mM MNI-caged-glutamate dissolved in HEPES-buffered solution, was placed adjacent to the dendrite of interest, and slight overpressure was applied to deliver the compound locally. A dendritic segment of interest was selected and imaged with high magnification to allow the identification of single spines. Single uncaging spots were placed near the heads of 15 spines. After this, a pointing protocol was started on the two-photon microscope, which illuminated all the selected spots sequentially, **c,** photoconverting MNI-caged-glutamate in its bioactive form. **d,**h, the somatic voltage transients from single spines (uEPSP) were recorded. **e,i,** from uEPSP, an expected response was calculated as arithmetic sums of an increasing number of single spines, with a prediction of a compound response that would be obtained with the same number of spines activation. **f,j,** then, in the same protocol, increasing numbers of spines were activated quasi-synchronously via uncaging, and the somatic voltage transients from compound responses were recorded. **f,g,** CA1 dendrites either displayed linear integration only via EPSPs or **j,k,** were capable of generating sudden supralinear dendritic spikes (red trace) when increasing numbers of spines were synchronously stimulated. **g,k,** plot of the magnitude of measured responses versus the corresponding arithmetic summation of uEPSPs. Black line is a linear fit to the data. **g,** increased number of stimulated spines result in a linear summation where the amplitude of measured responses is similar to the corresponding arithmetic summation of single spines. **k,** when the activation of multiple spines generates a dendritic spike, the measured amplitude is larger than the expected summation resulting in a deviation from the linearity, termed supralinear integration.

2.2.2. In vitro pharmacology

S-Lic was supplied by Bial–PORTELA & CA. S-Lic or ICA-121431 (Tocris Minneapolis, MN) were dissolved in DMSO, with a 0.1 % concentration of DMSO in ACSF. Control ACSF contained concentrations of DMSO equivalent to the drug-containing solution. Drug effects were analyzed 15 minutes after initiating the drug application.

2.3. Two-photon in vivo Ca^{2+} imaging, virus injections and head fixation

For Thy1-GCaMP6s mice intended for in vivo 2-photon imaging experiments, injection of an AAV led to labeling astrocytes with mCherry (rAAV2/1.GFAP.mCherry, total volume 250 nl, 20 nl/min) was carried out in addition for improved motion correction using an orthogonal imaging channel. Following virus injection, Optibond (Optibond^{TM} 3FL; two-component, 48% filled dental adhesive, bottle kit; Kerr; FL, USA) was applied thinly to the skull to aid adhesion of dental cement. Subsequently, a flat custom-made head post ring was applied with the aid of dental cement (Tetric Evoflow), the borehole was closed, and the surrounding skin was adapted with tissue glue.

2.3.1. Window implantation procedure

Cranial window surgery was performed to allow imaging from the dorsal hippocampal CA1 region. 30 minutes before induction of anesthesia, the analgesic buprenorphine was administered for analgesia (0.05 mg/kg body weight), dexamethasone (0.1 mg/20 g body weight), and ketoprofen (5mg/kg body weight) were given to inhibit inflammation/swelling and pain. Mice were anesthetized with 3-4% isoflurane in an oxygen/air mixture (25/75%) and then placed in a stereotactic frame. Eyes were covered with eye-ointment (Bepanthen, Bayer) to prevent drying, and body temperature was maintained at 37°C using a regulated heating plate (TCAT-2LV, Physitemp) and a rectal thermal probe. The further anesthesia was carried out via a mask with a reduced isoflurane dose of 1-2% at a gas flow of about 0.5 ml/minute. A circular craniotomy (Ø 3 mm) was opened within the head fixation ring above the right hemisphere hippocampus using a dental drill. Cortical tissue was aspirated until the alveus fibers above CA1 became visible. A custom-made cone-shaped silicone inset (upper diameter 3 mm, lower diameter 2 mm, length 1.5 mm, RTV 615, Movimentive) attached to a cover glass (Ø 5 mm, thickness 0.17 mm) was inserted and fixed with dental cement. Postoperative care included analgesia by administering buprenorphine twice daily (0.05 mg/kg body weight) and ketoprofen once daily (5 mg/kg body weight s.c.) on the three consecutive days after surgery. Animals were carefully monitored twice daily on the following 3 days, and recovered from surgery within 24-48 hours, showing regular activity and no signs of pain.

2.3.2. Two-photon Ca^{2+} imaging

We used a two-photon microscope (A1 MP, Nikon) equipped with a 25x long-working-distance, water-immersion objective (N.A.=1, WD=4 mm, XLPLN25XSVMP2, Olympus) controlled by NIS-Elements software (Nikon). GCaMP6s was excited at 940 nm using a Ti:Sapphire laser system (~60 fs laser pulse width; Chameleon Vision-S, Coherent) and a fiber laser system at 1070 nm (55 fs laser pulse width, Fidelity-2, Coherent) to excite mCherry (**Fig. 2.5**). Emitted photons were collected using gated GaAsP photomultipliers (H11706-40, Hamamatsu). Movies were recorded using a resonant scanning system at a frame rate of 15 Hz and a duration of 20 minutes per movie.
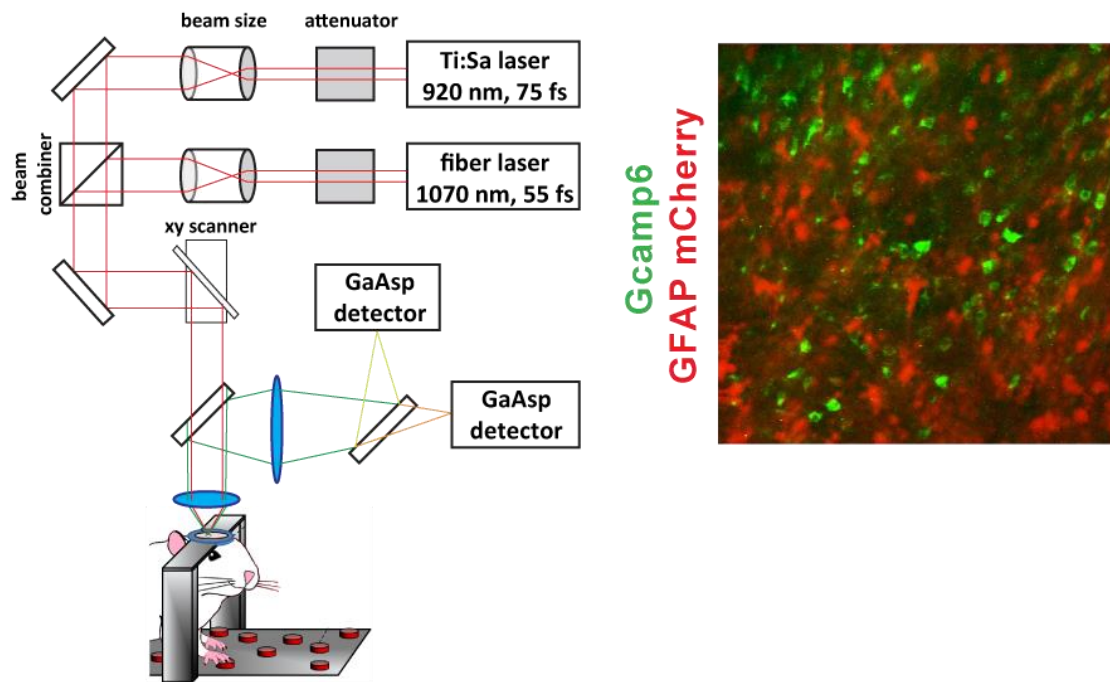
Fig. 2.5, Two-photon imaging in the CA1 region of the hippocampal formation. Setup of the 2-photon microscope for two-photon imaging. To allow efficient excitation of both Ca^{2+} indicator and mCherry GFAP, we established excitation with two pulsed laser sources at 920 and 1070 nm. Inset shows imaging in a representative field of view of the GCaMP6 signal from CA1 neurons (green) and the mCherry signal from astrocytes (red). Labeling of astrocytes with mCherry was carried out for improved motion correction using an orthogonal imaging channel.

2.3.3. Habituation and behavior on the linear track

Experiments were performed in head-fixed awake mice running on a linear track. Two weeks before the measurements, mice were habituated to the head fixation. Initially, mice were placed on the treadmill without fixation for 5 minutes at a time. Subsequently, mice were head-fixed but immediately removed if signs of fear or anxiety were observed. These habituation sessions lasted 5 minutes each and were carried out three times per day, flanked by 5 minutes of handling. During the following 3-5 days, sessions were extended to 10 minutes each. All experimental recordings were from experimental sessions of 20 minutes duration. After habituation, mice ran well on the treadmill for average distances between 9 and 27 meters per 20-minute session. The treadmill was a self-constructed linear horizontal treadmill, similar to (Royer et al., 2012). The belt surface was equipped with tactile cues. Belt position and running speed were measured by modified optical mouse sensors. All

stimulation and acquisition processes were controlled by custom-made software written in LabView. Detailed construction plans and LabView software are available upon request.
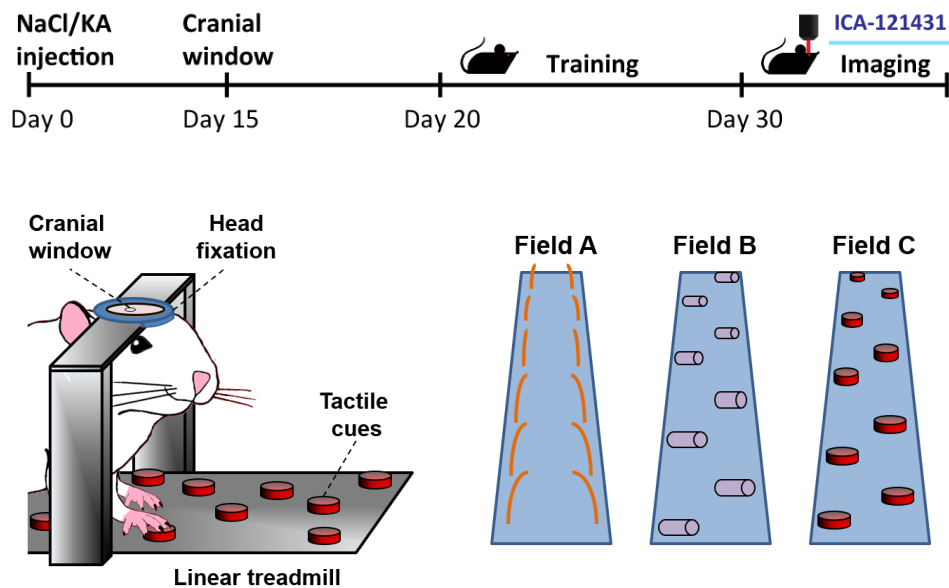
Fig. 2.6. Two-photon Ca²⁺ imaging in head-fixed sham-control and epileptic Thy1-GCaMP6s mice. Experimental timeline to investigate the activity of CA1 neurons from mice running on a linear track, enriched with spatial cues patterns.

2.3.4. Data analysis

All analyses on imaging data and treadmill behavior data were conducted in MATLAB using standard toolboxes, open access toolboxes, and custom-written code. To remove motion artifacts, recorded movies were registered using a Lucas–Kanade model (Greenberg and Kerr, 2009). In most cases, the red (mCherry) channel was used for motion correction. Individual cell locations and fluorescence traces were identified using a constrained nonnegative matrix factorization-based algorithm, and afterward, Ca²⁺ events were identified with a deconvolution algorithm (Pnevmatikakis et al., 2016). All components were manually inspected, and only those kept showed the shape and size of a CA1 pyramidal neuron and at least one Ca²⁺-event amplitude three standard deviations above noise level in their extracted fluorescence trace. I binarized individual cell fluorescence traces by converting the onsets of detected Ca²⁺ events to binary activity events.

2.3.5 Spatial tuning

To address spatial tuning of CA1 pyramidal neurons, we used spatial tuning vector analysis (Danielson et al., 2016). We restricted the analysis to running epochs, where a running epoch was defined as an episode of movement with a minimum duration of 2.5 s above a threshold of 4 cm/s in a forward direction. Only cells with 4 or more event onsets during all running epochs in a 20-minute session were included in the analysis. Mouse position was represented as vectors pointing towards the position on the linear track occupied by the mouse. We calculated the mean of the vectors at the times of all transient onsets during a session, weighted by the time spent in that bin. I addressed statistical significance by creating the null distribution for every spatially tuned cell. This was achieved by randomly shuffling the onset times and recalculating the spatial tuning vector 1000 times.

The p-value was calculated as the percentage of vector lengths arising from the shuffled distribution that was larger than the actual vector length (**Fig. 2.7**).
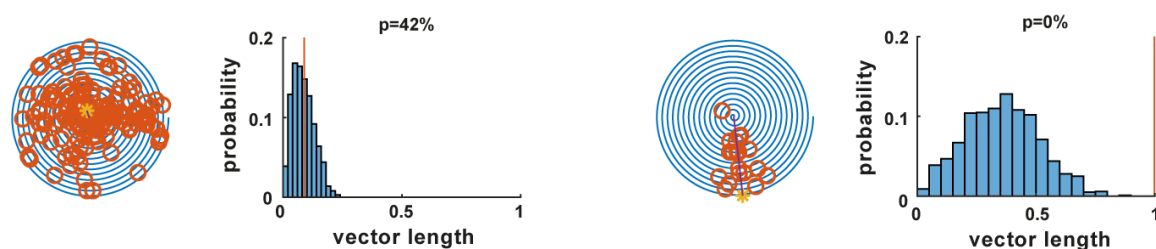
Fig. 2.7, Representative examples of spatial tuning in CA1 neurons. Spiral plots represent calcium events occurring during spatial navigation. One 360° pass around the spiral plot corresponds to a complete transition on the 150 cm linear track. Red dots indicate the activity of the CA1 neuron and represent a related transient vector. Computed sum of these vectors forms the tuning vector indicated by black straight lines. Histogram plots show tests vs. shuffled distributions of tuning vector length. The red vertical line indicates the tuning vector length of the CA1 neuron, shuffled distributions shown in blue. If the percentage of vector lengths arising from the shuffled distribution was >5% larger than the actual vector length, the cell is not considered coding for spatial information. In contrast, when the percentage is <5%, the cell is a place cell with different coding precision strengths depending on the tuning vector's length (long tuning vector showing high precise spatial tuning and short tuning vector showing lower and less spatial tuning).

2.3.6. Histochemistry

To verify successful viral transduction and the window position, animals were deeply anesthetized with ketamine (80 mg/kg body weight) and xylazine (15 mg/kg body weight). After confirming a sufficient depth of anesthesia, mice were heart-perfused with cold phosphate-buffered saline (PBS) followed by 4% paraformaldehyde (PFA) in PBS. Animals were decapitated, and the brain was removed and stored in 4% PFA in PBS solution. Fifty to 70 µm thick coronal slices of the hippocampus were cut on a vibratome (Leica). For nuclear staining, brain slices were kept for 10 min in a 1:1000 DAPI solution at room temperature. Brain slices were mounted, and the red, green, and blue channels were successively imaged under an epifluorescence or spinning disc microscope (Visitron VisiScope).
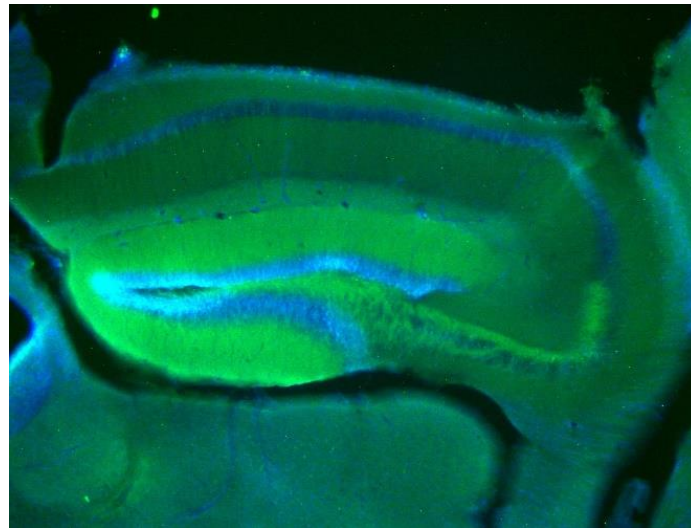
Fig. 2.4, Post hoc analysis in fixed coronal slice (70µm) of Thy1-GCaMP6s mouse previously implanted with a hippocampal window. Somata are stained with DAPI (blue), neuron cytosols are filled with GCaMP6s (green).

2.4. In vivo pharmacology

In vivo treatment with the specific $Na_v1.3$ antagonist ICA-121431 for behavioral experiments and in vivo 2-photon imaging was carried out at a 0.5 mg/kg body weight dose. ICA-121431 was solubilized in distilled water (concentration, 111.22 µM) and applied via gavage with a stainless-steel gavage cannula (20G, 30mm long, FST).

2.5. Behavior, object location, and object recognition memory

Three weeks after kainate/sham treatment, mice were habituated to handling by the experimenter for 10 minutes daily on 2 consecutive days prior to starting behavioral experiments. On experimental days, mice were moved from the animal holding facility to the experimental room at least 45 minutes before starting the experiments. The experimental room was quiet and had dim light conditions of around 20 lux, which was achieved by a single light spot pointing towards the ceiling. All experiments took place in the same acrylic glass arena that was 56 cm x 36 cm in size and had 20 cm high transparent walls without internal visual cues. Between animals, the arena was thoroughly cleaned using 70 % ethanol. The arena was placed on an infrared light board, and animal activity was monitored with an infrared camera above the arena and animal tracking software (Noldus X8.5, Ethovision). On the first three consecutive days, mice were placed in the empty arena for 10 minutes (**Fig. 2.8, habituation days 1-3**). After two days of break, treatment was started by administering animals twice per day via gavage with the drug or control substance. Animals received either 0.5 mg/kg body weight of ICA-121431 dissolved in water (Ampuwa) or plain water, 4 and 2 hours before starting experiments on every experimental day. On the first day of treatment, mice were again placed in the empty open field arena for 10 minutes (**Fig. 2.8, habituation day 4**). On the next day, mice were introduced to two identical objects (blue beaker bottle caps, diameter 5.5 cm) placed on opposite ends of a narrow side of the arena, 11.5 cm away from the walls, for 10 minutes (**Fig. 2.8, acquisition day 5**). Twenty-four hours later, one of the objects was displaced along the long side of the arena by 32 cm, and mice were given 5 minutes to explore (**Fig. 2.8, object location memory test, OLM, day 6**). On the next day, mice encountered the objects in the same position for 10 minutes as the day before to habituate them to the displacement (**Fig. 2.8, acquisition day 7**). Twenty-four hours later, a novel object, a transparent petri dish of the same diameter, replaced one of the familiar objects, and mice were given 5 minutes to explore (**Fig. 2.8, Novel object recognition test, NOR, day 8**). As an indicator of successful memory formation and recall, I compared exploration times of the objects. Successful memory formation is indicated by increased exploration of the displaced or novel object compared to the familiar object. I computed an exploration index according to the following formula (exploration time of displaced/novel object – exploration time of familiar object) / (exploration time of displaced/novel object + exploration time of familiar object)*100. Exploration times were manually scored by an experienced observer blinded to the treatment condition of the animal. I considered exploration when the nose of the animal was opposed to the object and pointed towards it. Time spent climbing onto the object was not considered exploration. I excluded trials in

which mice did not explore the objects for more than 3 seconds in both the habituation and recall trials, and if mice displayed a strong preference towards one of the two objects in habituation trials, indicated by a discrimination index of >20.
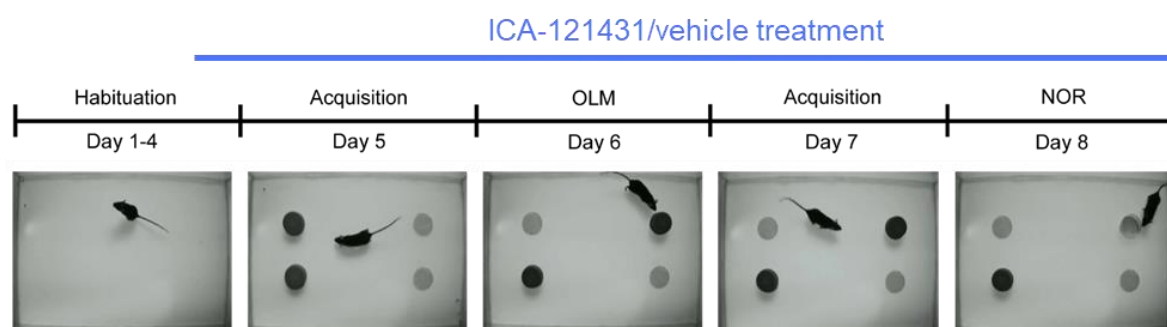
Fig. 2.8, Hippocampal-dependent memory in epileptic mice. Timeline of the behavioral experiments with in vivo inhibition of $Na_v1.3$ channels with ICA-121431. Days 1-4: habituation in the open field, with the application of either vehicle or ICA-121431 starting on the fourth day. Day 5-8: the object location memory (OLM) and object recognition memory (NOR) tests were sequentially performed.

2.5.1. Y maze spontaneous alternation test

To investigate Spatial Working Memory, the mice were placed for 10 minutes in a y-shaped arena made of red Plexiglas with three arms (40 cm long, 8 cm wide) arranged at a 120° angle. Spontaneous alternation behavior was analyzed by manually counting the number of three consecutive arm entries into different arms and dividing it by the number of potential alternations according to the following formula: (number of successful alternations / (total arm entries – 2). Arm entries were scored when all four paws of an animal were in an arm.
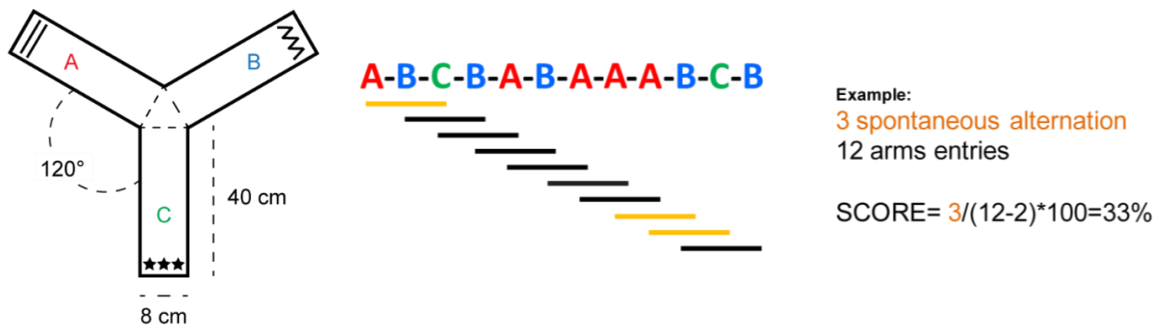
Fig. 2.9, Y maze spontaneous alternation test. a, Scheme representing the Y maze arena **b,** example of alternation score ranking.

Chapter 3

Results

3.1. *Altered intrinsic properties in epileptic CA1 excitatory neurons*

In this study, I investigated changes in chronic TLE using the well-established kainate acid animal model (Bedner et al., 2015; Bragin et al., 1999) that presents with neuropathological and electroencephalographic features similar to those observed in patients with temporal lobe epilepsy with Ammon's horn sclerosis.

I first investigated changes in the passive and active properties of epileptic neurons via patch-clamp recordings in-vitro, which were obtained from hippocampal CA1 excitatory cells in sham-control and epileptic animals. The resting membrane potential from epileptic neurons was significantly more depolarized compared to sham-control animals (**Table 1**). Eliciting intrinsic firing with somatic current injections revealed an increased action potential output frequency with a significantly lower firing threshold in epilepsy (**Fig. 3.1a-c**). Moreover, the fraction of neurons capable of generating burst-firing was higher in epilepsy (**Fig. 3.1d, e**). This is similar to the increase in burst-firing observed in other TLE animal models, such as the pilocarpine model (Becker et al., 2008; Sanabria et al., 2001).
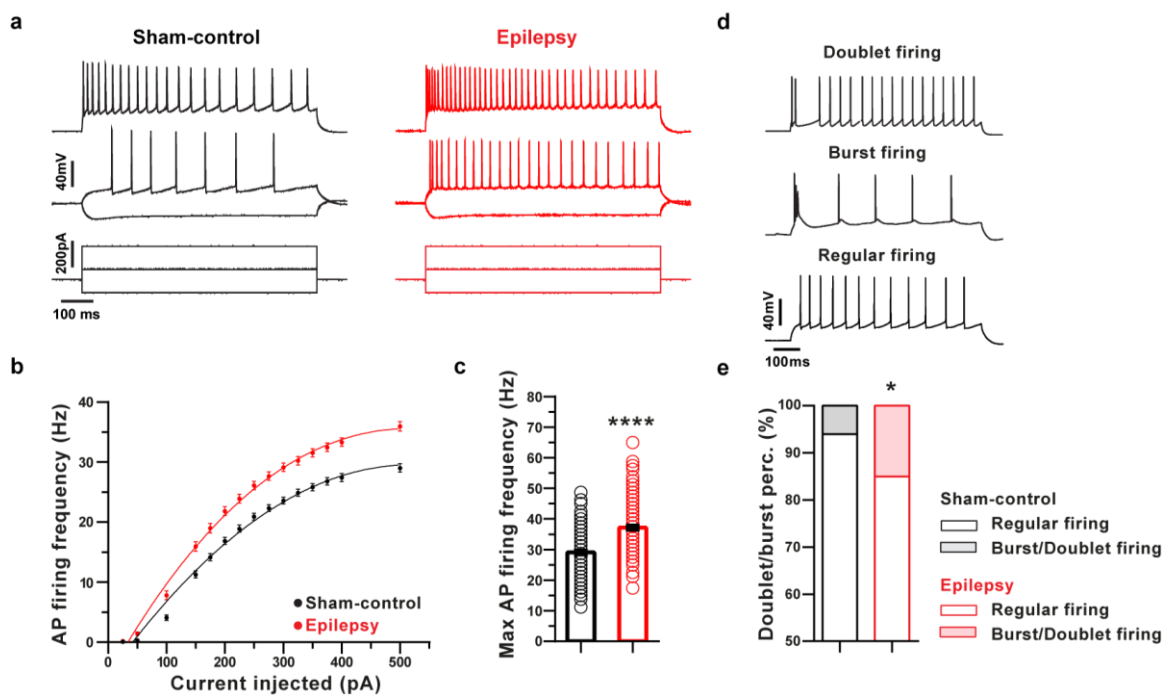
Fig. 3.1, Intrinsic firing properties of CA1 pyramidal neurons in sham-control and chronically epileptic mice. a, Representative examples of firing patterns to somatic current injection in a CA1 neuron from a sham-control and an epileptic mouse, respectively. **b,** Average firing frequencies for somatic current injections of different magnitude plotted for sham control and epileptic mice (n=132 and 137, respectively). **c,** Quantification of maximal firing frequency in sham-control and epileptic mice. Asterisks indicate (sham-control n=132, maximal action potential firing frequency 29.0±0.6 Hz vs. epileptic mice n=137, maximal action potential firing frequency 37.2±0.7, unpaired t-test p<0.0001). **d, e,** Incidence of doublet or burst firing. Panel d shows representative examples of doublet firing (uppermost trace, two action potentials separated from subsequent regular firing by a medium duration hyperpolarization), burst firing (middle trace, more than two action potentials riding on a pronounced slow depolarization), and regular firing (lowermost trace). Panel e shows the quantification of neurons classified according to their intrinsic discharge behavior. There was a significant increase of non-regular firing cells in epileptic mice (Fisher's exact test *p*=0.027, sham-control CA1 neurons n=132, 124/8/0 regular firing, doublet firing and burst firing neurons, epileptic CA1 neurons n=137, 117/14/6 regular firing, doublet firing and burst firing neurons, respectively). Error bars indicate mean ± SEM.

	Sham n= 132	Epilepsy n= 137
Passive properties		
Resting membrane potential (mV)	-77.3 ± 0.2	-74.6 ± 0.3[#]
Membrane resistance (MΩ)	144.4 ± 2.8	157.2 ± 3.9
Membrane time costant (ms)	28.1 ± 0.8	29.6 ± 0.1
Active properties		
Threshold (mV)	-56.5 ± 0.5	-58.6 ± 0.3[*]
Peak amplitude (mV)	85.2 ± 0.9	84.3 ± 0.8
Duration (ms)	1.2 ± 0.01	1.1 ± 0.01[#]
Peak dv/dt (V s)	226.7 ± 3.8	229.0 ± 3.8
Fast afterhyperpolarization (mV)	-49.3 ± 0.2	-50.9 ± 0.3[#]
Peak depolarization rate (V/s)	207.1 ± 5.0	221.4 ± 6.5
Frequency at 300 pA (Hz)	23.5 ± 0.5	29.3 ± 0.6[#]
Maximal frequency (Hz)	28.9 ± 0.6	37.1 ± 0.7[#]

unpaired student t-test * p<0.005   # p<0.0005   Liquid junction corretion -14mV

Table 1: Intrinsic active and passive membrane properties of CA1 pyramidal cells in sham-control and epileptic mice.

3.2. Altered dendritic integration via dendritic spikes in chronic epilepsy

To investigate changes in how CA1 excitatory neurons integrate inputs during chronic epilepsy and how the hippocampal output may be affected by an altered dendritic integration process, I combined patch-clamp experiments with 2-photon imaging and 2-photon glutamate uncaging in hippocampal slices from sham-control and epileptic mice (Losonczy & Magee, 2006; Remy et al., 2009).

Two-photon glutamate uncaging experiments allow us to deliver excitatory inputs onto multiple individual dendritic spines with high spatio-temporal precision while measuring the membrane potential changes in response to their activation. Patch-clamp recordings from CA1 pyramidal neurons were performed in whole-cell mode, and the cell morphology was visualized with a 2-photon microscope.

MNI-caged glutamate was then photoconverted, via 2-photon excitation, on its bioactive form, near the heads of 10–15 dendritic spines, evoking unitary excitatory postsynaptic potentials (uEPSPs) when the glutamate was released near a single spine or compound excitatory postsynaptic potentials (cEPSPs) when multiple spines were quasi-synchronously stimulated.

Responses of single spines to uncaging of glutamate were calibrated to ~1 mV in both sham-control and epileptic animals (1.09±0.42 mV, n=98 vs. 1.07±0.04 mV, n=85 dendrites, unpaired t-test, p=0.80, **Fig. 3.2a, c**). The rise and decay kinetics of uEPSPs from single spine activation were slightly but significantly faster in epileptic animals (**Fig. 3.2d, e**). This was also observed in miniature EPSC (mEPSC) recordings (**Fig. 3.2f-m**).

The distances of the uncaging sites from the somatic region were not different when comparing sham-control and epileptic mice (**Fig. 3.2b** 1st order dendrites sham-control 66.2±2.2 µm, n=101 vs. epileptic mice 64.9±2.3 µm, n=69; 2nd order dendrites sham-control 77.5±2.6 µm, n=54 vs. epileptic mice 80.6±2.8 µm, n=55; unpaired Student's t-test 1st order sham-control vs. epileptic mice p=0.68; 2nd order sham-control vs. epileptic mice p=0.43). Moreover, a morphological analysis did not show differences when I compared the density of dendritic spines along CA1 apical oblique dendrites from sham-control and epileptic mice (**Fig. 3.2l-n).**
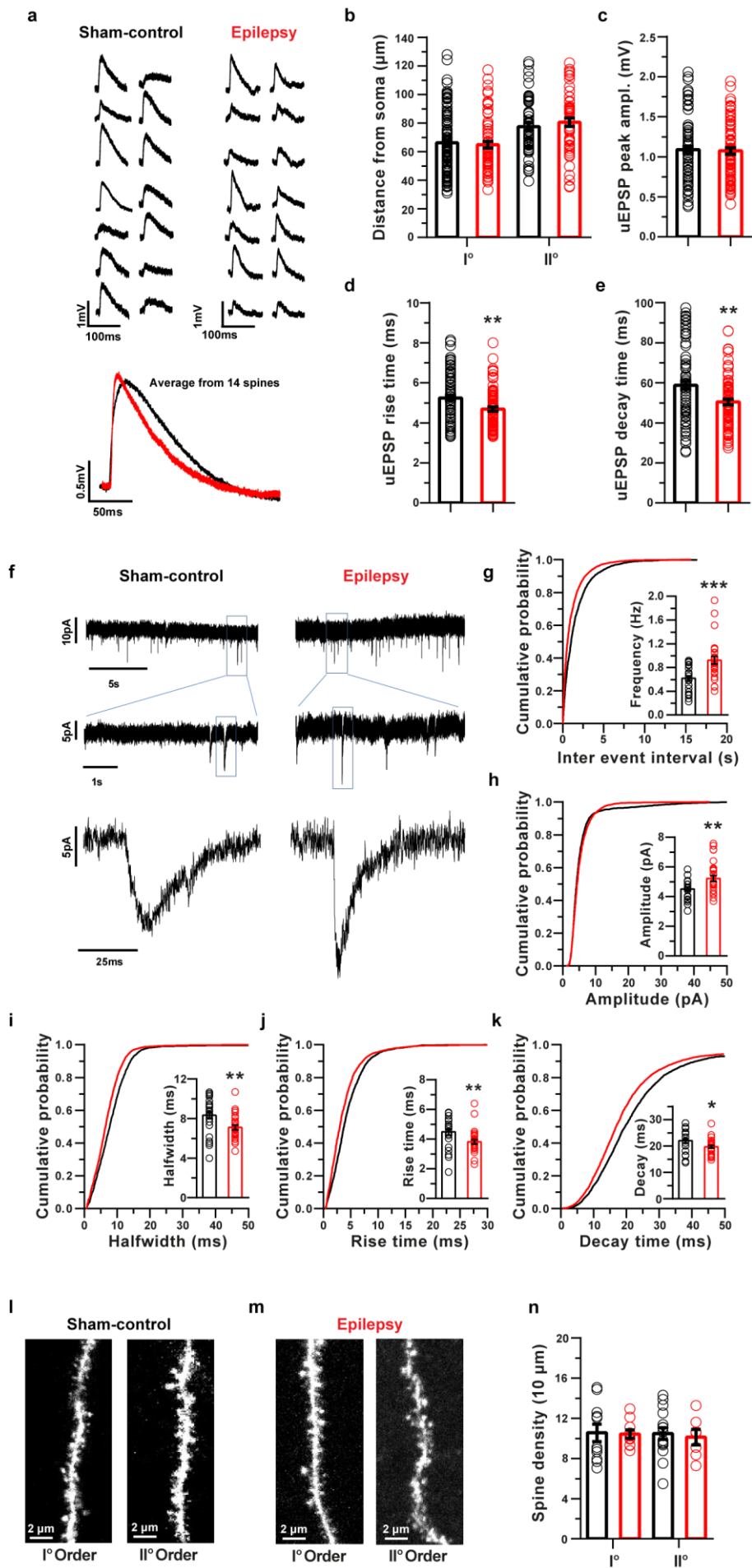
Fig. 3.2, Properties of single-spine uEPSPs and miniature EPSCs in CA1 pyramidal neurons from sham-control and epileptic mice. a-e, Properties of uncaging-evoked single spine EPSPs. **a,** Representative examples in sham-control and epileptic mice. Inset: Enlarged average single spine EPSPs showing fast kinetics of rise and decay in epileptic mice. **b,** Quantification of the distance of the uncaging site from the soma, not significant difference between groups (sham-control n=120 vs. epileptic mice n=99, unpaired t-test $p=0.90$). **c,** uEPSPs peak amplitude, not significant differences between groups, unpaired t-test $p=0.79$, **d,** 10-90% rise times. Rise times were significantly faster in epileptic animals, unpaired t-test $p=0.0021$. **e,** Decay time constants of uEPSPs were significantly smaller in epileptic animals. Unpaired t-test $p=0.0046$. **f-m,** Properties of miniature EPSCs recorded in the presence of tetrodotoxin and bicuculline (see Methods). **f,** Representative examples in sham-control and epileptic mice. Inset: Enlarged individual mEPSCs showing fast kinetics of rise and decay in epileptic mice. **g,** Inter-event intervals of mEPSCs show a significantly increased mEPSC rate in epileptic animals (unpaired t-test $p=0.0003$). **h,** mEPSC amplitudes were slightly increased (sham-control n=25 vs. epileptic n=28, unpaired t-test $p=0.0072$). **i-k,** mEPSC kinetics were faster in epileptic mice, as documented by decreased half-width (unpaired t-test $p=0.0053$), shortened rise times (unpaired t-test $p=0.0089$), and shortened decay time constants (unpaired t-test $p=0.021$). **l-n,** spine density quantification in 1st and 2nd order dendrites did not show differences between sham-controls and epilepsy animals (1st order dendrites n=11 and 10, 2nd order dendrites n=16 and 7 for sham-control and epileptic mice respectively, two-way ANOVA main effect, sham-control vs. epilepsy: $F_{(1\ 40)}=0.11$, $p=0.73$; 1st order vs. 2nd order: $F_{(1\ 40)}=0.079$, $p=0.77$; interaction: $F_{(1\ 40)}=0.026$, $p=0.87$; Bonferroni´s post-test, spine density pro 10µm in 1st order dendrites in sham-control vs. epilepsy p >0.99; spine density pro 10 µm in 2nd order dendrites in sham-control vs. epilepsy p >0.99).

I then went on to probe the capability of CA1 dendrites to generate dendritic spikes by activating multiple spines quasi-synchronously (interspine stimulation interval, 0.1ms). CA1 dendrites either displayed linear integration only or were capable of generating sudden supralinear dendritic spikes when increasing numbers of spines were synchronously stimulated (Losonczy & Magee, 2006; Remy et al., 2009) (representative examples in **Fig. 3.3a-c**). In linearly integrating dendritic branches, the linear summation of single spine uEPSPs was augmented in epileptic animals in 1st order branches emanating from the main dendritic trunk (n=35 and 26 in sham-control vs. epileptic mice). Linearly integrating 2nd order dendrites did not show differences in EPSP summation (**Fig. 3.3d, f**, n=23 and 15 in control vs. epileptic mice, two-way ANOVA main effect, sham-control vs. epilepsy: $F_{(1\ 95)}=7.38$,

p=0.0078; 1st order vs. 2nd order: $F_{(1\ 95)}$=4.33, p=0.040; interaction: $F_{(1\ 95)}$=0.32, p=0.57; Bonferroni´s post-test, 1st order dendrites sham-control vs. epilepsy p=0.018; 2nd order dendrite sham-control vs. epilepsy p=0.35).
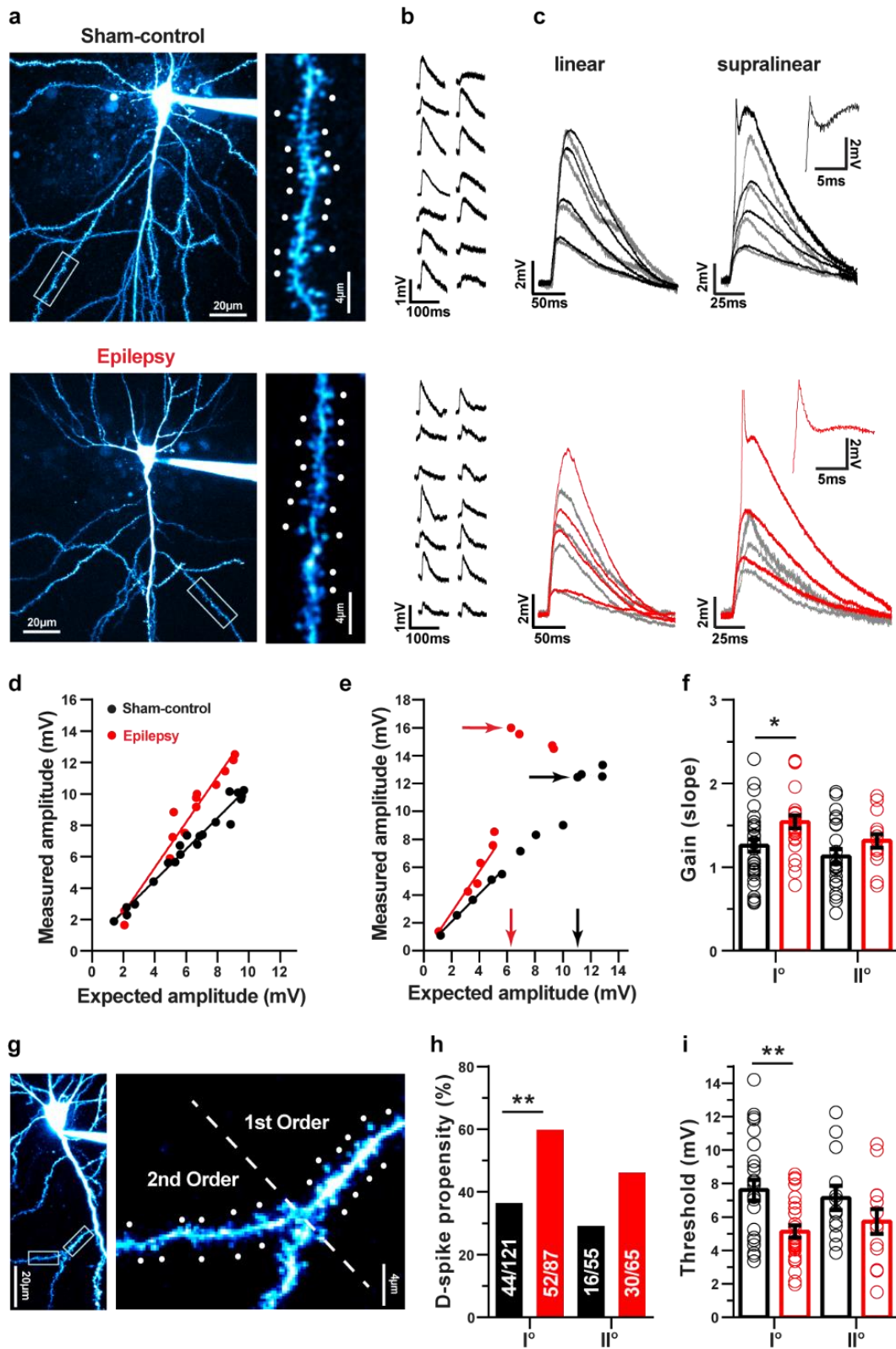
Fig. 3.3, Probing dendritic integration in chronic epilepsy. a, CA1 pyramidal neurons filled with a fluorescent dye via the somatic patch recording, close up of a dendritic segment with uncaging targeting points at spines. **b,** Responses to single-spine stimulation with 2P-uncaging of MNI-glutamate measured with somatic patch recording. **c,** Representative recordings of compound linear and supralinear EPSPs. Grey lines are expected EPSPs from linear summation of single spine responses. Examples of a branch with linear integration (left panels) and a branch capable of supralinear integration (right panels) are shown for sham-control (black) and epileptic mice (red). **d,** Examples of linearly integrating dendrites in sham-control (black) and epileptic animals (red). **e,** Examples of dendrites capable of generating supralinear dendritic spikes in sham-control (black) and epileptic animals (red). Occurrence of dendritic spikes and their voltage threshold are indicated with arrows. **f,** Quantification of the slope of the linear phase in linearly integrating 1st and 2nd order dendrites in sham-control (black) and epileptic mice (red). Asterisks indicate Bonferroni´s post-tests $p=0.0176$. **g,** Representative dendrite with 1st and 2nd order branches. **h,** The propensity for dendritic spikes is enhanced in 1st order dendrites in epileptic animals (red) compared to sham-controls (black). Asterisks indicate Fisher's exact test $p=0.0011$. **i,** The threshold for generation of dendritic spikes, measured as indicated with arrows in panel **e,** is reduced in 1st order dendrites of epileptic animals, but not in 2nd order dendrites. Asterisks indicate Bonferroni´s post-test, $p=0.0017$.

The difference in linear summation was normalized by application of the Na⁺ channel blocker tetrodotoxin, indicating that it is caused by increases in voltage-gated Na^+ currents (**Fig. 3.4**, sham-control and epileptic n=7 and 6, respectively, 2-way repeated measures ANOVA main effect, sham-control vs. epilepsy: $F_{(1\ 11)}=0.88$, $p=0.37$; ACSF vs. TTX: $F_{(1\ 11)}=26.96$, $p=0.0003$; interaction: $F_{(1\ 11)}=10.15$, $p=0.0087$; Bonferroni´s post-test, ACSF vs. TTX in epilepsy $p=0.0003$).
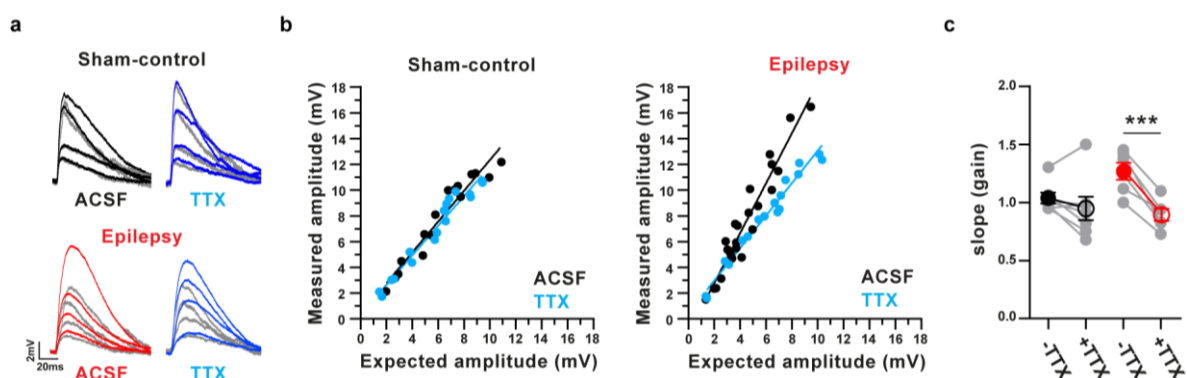

Fig. 3.4, Effects of TTX on EPSP summation in linearly integrating 1st order CA1 pyramidal neuron dendrites. a, Examples of compound uEPSPs in sham-control and epileptic CA1 pyramidal cells. Grey lines indicate traces derived from the arithmetic summation of single-spine EPSPs and

represent compound EPSPs that would be obtained with a purely linear summation. In epileptic mice, measured compound EPSPs were larger than expected from linear summation. **b,** Plotting measured EPSPs vs. EPSP sizes expected from arithmetic summation in ACSF and following application of 500 nM tetrodotoxin (TTX). The slope of the fitted line describing summation is reduced in epileptic but not in control animals. **c,** Quantification of linear summation, and the TTX effects (sham-control and epileptic n=7 and 6, respectively, 2-way repeated measures ANOVA main effect, sham-control vs. epilepsy: $F_{(1\ 11)}=0.88$, $p=0.37$; ACSF vs. TTX: $F_{(1\ 11)}=26.96$, $p=0.0003$; interaction: $F_{(1\ 11)}=10.15$, $p=0.0087$; Asterisks indicate Bonferroni´s post-test, ACSF vs. TTX in epilepsy $p=0.0003$). No effect of TTX on uEPSP peak amplitude, uEPSP rise time, and uEPSP decay time constant was detected (two-way repeated-measures ANOVA n.s. for all parameters).

Strikingly, the fraction of dendrites capable of generating dendritic spikes was significantly increased in 1st order dendrites from epileptic neurons, but not in 2nd order dendrites (**Fig. 3.3e, g, h**, 1st order dendrites 36% vs. 60%, Fisher's exact test $p=0.0011$, 2nd order dendrites 29% vs. 46%, Fisher's exact test $p=0.062$).

I next compared the properties of dendritic spikes in those branches capable of generating them. The threshold for the generation of dendritic spikes was calculated by determining the expected somatic voltage at which a dendritic supralinearity first occurred (indicated by arrows at the x-axis, **Fig. 3.3e**). In epileptic animals, the voltage threshold to generate dendritic spikes was significantly reduced in 1st order but not 2nd order dendrites (**Fig. 3.3i**, 1st order dendrites n=25 and 27, 2nd order dendrites n=13 and 13 for sham-control and epileptic mice respectively, two-way ANOVA main effect, sham-control vs. epilepsy: $F_{(1\ 74)}=9.92$, $p=0.0024$; 1st order vs. 2nd order: $F_{(1\ 74)}=0.012$, $p=0.91$; interaction: $F_{(1\ 74)}=0.77$, $p=0.38$; Bonferroni´s post-test, threshold in 1st order dendrites in sham-control vs. epilepsy $p=0.0017$), meaning a required lower number of activated spines to elicit dendritic spikes in epilepsy. The reduction was remarkably pronounced in some 1st order dendrites from epileptic animals, with dendritic spikes sometimes being generated with as few as 1-3 spines and somatic voltages of as little as ~3 mV (see **Fig. 3.5** for dendritic spike elicited with a single spine stimulation).
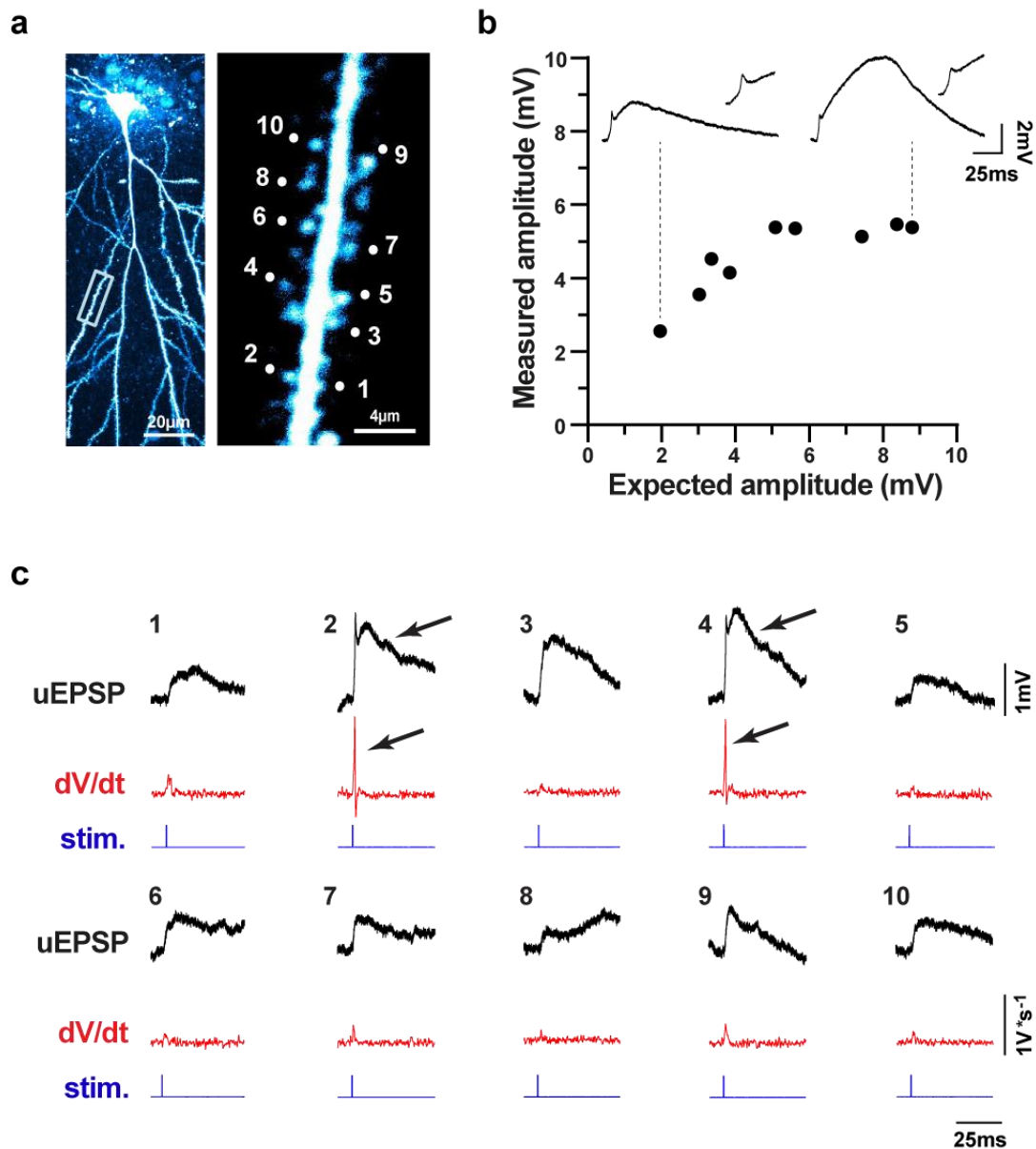
Fig. 3.5, Dendritic spike elicited with stimulation of only a single spine. a, Micrograph showing the 1st order dendrite, with an enlarged view showing the uncaging points. **b,** Uncaging resulted in a dendritic spike already with single-spine stimulation, with more spines being stimulated synchronously, resulting in a larger slow dendritic spike component (see insets for voltage traces of entire dendritic spike and enlarged fast phases of the dendritic spikes). **c,** Responses to individual single spines (corresponding to the spines shown in panel a). Dendritic spikes are elicited to spines 2 and 4 (indicated by arrows, note the large rate of rise indicated in the dV/dt traces in red).

A further characteristic of dendritic spikes is the rate of rise of the initial fast phase that reflects the contribution of voltage-gated sodium channels. The maximal rate of rise was determined from the first derivation of the voltage trace (indicated in **Fig. 3.6a**). In 1st order dendrites, but not 2nd order dendrites, I observed a significant increase in the maximal rate of rise (**Fig. 3.6b**,

1st order dendrites n=44 and 52, 2nd order dendrites n=16 and 30 in sham-control and KA, respectively, two-way ANOVA main effect, sham-control vs. epilepsy: $F_{(1\ 139)}$=1.86, p=0.18; 1st order vs. 2nd order: $F_{(1\ 139)}$=1.96, p=0.16; interaction: $F_{(1\ 139)}$=5.08, p=0.025; Bonferroni´s post-test, rate of rise in 1st order dendrites in sham-control vs. epilepsy p=0.0025; 1st vs. 2nd order dendrites rate of rise in epilepsy p=0.0074).

Previous studies on supralinear integration have demonstrated that maximum dendritic spike dV/dt follow a bimodal distribution, resulting in weak and strong dendritic spikes (Losonczy et al., 2008; Remy et al., 2009). The fraction of dendrites capable of generating strong dendritic spikes was significantly increased in 1st order dendrites from epileptic neurons, but not in 2nd order dendrites (**Fig. 3.6c**)

In contrast to the fast phase of the dendritic spikes, the subsequent slower depolarization was not different in sham-control vs. epileptic animals (**Fig. 3.6d**, 1st order dendrites n=42 and 47, 2nd order dendrites n=16 and 29, in sham-control and epilepsy, respectively, area under the curve of slow depolarization two-way ANOVA main effect, sham-control vs. epilepsy: $F_{(1\ 130)}$=3.51, p=0.063; 1st order vs. 2nd order: $F_{(1\ 130)}$=1.83, p=0.18; interaction: $F_{(1\ 130)}$=0.17). These results collectively show a dramatically augmented excitability of proximal, 1st order dendrites in epileptic animals, reflected in the prevalence and properties of dendritic spikes.
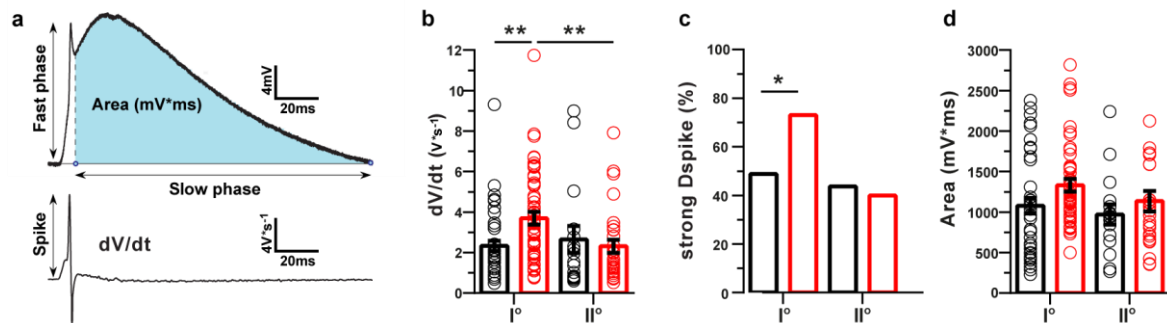
Fig 3.6, Dendritic spikes properties a, The maximal rate of rise of the fast phase was determined from the first derivation of the voltage trace, the slow phase is indicated in blue **b,** The fast phase of dendritic spikes is accelerated in 1st order dendrites from epileptic mice (panel k, asterisks indicate Bonferroni´s post-test, rate of rise in 1st order dendrites in sham-control vs. epilepsy p=0.0025; 1st vs. 2nd order dendrites rate of rise in epilepsy p=0.0074). **c,** the propensity for strong dendritic spikes (dV/dt >2V*s^{-1}) is enhanced in 1st order dendrites in epileptic animals (red) compared to sham-controls (black). Asterisks indicate Fisher's exact test p=0.02. **d,** the area of the slow phase was unchanged between sham-controls and epilepsy.

3.3. Reduced synchrony detection by dendritic spikes in chronic epilepsy

Synchronous stimulation is required for the generation of dendritic spikes in normal pyramidal neurons. This synchrony-dependence is thought to underlie the ability of dendritic spikes to detect the coincident activity of specific presynaptic ensembles converging onto a single dendritic branch (Losonczy et al., 2008). I, therefore, tested how dendritic spike generation depends on input synchrony by systematically changing the inter-spine stimulation interval time in control and epileptic animals (representative examples in **Fig. 3.7a**, sham-control in black, epilepsy in red).

Neighboring dendritic spines were stimulated quasi-synchronously with an interval time of 0.1ms to evoke dendritic spikes. Subsequently, the time between the individual spine stimulations was gradually increased in steps ranging from 0.1ms to 5ms.

Epileptic animals exhibited a remarkable loss of their capability to respond to synchronous inputs via selective generation of dendritic spikes. While sham-control animals exhibited a steep decrease in dendritic spike generation when stimulation was less synchronous, epileptic animals continued to generate dendritic spikes even with very asynchronous stimulations (**Fig. 3.7b,** n=12 and 11 in sham-control vs. epileptic mice, Fisher's exact test, p<0.001 indicated with asterisks, see figure legend).

Correspondingly, the maximal rate of rise of the fast phase of dendritic spikes (dV/dt) also showed a much less pronounced reduction with less synchronous stimulation (**Fig. 3.7c,** two-way repeated-measures ANOVA main effects, sham-control vs. epilepsy: $F_{(1\ 21)}=32.34$, p<0.0001; inter-spine time: $F_{(4\ 84)}=22.59$, p<0.0001; interaction: $F_{(4\ 84)}=9.87$, p<0.0001; Bonferroni´s post-tests indicated with asterisks, p<0.003, individual p-values see legend). Intriguingly, in some cases, dendritic branches from epileptic animals were capable of generating multiple sequential spikes (n=2 of 11 branches, example in **Fig. 3.7a,** blue arrow). Together with the lower threshold required to evoke dendritic spike, these data suggest that in epilepsy, supralinear responses can be generated by activation of few spines, with degraded requirements for input synchrony compared with sham-control animals.
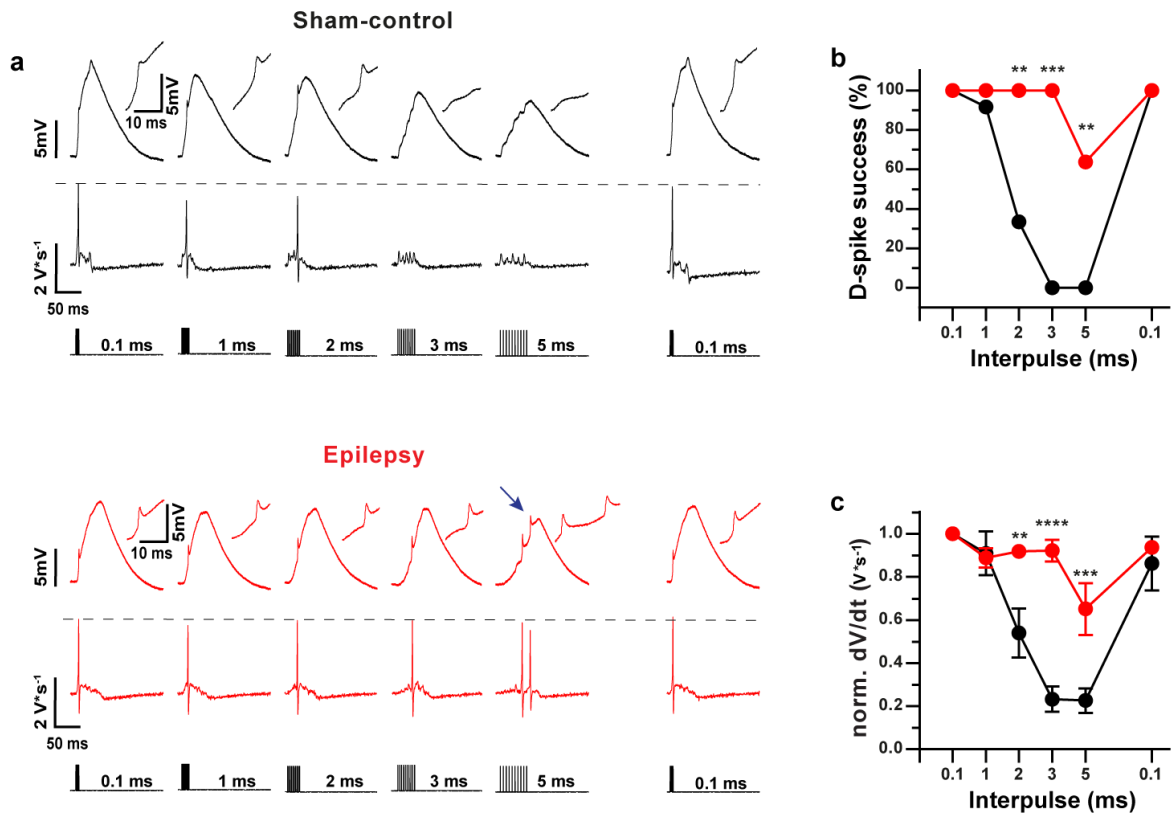
Fig. 3.7, Degraded synchrony detection in epileptic mice. a, Representative example traces showing input synchrony dependence of dendritic spikes in CA1 neurons from sham-control and epileptic mice. Changing the inter-spine stimulation interval (lowermost row) systematically affects dendritic spike generation in control and epileptic animals. Upper rows show somatic voltage response, middle rows show the first derivation of the voltage trace (dV/dt). Note that the rightmost response is again with 0.1 ms inter-spine stimulation intervals, applied following the longer intervals. **b, c,** Rate of spike occurrence in % of uncaging stimulations (D-spike success) and dendritic-spike strength expressed as the maximal rate of rise (dV/dt) of the fast phase of the dendritic spike. Asterisks in b correspond to significance in Fisher's exact test, with the following p-values: 2 ms $p=0.0013$; 3 ms $p<0.0001$; 5 ms $p=0.0013$. Asterisks in c correspond to significances in Bonferroni´s post-tests for inter-spine stimulation intervals 2 ms $p=0.0013$; 3 ms $p<0.0001$; 5 ms $p=0.0003$.

3.4. Reduced dendritic spike inactivation in chronic epilepsy

Supralinear integration powerfully detects and amplifies synchronous synaptic inputs and thus requires a specific mechanism to shape and constrain its activity. Indeed, sparse dendritic spiking is thought to be regulated through the inactivation of dendritic spikes. Previous studies have demonstrated how the generation of dendritic spikes leads to a subsequent inactivation of supralinear integration (Remy et al., 2009), caused by the strong progressive reduction of the fast component, which reflects the inactivation of dendritic Na^+ channels. This is particularly relevant since in vivo studies from CA1 pyramidal neurons have shown that these neurons receive synchronized inputs at theta frequencies ranging from 5 to 10 Hz during behavior (Buzsaki, 2002).

Following my first findings highlighting an aberrant dendritic overexcitability in epilepsy, I investigated if the inactivation mechanism that usually constrains supralinear integration in healthy CA1 hippocampal neurons may be affected during chronic epilepsy. I performed 2-photon glutamate uncaging on apical oblique dendrites, evoking subsequent dendritic spikes in a train of 5 stimulation at 10Hz frequency using for each stimulation the same number of spines (quasi-synchronous compound stimulation of 10 spines with interval time 100ms).

In control animals, dendritic spike inactivation was observed similar to published data, indicated by a progressive reduction of dendritic spike dV/dt until dendritic spike failure (black traces in **Fig. 3.8a,** quantification in **Fig. 3.8b,c**). In epileptic animals, this reduction in dendritic spike dV/dt, as well as inactivation of spike generation, was significantly less pronounced (**Fig. 3.8a-c,** statistical results see figure legend).

Thus, collectively, the results show that dendritic spike generation is strongly enhanced and that multiple mechanisms that underlie the sparse generation of dendritic spikes in normal animals are severely degraded in epilepsy.
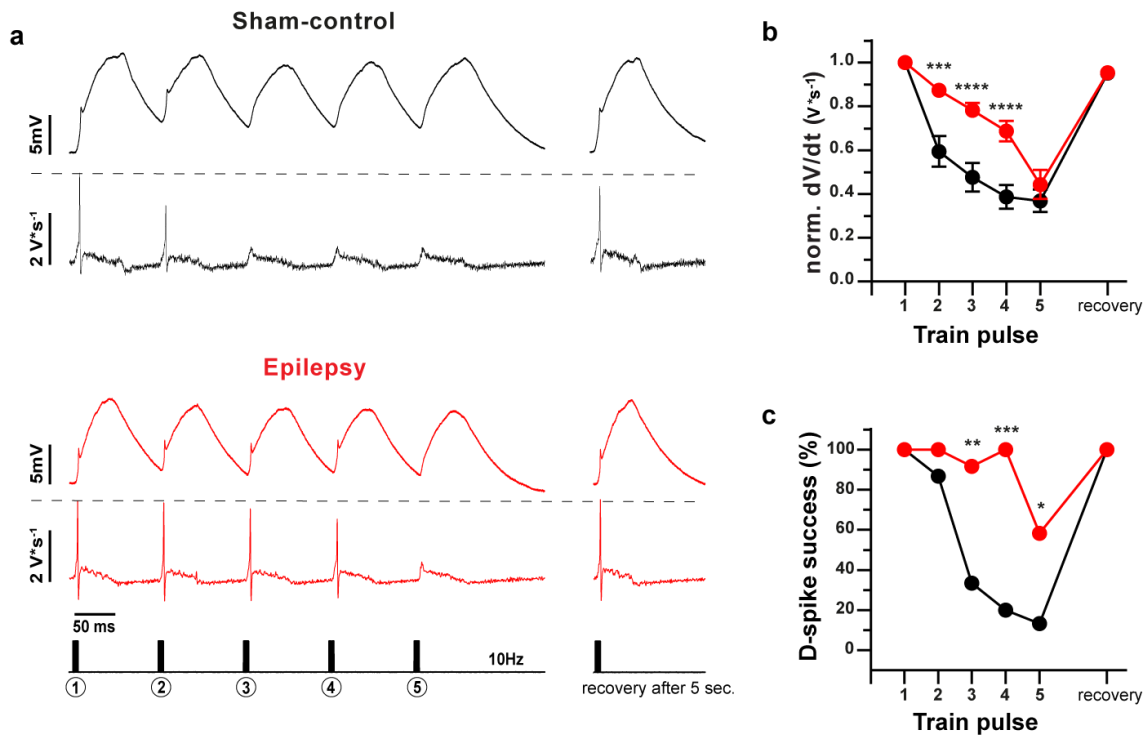
Fig. 3.8, Degraded dendritic spike inactivation in chronic epilepsy. a, Representative somatic voltage recordings from a sham-control (black) and epileptic (red) mouse (upper trace) with the corresponding first derivation of the voltage trace (dV/dt). Dendritic spikes were repetitively elicited with synchronous stimulation at 10 Hz (lowermost trace). **b,** Spike strength (dV/dt) decreases steeply with repetitive stimulation in control (black) but not in epileptic animals (red). Sham-control n=15, epileptic mice n=12. Two-way repeated-measures ANOVA revealed main effects, sham-control vs. epilepsy: $F_{(1\ 25)}$=12.51, p<0.0016; repetitive stimulation: $F_{(4\ 100)}$=80.57, p<0.0001; interaction: $F_{(4\ 84)}$=8.30, p<0.0001); asterisks indicate Bonferroni´s post-test, dV/dt for 2nd stimulation p=0.0006, 3rd stimulation p=0.0001, 4th stimulation p=0.0002. **c,** The fraction of stimuli successfully generating dendritic spikes also strongly decreased with repetitive stimulation. N-numbers as above, asterisks indicate Fisher's exact test, 3rd stimulation p=0.001, 4th stimulation p=0.0001, 5th stimulation p=0.037).

3.5. Involvement of Na⁺ channels in augmented dendritic integration

The increased incidence of dendritic spikes, as well as the increased rate of rise of the fast phase of the dendritic spikes, suggests up-regulation of Na^+ channels as a potential mechanism.

To investigate whether Na^+ channel upregulation leads to the aberrant dendritic integration in epilepsy, I pharmacologically target specific Na^+ channel isoforms and examined their role. I first used the Na^+ channel blocker and anticonvulsant Eslicarbazepine (S-Lic) (300

µM), which is known to affect $Na_v1.2$ and 1.6 channels but not $Na_v1.3$ or 1.1 channels (Holtkamp et al., 2018).

Individual unitary EPSPs elicited by 2-photon glutamate uncaging onto the single spines did not change with the addiction of S-Lic, and their kinetics properties were also unchanged (**Fig. 3.9**).
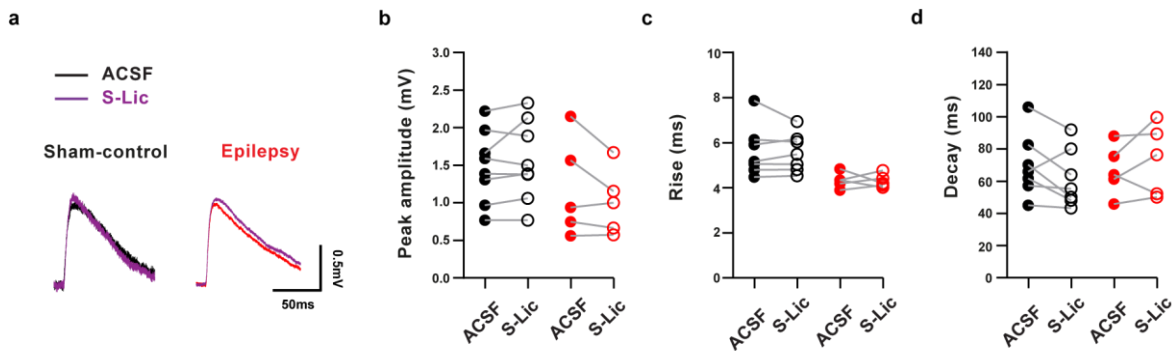
Fig. 3.9, Effects of S-Lic on the properties of uEPSPs. a, Representative examples of single spine uEPSPs in sham-control (black) and epileptic mice (red). uEPSPs following application of S-Lic (300 µM, violet) are superimposed on the corresponding uEPSPs in control ACSF, respectively. **b-d,** Effect of S-Lic on peak amplitude, 20-80% rise times and decay time constants of uEPSPs in control (black symbols) and epileptic mice (red symbols, S-Lic: n=7 and 5 for sham-control and epileptic mice). Peak amplitude and decay time constant of the uEPSP showed no significant effects of epilepsy vs. sham-control, or effects of Na^+ channel blocker (Two-way repeat measures ANOVA n.s. for all parameters). The uEPSP rise time were significantly faster in epileptic mice (two-way repeated-measures ANOVA, main effect, sham-control vs. epilepsy: $F_{(1\ 10)}=7.95$, $p=0.018$; ACSF vs. S-Lic: $F_{(1\ 10)}=0.083$, $p=0.78$; interaction: $F_{(1\ 10)}=0.29$, $p=0.87$).

Then I tested the effect of S-Lic on supralinear integration, stimulating multiple spines at apical oblique dendrites via 2-photon glutamate uncaging.

Application of S-Lic also did not alter the threshold for eliciting dendritic spikes in either control or epileptic animals (**Fig. 3.10c,g**, spike thresholds indicated with dashed lines, quantification in **Fig. 9d,h**, n=8 and 5 in sham-control vs. epilepsy; two-way repeated measures ANOVA main effect, sham-control vs. epilepsy: $F_{(1\ 11)}=5.82$, $p=0.044$; ACSF vs. S-Lic: $F_{(1\ 11)}=0.86$, $p=0.37$; interaction: $F_{(1\ 11)}=0.47$, $p=0.51$, Bonferroni's post-test n.s.). Likewise, S-Lic did not affect the rate of rise of dendritic spikes in epileptic animals (**Fig. 9a-f,** two-way repeated measures ANOVA main effect, sham-control vs. epilepsy: $F_{(1}$

$_{11)}$=27.76, p=0.0003; ACSF vs. S-Lic: $F_{(1\ 11)}$=1.30, p=0.28; interaction: $F_{(1\ 11)}$= 2.51, p=0.14, Bonferroni's post-test n.s.).
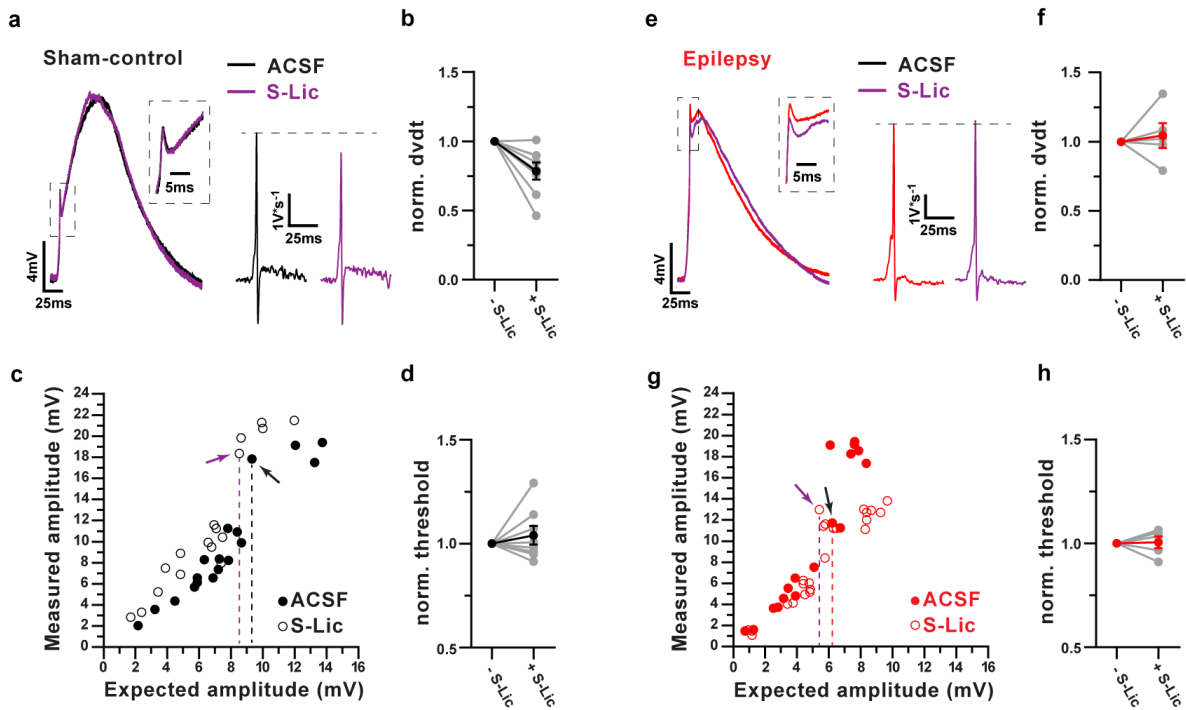
Fig. 3.10, The Na$_v$1.2/1.6 Na$^+$ channel blocker S-Lic does not affect the enhanced dendritic excitability in epilepsy. a, Representative effects of the Na$^+$ channel blocker S-Lic at concentrations of 300 µM on dendritic spikes (insets show magnification of the fast phase of the dendritic spike), and on the first derivation of the voltage trace (dV/dt) in sham-control (**a-b**) and epileptic mice (**e-f**). **c, g,** Effects on the dendritic spike threshold in sham-control and epileptic mice (arrows indicate the occurrence of dendritic spikes and dashed lines indicate thresholds). Two-way ANOVA revealed no significant effects of S-Lic on the rate of rise or threshold of dendritic spikes in control (b-d) and epileptic animals (**f-h**).

Those results suggest that Na$_v$1.2 or 1.6 isoforms are not involved in aberrantly enhanced dendritic integration in epilepsy. Nevertheless, as expected from previous studies, the block of Na$_v$1.2/1.6 with S-Lic significantly inhibited somatic action potential generation in epilepsy (**Fig. 3.11**).
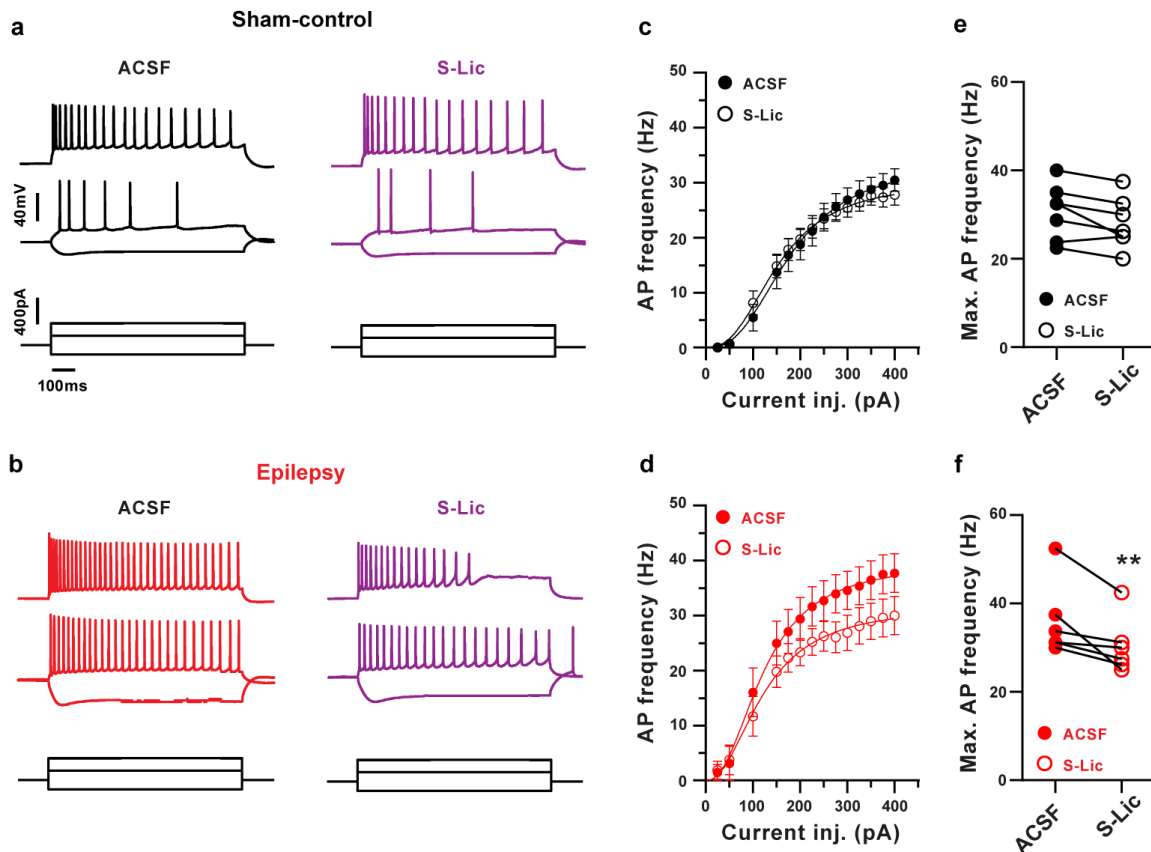
Fig. 3.11, Effects of S-Lic on intrinsic firing properties of CA1 pyramidal neurons in sham-control and epileptic mice. a-d, Representative examples of S-Lic effects in sham-control animals (panels a and c) and epileptic animals (panels b and d). **c,d,** Action potential frequencies induced by somatic current injection of different magnitudes in sham-control and epileptic mice (sham-control, black symbols and epileptic mice, red symbols). **e,f,** Effects of S-Lic at current injections at which firing rates in ACSF were maximal. Differences in maximal action potential frequency tested with two-way repeated-measures ANOVA, S-Lic two-way repeated-measures ANOVA main effect, sham-control vs. epilepsy: $F_{(1\ 12)}=1.48$, $p=0.25$; ACSF vs. S-Lic: $F_{(1\ 12)}=19.98$, $p=0.0008$; interaction: $F_{(1\ 12)}=2.57$, $p=0.14$; Bonferroni´s post-test, max action potential frequency (Hz) in sham-control ACSF vs. S-Lic $p=0.098$; max action potential frequency (Hz) in epilepsy ACSF vs. S-Lic $p=0.0034$. ICA-121431 main effect, sham-control vs. epilepsy: $F_{(1\ 10)}=11.66$, $p=0.0066$; ACSF vs. ICA-121431: $F_{(1\ 10)}=1.67$, $p=0.23$; interaction: $F_{(1\ 10)}=2.28$, $p=0.16$.

I then focused my attention on a different Na^+ channel isoform. $Na_v1.3$ channels are generally down-regulated in early ontogenesis but have exhibited increased expression in epilepsy (Lin et al., 2017). I used the selective $Na_v1.3$ blocker ICA-121431 (McCormack et al., 2013) (100 nM) to investigate the role of this channel subunit in dendritic spikes. ICA-121431, as well as S-Lic, did not alter the properties of uncaging-evoked single-spine EPSPs (**Fig. 3.12**).
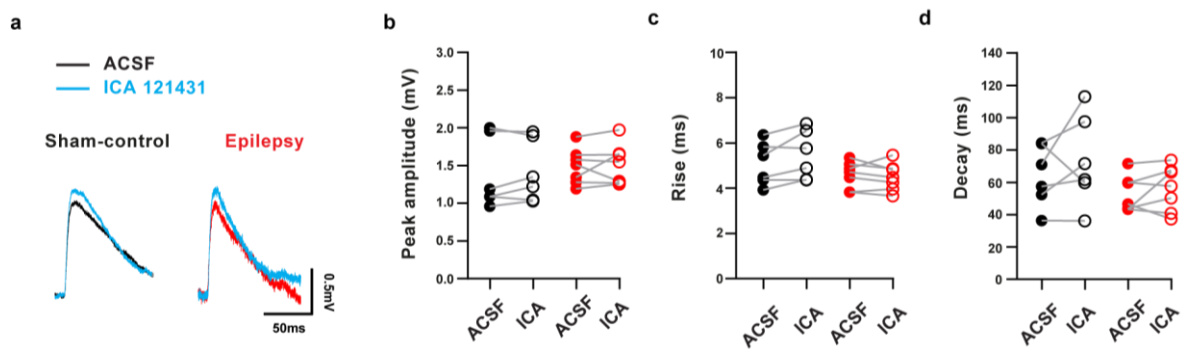
Fig. 3.12, Effects of ICA-121431 on the properties of uEPSPs. a, Representative examples of single spine uEPSPs in sham-control (black) and epileptic mice (red). uEPSPs following application of ICA-121431 (100 nM, blue) are superimposed on the corresponding uEPSPs in control ACSF, respectively. **b-d,** Effect of ICA-121431 on peak amplitude, 20-80% rise times, and decay time constants of uEPSPs in control (black symbols) and epileptic mice (ICA-121431: n=6 and 8 for sham-control and epileptic mice). Peak amplitude and decay time constant of the uEPSP showed no significant effects of epilepsy vs. sham-control, or effects of Na^+ channel blocker (Two-way repeat measures ANOVA n.s. for all parameters).

However, in epileptic, but not in sham-control animals, ICA-121431 (100 nM) significantly increased the dendritic spike threshold (**Fig. 3.13c, g,** spike thresholds indicated with dashed lines, **Fig. 3.13d, h** for summary, n=5 and 7 in sham-control vs. epilepsy, two-way repeated-measures ANOVA main effect, sham-control vs. epilepsy: $F_{(1\ 10)}=0.008$, $p=0.93$; ACSF vs. ICA-121431: $F_{(1\ 10)}=6.24$, $p=0.032$; interaction: $F_{(1\ 10)}=7.10$, $p=0.024$; Bonferroni´s post-test epilepsy ACSF vs. ICA-121431 $p=0.0050$). Likewise, ICA-121431 decreased the rate of rise of dendritic spikes only in epileptic animals (see insets for dV/dt traces in **Fig. 3.13a, e**, summary in **Fig. 3.13b, f,** two-way repeated-measures ANOVA main effect, sham-control vs. epilepsy: $F_{(1\ 10)}=0.050$, $p=0.82$; ACSF vs. ICA-121431: $F_{(1\ 10)}=5.36$, $p=0.043$; interaction: $F_{(1\ 10)}=2.50$, $p=0.14$; Bonferroni´s post-test epilepsy ACSF vs. ICA-121431 $p=0.025$). The slow phase of the dendritic spike was unaffected by ICA-121431 (two-way repeated measures ANOVA, n.s.).
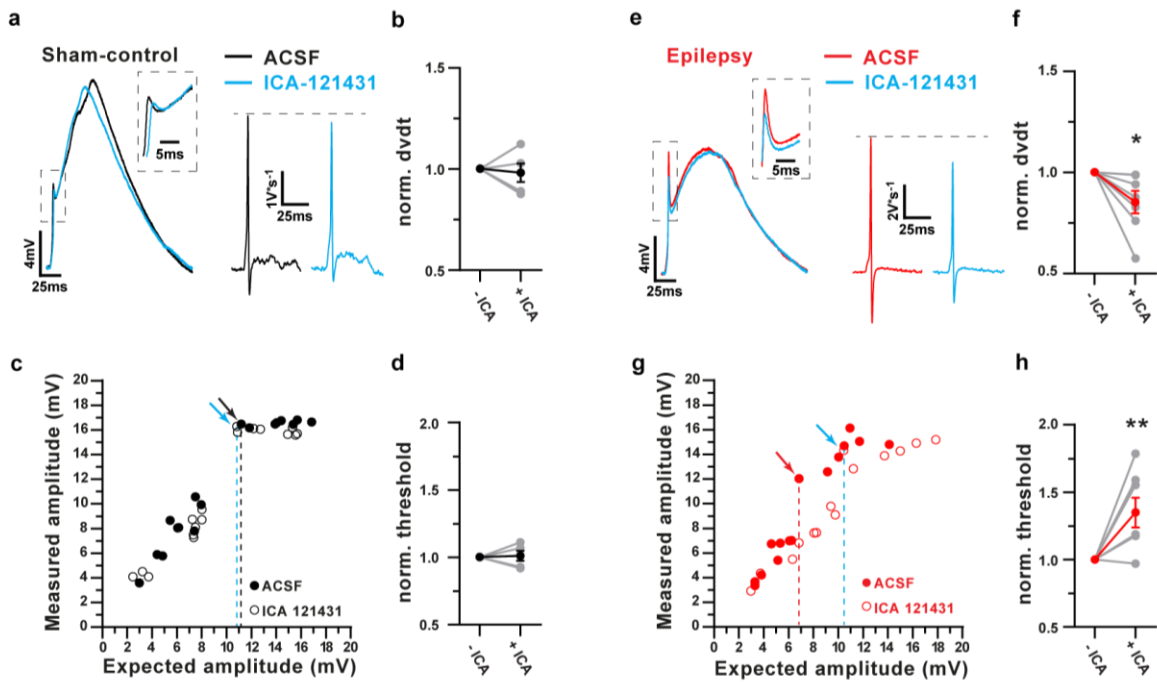
Fig. 3.13, The Na$_v$1.3 specific blocker ICA-121431 reverses enhanced dendritic excitability. a, e,** Representative examples of the effects of the Na$_v$1.3 specific blocker ICA-121431 (100 nM) on dendritic spikes (insets show magnification of the fast phase of the dendritic spike), and on the first derivation of the voltage trace (dV/dt) in sham-control and epileptic animals. **b, f, Effects of ICA-121431 at concentrations of 100 nM on the maximal rate of rise of the dendritic spike in sham-control (b) and epileptic mice (f). Asterisk indicates Bonferroni´s post-test, *p*=0.023. **c, g,** Representative examples of effects on the dendritic spike threshold in sham-control and epileptic mice (arrows indicate the occurrence of dendritic spikes and dashed lines indicate thresholds). **d, h,** Quantification of the effects of ICA-121431 on the dendritic spike threshold in sham-control (d) and epileptic mice (h). Asterisk indicates Bonferroni's post-test *p*=0.0050.

I then tested if, in addition to the significant effects on dendritic integration in epileptic animals, blocking Na$_v$1.3 channels also affects the somatic firing. Surprisingly, ICA-121431 had no effects on action potential generation induced by somatic current injection in either control or epileptic animals (**Fig. 3.14**, n=6 in both groups, two-way repeated-measures ANOVA main effect, sham-control vs. epilepsy: $F_{(1\ 10)}$=11.66, *p*=0.0066; ACSF vs. ICA-121431: $F_{(1\ 10)}$=1.67, *p*=0.23; interaction: $F_{(1\ 10)}$=2.28, *p*=0.16, Bonferroni's post-tests n.s.). These results suggest that the Na$_v$1.3 blocker ICA-121431 selectively affects dendritic spikes and not the somatic firing, while S-Lic does the converse, highlighting a specific novel

mechanism in chronic epilepsy, constrained at the dendritic level, in which $Na_v1.3$ channels play a fundamental role leading to an aberrant integration.
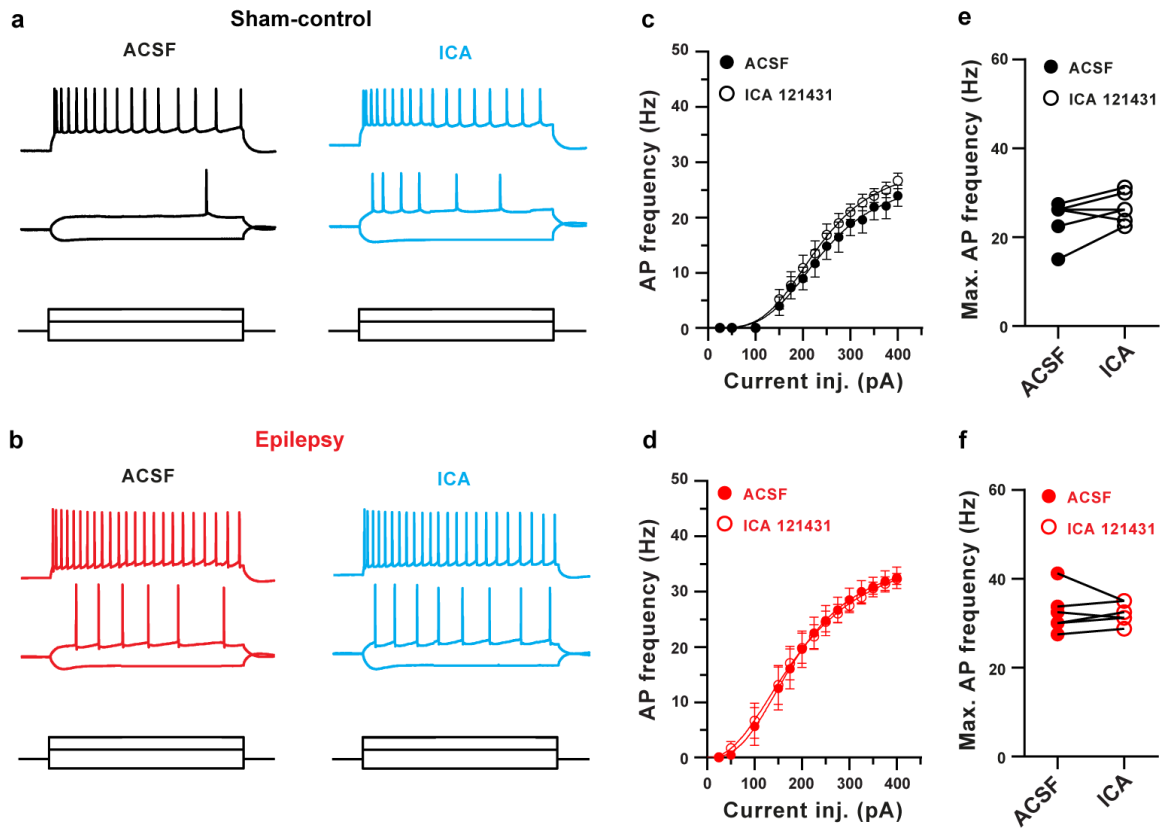
Fig. 3.14, Effects of ICA-121431 on intrinsic firing properties of CA1 pyramidal neurons in sham-control and epileptic mice. a-d, Representative examples of ICA-121431 effects in sham-control animals (panels a and c) and epileptic animals (panels b and d). **c,d,** Action potential frequencies induced by somatic current injection of different magnitudes, in sham-control and epileptic mice. **e,f,** Effects of ICA-121431 at current injections at which firing rates in ACSF were maximal. Differences in maximal action potential frequency tested with two-way repeated-measures ANOVA, S-Lic two-way repeated-measures ANOVA main effect, sham-control vs. epilepsy: $F_{(1\ 12)}=1.48$, $p=0.25$; ACSF vs. S-Lic: $F_{(1\ 12)}=19.98$, $p=0.0008$; interaction: $F_{(1\ 12)}=2.57$, $p=0.14$; Bonferroni´s post-test, max action potential frequency (Hz) in sham-control ACSF vs. S-Lic $p=0.098$; max action potential frequency (Hz) in epilepsy ACSF vs. S-Lic $p=0.0034$. ICA-121431 main effect, sham-control vs. epilepsy: $F_{(1\ 10)}=11.66$, $p=0.0066$; ACSF vs. ICA-121431: $F_{(1\ 10)}=1.67$, $p=0.23$; interaction: $F_{(1\ 10)}=2.28$, $p=0.16$.

3.6. Role of Na$_v$1.3 in the altered place-related firing of CA1 neurons

These data point towards a substantial decrease in the specificity of dendritic spikes and degraded input feature detection. I hypothesized that an altered dendritic integration might contribute to degraded place coding in CA1 neurons in vivo during chronic epilepsy. I, therefore, examined the activity of CA1 neurons and investigated the place coding using 2-photon Ca^{2+} imaging in head-fixed sham-control and epileptic Thy1-GCaMP6s mice running on a linear track equipped with spatial cues (**Fig. 3.15**).

As described in previous studies, the activity of CA1 neurons was higher during locomotion in both the sham-control and epileptic mice. Additionally, I observed a markedly increased activity of CA1 neurons in epileptic animals compared to sham control animals, both during immobility and locomotion (**Fig. 3.16,** n=1022 CA1 neurons in 5 sham-control mice and 1697 CA1 neurons in 6 epileptic mice, statistics see figure legend).
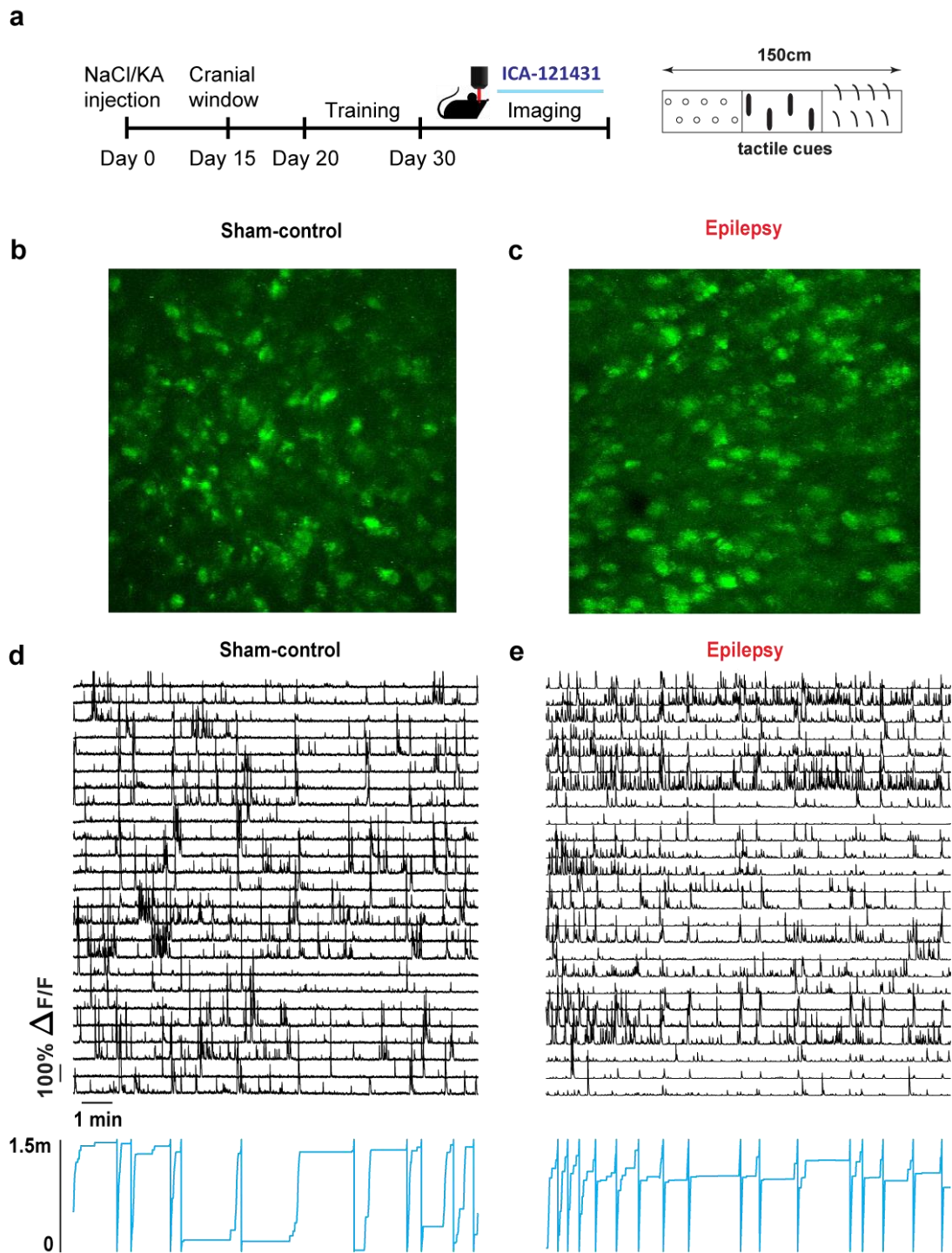
Fig. 3.15, Two-photon Ca²⁺ imaging in head-fixed sham-control and epileptic Thy1-GCaMP6s mice. a, Experimental timeline protocol to investigate the activity of CA1 neurons in mice running on a linear track, enriched with specific spatial cues patterns. **b, c,** Representative CA1 fields of view obtained for in vivo imaging. **d,e,** Representative examples of activity in a subset of the CA1 neurons from the fields of view shown in panels b and c. Upper traces indicate ΔF/F traces from a subset of CA1 neurons, lower blue traces indicate position of the mouse along the linear track.
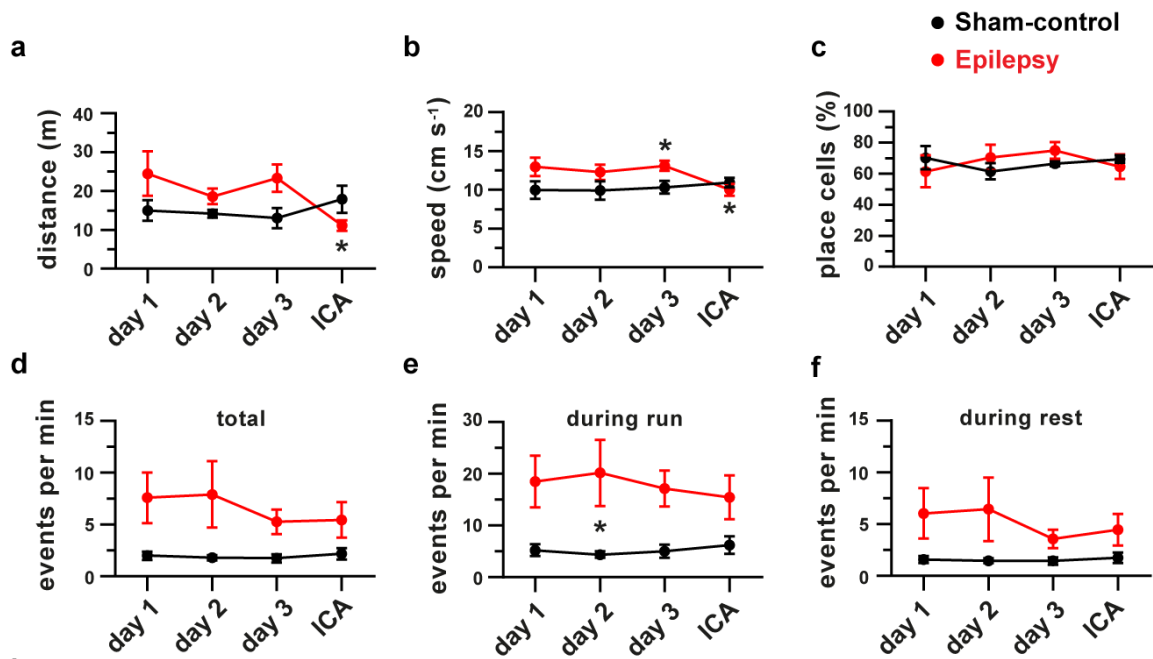
Fig. 3.16, Activity of CA1 neurons. **a,** Locomotion on the linear track, total distance run per session (travel distance, a), as well as the average running speed for sham-control and epileptic animals (b). Days 1-3 represent sessions on three consecutive days without ICA-121431, before one session with ICA-121431 (ICA) application. During days 1-3, these parameters were stable and did not differ between sham-control and epileptic animals (n=5 and 6 for sham-control and epilepsy, respectively, two-way ANOVA, n.s.). When comparing the distance run on day 3 with day 4 (ICA-121431 application), ANOVA revealed main effects of sham-control vs. epilepsy: $F_{(1\ 9)}=0.35$, $p=0.056$; baseline vs. ICA-121431: $F_{(1\ 9)}=1.73$, $p=0.22$; and a significant interaction: $F_{(1\ 9)}=9.5$, $p=0.013$, asterisk in panel c indicates Bonferroni´s post-test, $p=0.019$). When comparing the average speed on day 3 with day 4 (ICA-121431 application), ANOVA revealed main effects, sham-control vs. epilepsy: $F_{(1\ 9)}=1.10$, $p=0.31$; baseline vs. ICA-121431: $F_{(1\ 9)}=5.91$, $p=0.037$; interaction: $F_{(1\ 9)}=12.96$, $p=0.0057$). Asterisks in panel d indicate Bonferroni´s post-tests, Sham-control vs. epilepsy, $p=0.028$; speed in epileptic mice before and after ICA-121431 treatment, $p=0.0031$. **c,** Fraction of place-coding neurons of the neurons active during running (activity criterion as used for place cells >4 events detected during running episodes). There was no significant difference between groups, or due to ICA-121431 application (two-way ANOVA, n.s.). **d-f,** Average number of detected Ca^{2+} events during the total duration of the session (d), during only locomotion (run, e), or immobility (rest, f). Frequencies of Ca^{2+} events during the total duration of the session were significantly higher in epileptic mice during days 1-3 (two-way ANOVA main effect, sham-control vs. epilepsy: $F_{(1\ 9)}=5.12$, $p=0.049$; Day sessions: $F_{(2\ 18)}=0.67$, $p=0.52$; interaction: $F_{(2\ 18)}=0.53$, $p=0.59$). Similar findings were obtained during running (two-way ANOVA main effect, sham-control vs. epilepsy: $F_{(1\ 9)}=7.07$, $p=0.026$; Day sessions: $F_{(2\ 18)}=0.16$, $p=0.84$; interaction: $F_{(2\ 18)}=0.38$, $p=0.68$. Asterisk indicates Bonferroni´s post-test, sham-control vs. Epilepsy, $p=0.031$), but not during resting (two-way ANOVA, n.s.). No effects of ICA-121431 treatment on event frequencies were detected (two-way ANOVA, n.s.).

CA1 neurons that exhibited significant place-related activity (Danielson et al., 2016) were found in both sham-control and epileptic mice (examples of representative neurons in **Fig. 3.17,** spiral plots show place coding, rightmost distributions show tests vs. shuffled distributions for each cell). In both sham-control and epileptic mice, place-related firing fields tiled the extent of the linear track (**Fig. 3.18a**, upper panels all significantly place-coding CA1 neurons from a representative sham-control and epileptic mouse, respectively**, Fig. 3.19** for data from all sham-control and epileptic mice). It was apparent from visual inspection of these data that place-related firing of significantly place-coding cells appeared to be less specific in epileptic animals, consistent with published work demonstrating degraded place coding in epilepsy (Lenck-Santini et al., 2008; Zhou et al., 2007; Shuman et al., 2020; Ewell et al., 2019). I quantified the precision of spatial coding using a spatial tuning vector measure (Danielson et al., 2016), see also place vectors in spiral plots in **Fig. 3.17**), where higher place coding specificity corresponds to greater vector lengths. Indeed, I found the distribution of place vector lengths was significantly shifted to shorter values in epileptic mice, implying degraded place coding (**Fig. 3.18b,** cf. left and right panel). This difference was stable over multiple imaging sessions (**Fig. 3.18c**), indicating decreased specificity of place coding in epileptic animals. In the presence of ICA-121431, vector lengths significantly increased in epileptic, but not in sham-control mice (cumulative distributions of vector lengths for all cells in **Fig. 3.18b**). Correspondingly, ICA-121431 also caused an increase of the average vector lengths calculated per mouse in epileptic, but not in sham-control mice (**Fig. 3.18d,** n=6 and 5 mice respectively, repeated-measures two-way ANOVA main effects, sham-control vs. epilepsy: $F_{(1, 9)}=6.29$, $p=0.033$; baseline vs. ICA-121431 treatment: $F_{(1, 9)}=3.92$, $p=0.079$; interaction: $F_{(1, 9)}=5.64$, $p=0.042$; Bonferroni´s post-test sham-control vs. epilepsy $p=0.0095$, epileptic mice before ICA-121431 treatment vs. ICA-121431 treated epileptic mice $p=0.0207$). When I computed the effects on average vector lengths in each animal, the effect of ICA-121431 was significantly larger in epileptic mice, as expected (**Fig. 3.18e,** Mann-Whitney U-test, $p=0.03$). These experiments suggest that blocking $Na_v1.3$ channels in vivo significantly reverse degraded place coding in epilepsy.
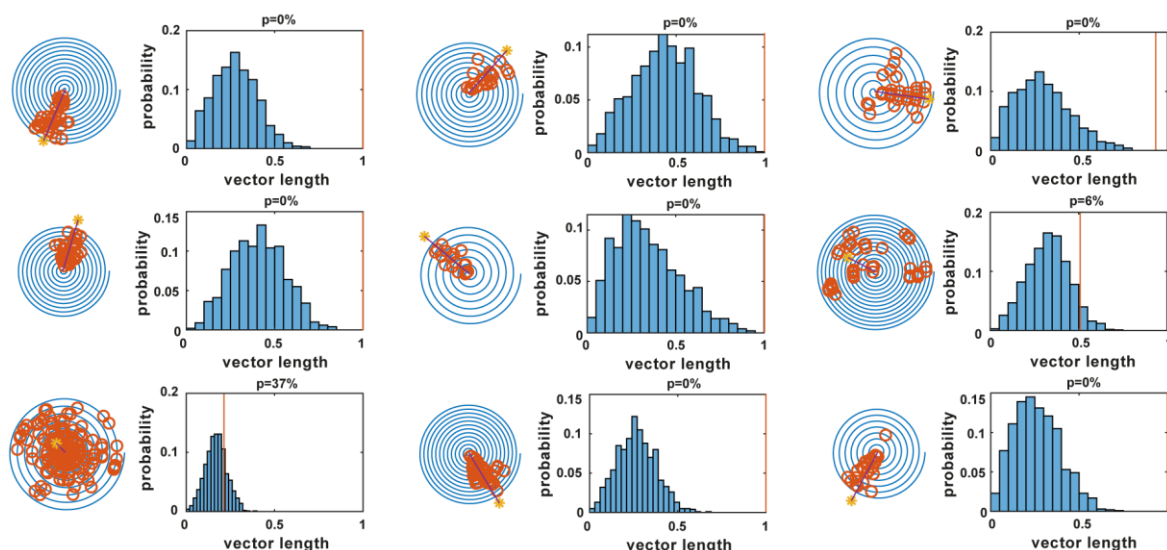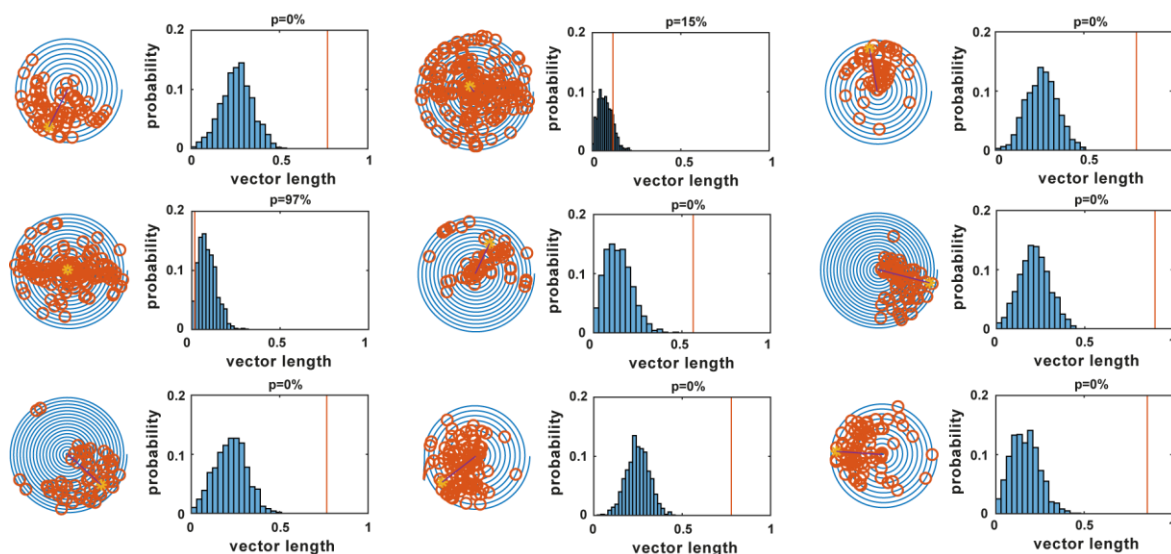
Fig. 3.17, Representative examples of significantly place-coding CA1 neurons. Examples from sham-control and epileptic mice as indicated. Spiral plots are shown on the left. One 360° pass around the spiral plot corresponds to a complete transition on the 150 cm linear track. Red dots indicate the activity of the CA1 neuron. Computed place vectors indicated by dark blue straight lines. Distributions on the right show tests vs. shuffled distributions for each cell (see Methods for details). The red vertical line indicates the vector length of the CA1 neuron, shuffled distributions shown in blue.

a

Sham-control

Epilepsy

Sham + ICA-121431

Epilepsy + ICA-121431

b

Sham before treatment
Sham ICA-121431

Epilepsy before treatment
Epilepsy ICA-121431

c

d

e
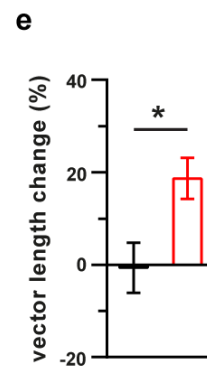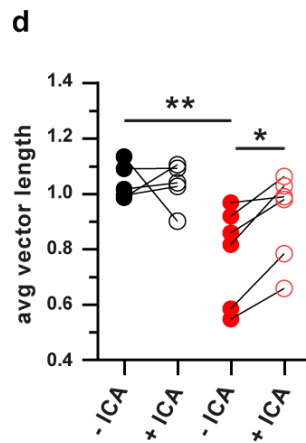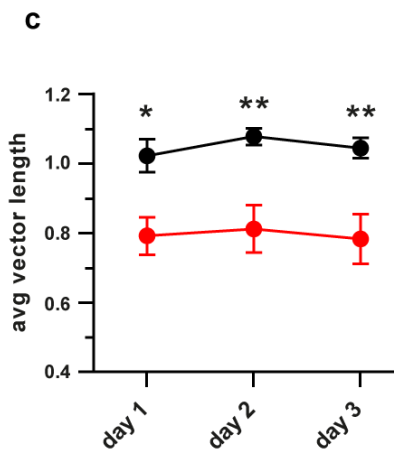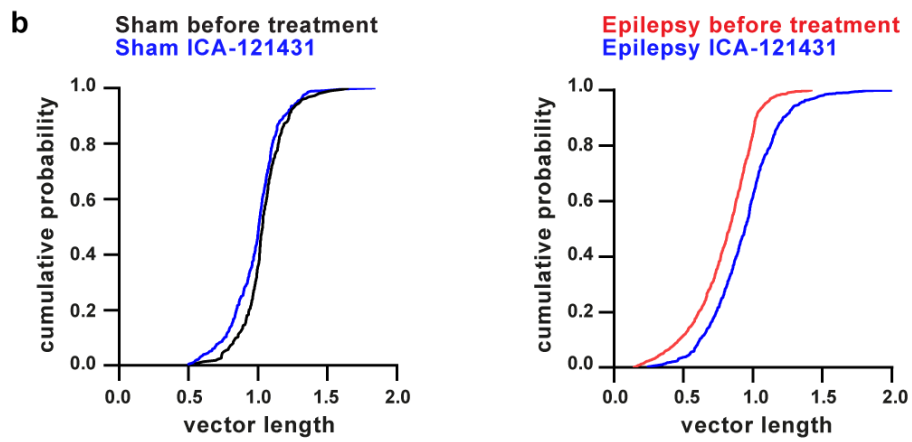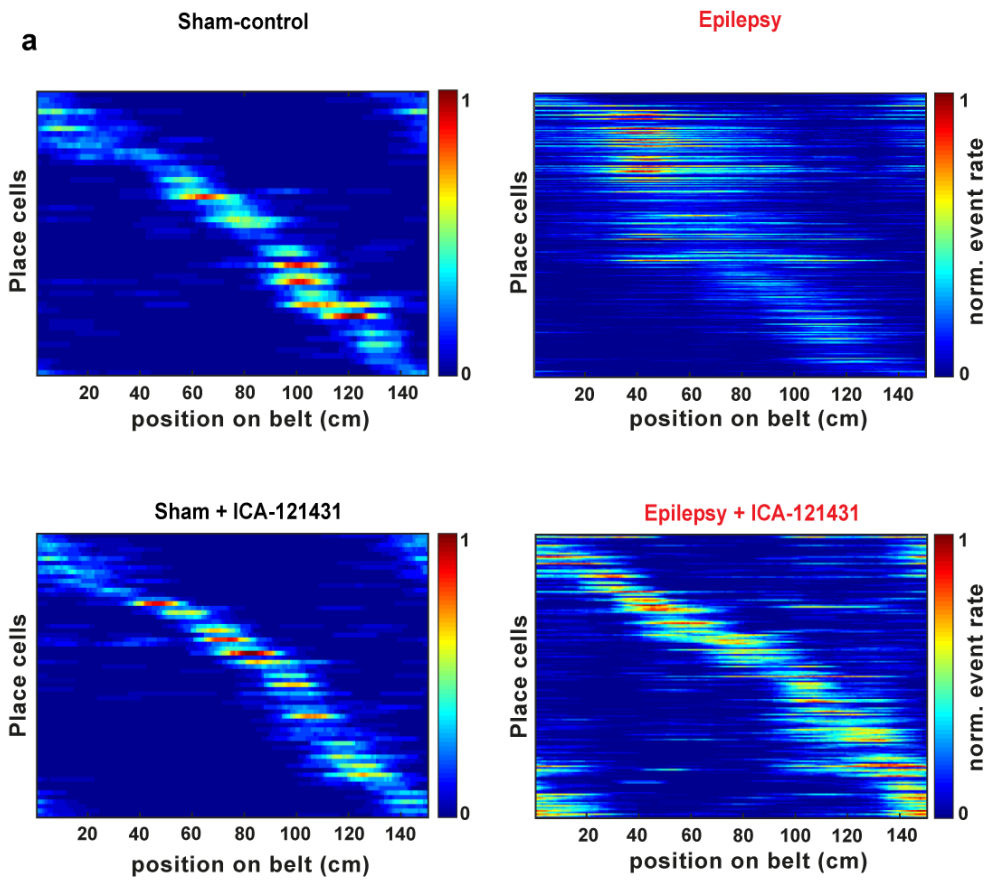
Fig. 3.18, Role of Na$_v$1.3 up-regulation in altered place-related firing of CA1 neurons and spatial learning in vivo. a, Analysis of place coding. Spiral plots for three representative CA1 neurons in a sham-control mouse (left panels) and an epileptic mouse (right panels). One 360° pass around the spiral plot corresponds to a complete transition on the 150 cm circular linear treadmill. Grey circles indicate event onsets in the CA1 neuron. Computed place vectors indicated by black straight lines. Distributions on the right show tests vs. shuffled distributions for each cell (see Methods for details). The red vertical lines indicate the vector length of the CA1 neuron, shuffled distributions shown in blue. **f,** All significantly place-coding CA1 neurons from a representative sham-control (left panels) and epileptic mouse (right panels). Lower panels show the same mice following treatment with ICA-121431. **g,** Cumulative distributions of place vector lengths for sham-control (left panel) and epileptic mice (right panel). Blue curves indicate the cumulative distribution of vector lengths after the application of ICA-121431. **h,** Differences between average vector lengths in sham-control (black) and epileptic animals (red) were stable over imaging sessions on three consecutive days. Two-way ANOVA main effect, sham-control vs. epilepsy: $F_{(1\ 27)}=31.12$, $p<0.0001$; subsequent days: $F_{(2\ 27)}=0.2623$, $p=0.7727$; interaction: $F_{(2\ 27)}=0.05973$, $p=0.9421$; asterisks indicate Bonferroni´s post-test, day 1 $p=0.02$, day 2 $p=0.0066$ and day 3 $p=0.0074$. **i,** Average vector lengths calculated per mouse in sham-control (black) and epileptic mice (red). Asterisks indicate Bonferroni's post-tests sham-control vs. epilepsy $p=0.0095$, epileptic mice before ICA-121431 treatment vs. ICA-121431 treated epileptic mice $p=0.0207$. **j,** Percent change in vector length caused by ICA-121431, quantified for each animal and averaged. Asterisk indicates Mann-Whitney U-test, $p=0.03$.
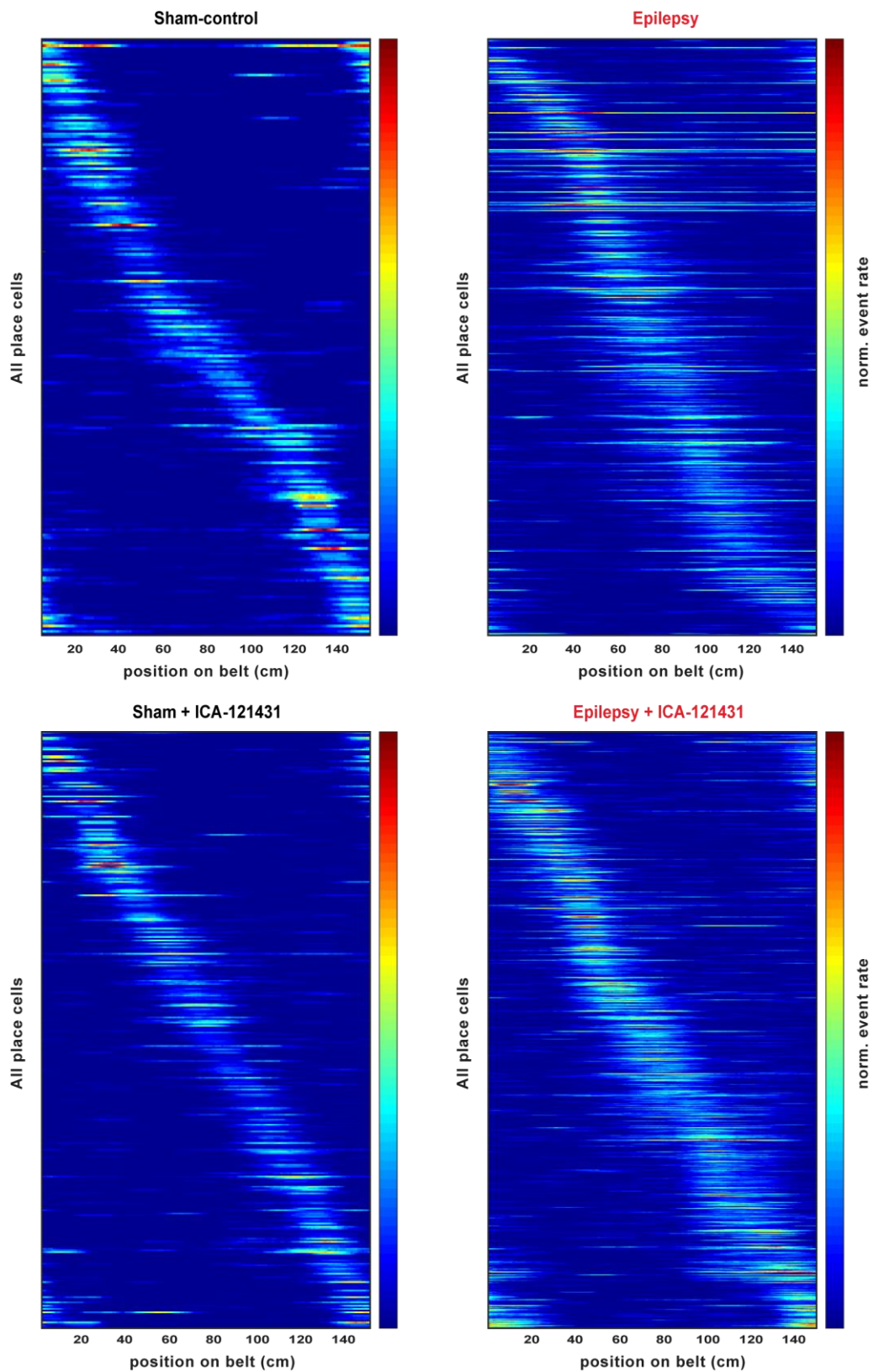
Fig. 3.19, Place-related activity in all CA1 pyramidal cells that displayed significant place coding. Panels show all CA1 neurons in sham-control and epileptic mice, both before and during application of ICA-121431.

3.7. Inhibiting Na$_v$1.3 channels normalize degraded memory in epileptic mice

I next investigated if inhibition of Na$_v$1.3 channels with ICA-121431 in vivo restores performance in a hippocampus-dependent task using well-established tests for spatial learning and working memory. Sham-control and epileptic animals were treated with vehicle or ICA-121431, and open field, object location memory test, novel object recognition test, and Y maze spontaneous alternation test were sequentially performed (**Fig. 3.20**).

After three days of habituation in the open field arena, the mice received vehicle or ICA-121431 treatment (**Fig. 3.21**). Apart from the first day, the exploration times were similar with respect to distance traveled during the session and time spent in the center of the open field in sham-control vs. epileptic groups. Moreover, the animals treated with ICA-121431were similar in locomotion and exploration to the vehicles treated groups (**Fig. 3.21**).
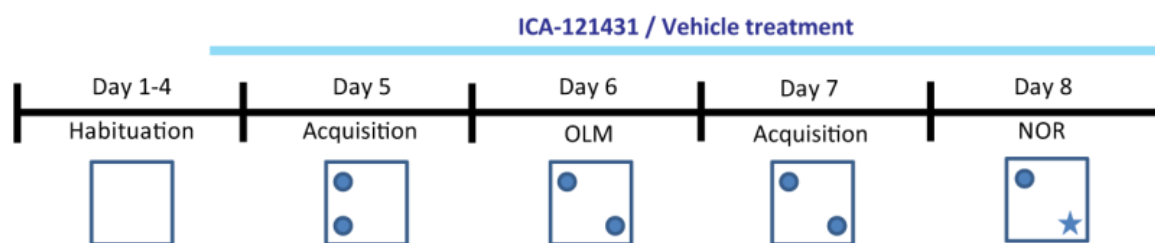
Fig. 3.20, Timeline of the behavioral experiment. Four days of habituation in the open field, with the application of either vehicle or ICA-121431 on the fourth day. After habituation to the open field, the object location memory (OLM) and object recognition memory (NOR) test were sequentially performed, vehicle or ICA-121431 treatment was delivered during all the consecutive days.
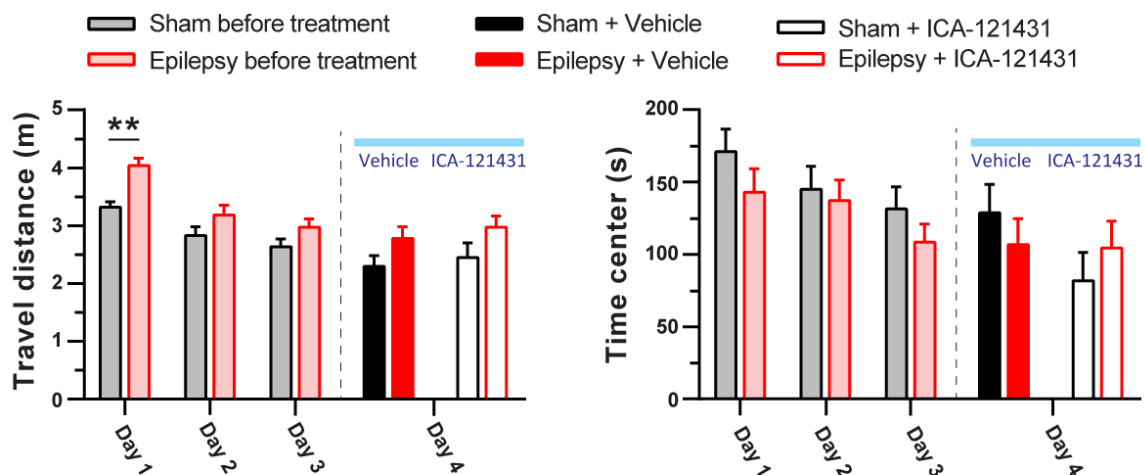
Fig. 3.21, Locomotor behavior in the open field. Four days of habituation in the open field, with the application of either vehicle or ICA-121431 on the fourth day. Animals habituated to the open field on days 1-3, with progressively less exploration on consecutive days. Left panel shows exploration times. Apart from the first day, the exploration times were similar with respect to distance traveled during the session and time spent in the center of the open field in sham-control vs. epileptic groups (n=24 and 29 in sham-control and epileptic mice, two-way ANOVA main effect, sham-control vs. epilepsy: $F_{(1\ 51)}=8.45$, $p=0.0054$; days 1-3 sessions: $F_{(2\ 102)}=39.27$, $p<0.0001$; interaction: $F_{(2\ 102)}=2.14$, $p=0.12$. Bonferroni´s post-test, sham-control vs. epilepsy day 1 $p=0.0015$, sham-control day1 vs. day2 $p=0.0053$; day1 vs. day3 $p<0.0001$; day2 vs. day3 $p=0.62$, travel distance in epileptic mice day1 vs. day2 $p<0.0001$; day1 vs. day3 $p<0.0001$; day2 vs. day3 $p=0.39$. There was no effect of ICA-121431 application when comparing against the values from day 3 of habituation, after habituation to the open field (two-way ANOVA, n.s.). Right panel shows time spent in the center, >5 cm away from walls. Two-way ANOVA main effect, sham-control vs. epilepsy: $F_{(1\ 51)}=1.2$, $p=0.28$; day 1-3 sessions: $F_{(2\ 102)}=7.32$, $p=0.0011$; interaction: $F_{(2\ 102)}=0.59$, $p=0.56$. Bonferroni´s post-test, sham-control day1 vs. day3 $p=0.02$. Epilepsy group day1 vs. day3 $p=0.030$.

I used the object location memory test (OLM) (**Fig. 3.22**), in which animals first learn the spatial arrangement of two objects, and then in a subsequent session, one of the objects is displaced. Normally the animals tend to spend more time exploring an object that has been relocated in a novel position. The discrimination index is an indicator of successful memory formation and recall, which compared exploration times of the novel object location (displaced object) versus the time spent with the familiar one (not changed object position). Subsequent sessions for the OLM test were carried out either in the presence of vehicle or ICA-121431. During the acquisition of the object position for the OLM test, mice did not discriminate between the two objects (**Fig. 3.22a,b** upper panels, **Fig. 3.22c,** two-way ANOVA, n.s.). In the OLM trial with a displaced object, vehicle-treated sham-control mice discriminated the new object, while vehicle-treated epileptic animals did not (**Fig. 3.22a** lower panels, n=17 and 15, respectively, filled bars in **Fig. 3.22d**). Importantly, administration of ICA-121431 by gavage (see methods) recovered memory performance to control levels in epileptic animals (**Fig. 3.22b,** lower panels, n=7 and 8 for sham-control and epileptic animals, respectively, empty bars in **Fig. 3.22d**). Two-way ANOVA revealed a main effect of vehicle vs. ICA-121431 treatment (vehicle vs. ICA-121431: $F_{(1\ 43)}=5.95$, $p=0.019$; sham-control vs. epilepsy: $F_{(1\ 43)}=1.17$, $p=0.29$; interaction: $F_{(1\ 43)}=3.91$, $p=0.054$ Bonferroni's post-tests indicated with asterisks).
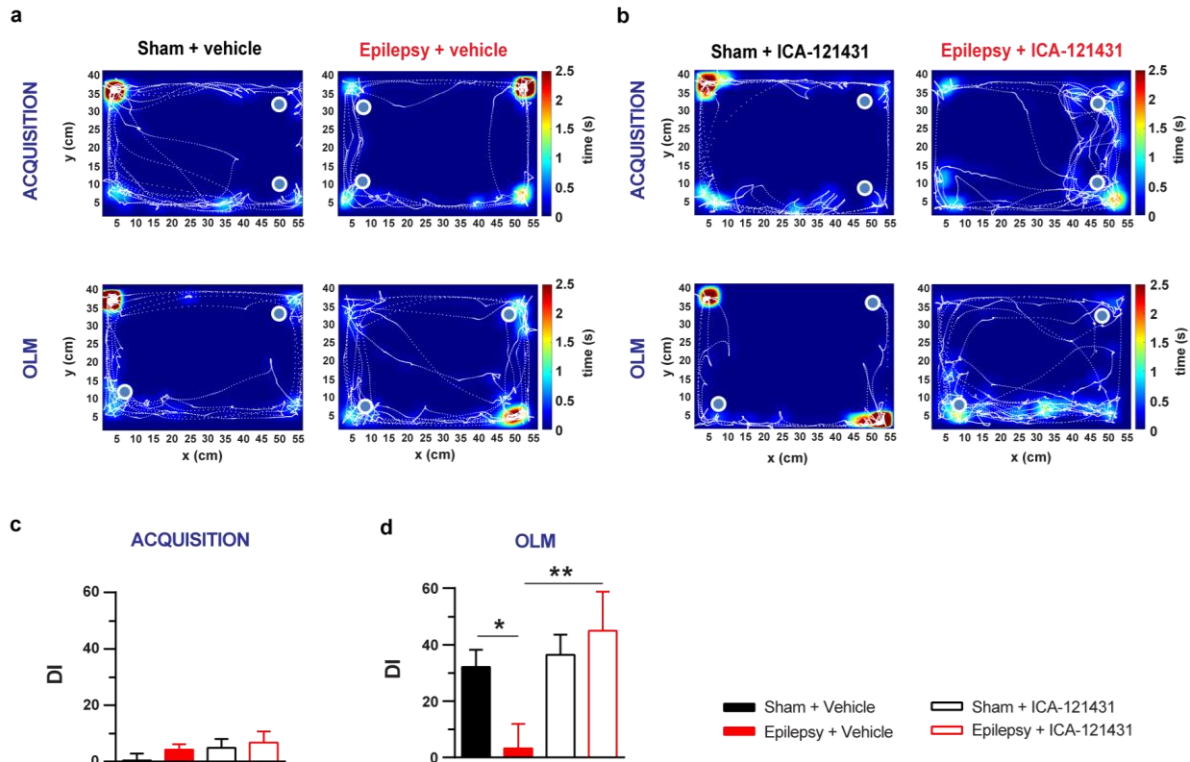
Fig. 3.22, Inhibiting Na$_v$1.3 channels normalizes hippocampal-dependent memory in epileptic mice. a, b, Representative examples of sessions with tracking data in sham-control and epileptic animals with vehicle application (b) and ICA-121431 application (c), respectively. Occupancy times are color-coded (calibration see scale bar). **c,** The discrimination index (DI) indicating if mice preferentially explore an object during the acquisition session. DI was close to zero, indicating that mice did not discriminate between the two objects in any group. **d,** DI in the OLM session. Vehicle-treated sham-control mice discriminated the new object, while vehicle-treated epileptic animals did not (black and red filled bars, respectively). Administration of ICA-121431 by gavage recovered memory performance to control levels in epileptic animals (empty bars). Asterisks indicate Bonferroni´s post-test, sham-control vehicle-treated vs. epilepsy vehicle-treated *p*=0.0193; epilepsy vehicle-treated vs. epilepsy ICA-121431 treated *p*=0.0057.

Following the OLM task, I tested the ICA-121431 treatment with the Novel Object Recognition (NOR) task. The NOR task is also used to evaluate cognition, particularly recognition memory, and like the OLM is based on the spontaneous tendency of animals to spend more time exploring a novel object than a familiar one. During habituation, the animals are allowed to freely explore the two identical objects used during the previous OLM test. The next day, one of the two objects is replaced with a new one different in shape and color but similar in volume, and the mice are allowed to explore the familiar and the novel object.

This test is based on the spontaneous tendency of rodents to spend more time exploring a novel object than a familiar one, and a discrimination index is used to test long-term recognition memory.

In contrast to the OLM trial, novel object recognition (NOR) was not impaired in epileptic animals (**Fig. 3.23a,c,d**), consistent with previous reports (Bui et al., 2018). ICA-121431 treatment did not alter performance in the NOR trial in either sham-control or epileptic mice (**Fig. 3.23b-d** n-numbers as for OLM trials).
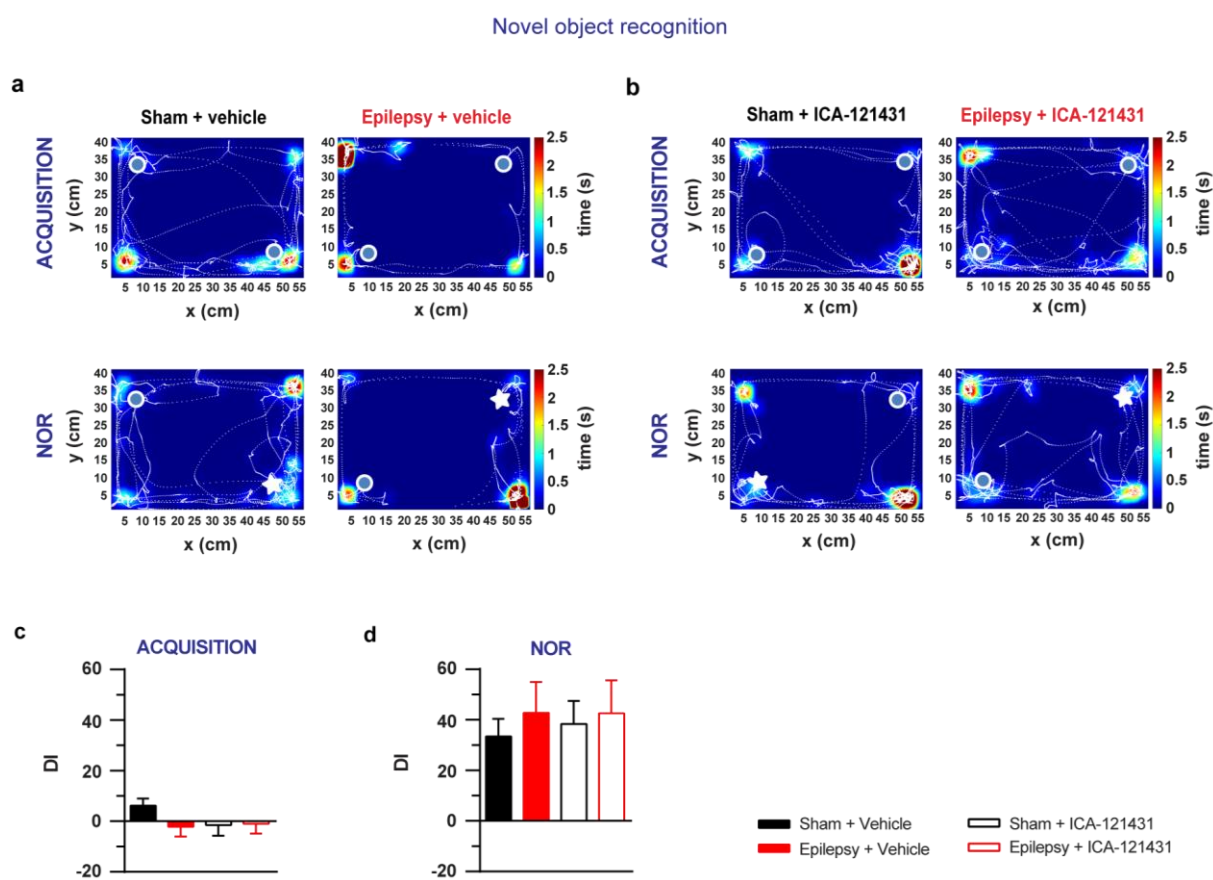
Fig. 3.23, Novel object recognition (NOR) test. a, b, Representative examples of sessions with tracking data in sham-control and epileptic animals with vehicle application (c) and ICA-121431 application (d), respectively. Occupancy times are color-coded (calibration see scale bar). e, g, time spent exploring the objects. Exploration times were not different between groups (two-way ANOVA, n.s.). c, The discrimination index (DI) indicating if mice preferentially explore an object during the acquisition session. DI was close to zero, indicating that mice did not discriminate the two objects in any group (no differences between groups, two-way ANOVA, n.s.). d, DI in the NOR session. In all groups, animals discriminated the novel object. There were no differences between groups (two-way ANOVA, n.s.).

In addition to degraded spatial learning, cognitive deficits in TLE have been demonstrated to affect behavioral tasks requiring working memory in patients (Cánovas et al.,2011) as well as in animal models (Gröticke et al., 2008; Van Den Herrewegen et al., 2019; Rattka et al., 2013). Therefore, I investigated if inhibition of Nav1.3 channels with ICA-121431 in vivo restores performance in working memory using the Y maze spontaneous alternation test (**Fig. 3.24a**). The Y maze is widely used to assess behavioral tasks in cognition research, and even if it is not a purely hippocampal-dependent task since different areas of the CNS, including the prefrontal cortex, basal forebrain, and septum, are involved in the performance of this task, the spontaneous alternation test has been demonstrated to be strongly sensitive to hippocampal damage and cognitive deficits. (Hashemi et al., 2019; Liu et al., 2019).

The test is dependent on the spontaneous animal's willingness and curiosity to explore the new environment. The mice tend to explore a new arm of the Y maze rather than returning to one arm previously visited.

If the mice choose a different arm in three consecutive entries than the one it arrived from, it accomplishes an alteration. This is considered a successful performance, whereas returning to the previously explored arm is considered an error. The number of arms the mice explored during the test and the total number of three consecutive different arm entries are used to calculate the alternation score and quantify performance during the task.

ANOVA revealed main effects on the alternation score of kainate treatment (sham-control vs. epilepsy: $F_{(1\ 44)}$=7.36, p=0.0095), but the effects of ICA-121431 treatment did not reach statistical significance ($F_{(1\ 44)}$=2.86, p=0.098; interaction: $F_{(1\ 44)}$=0.82, p=0.59, (**Fig. 3.24b,c**). Thus, the effects of ICA-121431 seem to be most prevalent for spatial tasks with a strong hippocampal contribution.

Together these behavioral experiments revealed how the pharmacological inhibition of Nav1.3 channels with ICA-121431 restores cognitive performance in a hippocampus-dependent task during chronic epilepsy. Thus, modulation of Nav1.3 channels may be exploited to correct epilepsy-induced enhanced dendritic excitability and to reverse cognitive impairments, in particular degraded spatial memory and learning, in chronic TLE.

Y Maze spontaneous alternation test
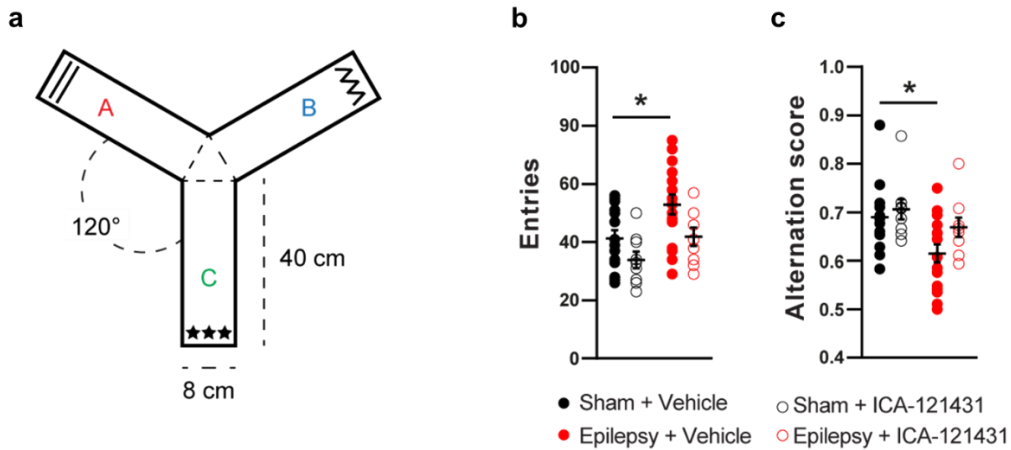
Fig. 3.24, Y maze spontaneous alternation test. a, Scheme representing the Y maze arena. For those experiment we tested sham-controls vehicle-treated (n=14), sham-controls ICA-121431 treated (n=9), epilepsy vehicle-treated (n=16) and epilepsy ICA-121431 treated (n=9) mice. **b,** Vehicle-treated epileptic animals showed a significantly higher number of entries compared with Sham-control vehicle or ICA-121431 treated, and epilepsy ICA-121431 treated mice reflecting the increased locomotion in epilepsy observed during calcium imaging experiment. (vehicle vs. ICA-121431: $F_{(1\ 44)}=7.46$, $p=0.0090$; sham-control vs. epilepsy: $F_{(1\ 44)}=8.47$, $p=0.0056$; interaction: $F_{(1\ 44)}=0.29$, $p=0.059$ Bonferroni's post-tests indicated with asterisks).

c, The alternation score was significantly lower in epilepsy animals treated with vehicle, (vehicle vs. ICA-121431: $F_{(1\ 44)}=2.86$, $p=0.97$; sham-control vs. epilepsy: $F_{(1\ 44)}=7.36$, $p=0.0095$; interaction: $F_{(1\ 44)}=0.81$, $p=0.37$ Bonferroni's post-tests indicated with asterisks). Conversely, the epilepsy group treated with ICA-121431 showed no differences when compared to the Sham-control animals.

Chapter 4

Discussion

In chronic epilepsies, cognitive deficits are observed in about 70-80% of patients (Helmstaedter et al., 2012; Elger et al., 2004), especially in TLE, because of the involvement of memory-relevant hippocampal structures (Helmstaedter et al., 2001, 2009). Even though deficits regarding attention, language, working memory, and spatial memory have been described that have a sizeable impact on the quality of life of TLE patients (Williams, 2003; Wilkinson et al., 2012), less effort has been directed towards understanding the biology underlying these impairments. Indeed, there is no treatment available that directly targets cognitive dysfunction in TLE.

Within the context of epilepsy comorbidities, investigating how individual neurons integrate thousands of synaptic inputs they receive might provide the key to understand memory impairments. Active properties of hippocampal CA1 pyramidal neuron dendrites have a critical role in this process, driving input feature selective tuning and plasticity (Poirazi & Mel, 2001; Wu & Mel, 2009).

In most pyramidal neurons, dendrites can generate regenerative dendritic spikes in a summation process termed supralinear integration (Schiller et al., 1997; Hausser et al., 2000; Nevian et al., 2007; Yuste, 2011). Dendritic spikes are a cornerstone of dendritic integration, which amplify spatiotemporally synchronous inputs and drive sharply tuned neuronal responses (Ariav et al., 2003; Golding & Spruston, 1998; Losonczy & Magee, 2006). They constitute a powerful signal for the induction of different types of synaptic plasticity (Remy & Spruston, 2007), including forms of potentiation that are thought to be independent of postsynaptic firing (Golding et al., 2002). Moreover, dendritic spikes have been proposed to drive place-related firing in CA1 neurons (Sheffield & Dombeck, 2017).

This active form of dendritic electrogenesis relies on voltage-gated ion channels (Ariav et al., 2003; Losonczy & Magee, 2006; Gasparini et al., 2004). In epilepsy and numerous other CNS disorders, the expression and the function of these active conductances are profoundly altered in CA1 dendrites. Indeed, in many models of acquired epilepsy, changes in K^+ channels (Bernard et al.,2004), T-type Ca^{2+} channels (Su et al., 2002; Yaari et al., 2007; Becker 2008), HCN channels (Jung et al., 2007; 2010), and Na^+ channels (Chen et al., 2011; Sanabria et

al., 2011; Royeck et al., 2015) have been identified as a cause of abnormal neuronal excitability. However, these studies have mainly focused on larger caliber, apical dendrites of pyramidal neurons, primarily because of the difficulties obtaining direct patch-clamp recording from thin dendrites.

Although 80% of the excitatory inputs to glutamatergic neurons impinge on small caliber dendrites, investigation of the integrative properties of these compartments and how they change in chronic epilepsy has only recently begun (Royeck et al., 2015; Kelly & Beck, 2017). Moreover, despite the critical importance of dendritic spikes for neuronal integration, changes in supralinear integrative properties have not been examined in TLE.

Starting from the large body of data examining dendritic ion channel changes in epilepsy and the importance of dendritic spikes in input-output computations, I hypothesized that supralinear integration may be strongly disturbed. This, in turn, may contribute to cognitive deficits in acquired epilepsies.

In this thesis, I described a Na^+ channel-dependent mechanism underlying a major change in hippocampal dendritic integration in chronic epilepsy that degrades place coding in-vivo and causes deficits in spatial memory. Strikingly, this mechanism can be pharmacologically targeted to restore impaired dendritic integration and disturbed memory function.

4.1 Dysfunctional dendritic integration in chronic epilepsy

Dendrites of CA1 excitatory neurons either display linear integration or are capable of additionally generating supralinear dendritic spikes. Importantly, dendritic spikes are only generated when stimulation of neighboring spines is strong and synchronous enough to recruit voltage-gated sodium channel activation (Gasparini et al., 2004; Losonczy & Magee, 2006; Larkum et al., 2009; Remy et al., 2009). In this study, I showed that the properties of dendritic spike generation are markedly altered in CA1 pyramidal neurons in chronic epilepsy. Specifically, the fraction of proximal dendritic branches generating dendritic spikes is almost doubled in epileptic animals. In addition, in those dendrites that generate dendritic spikes, virtually all properties that confer input-specificity to supralinear responses are degraded.

First, the threshold for eliciting dendritic spikes is significantly lowered in epileptic animals, with dendritic spikes sometimes being generated from very few synaptic inputs (1-3 spines) and somatic voltages as little as ~3 mV. Altered excitability within the dendritic arbor might affect the development of short- and long-term plasticity (Losonczy et al., 2008) or alter

somatic action potentials backpropagation into the distal dendritic arbor, promoting epileptiform activity and providing one plausible proconvulsant mechanism.

Second, even very asynchronous synaptic stimulations can generate dendritic spikes in epileptic animals. In healthy CA1 pyramidal neurons, the restriction to only synchronous clustered excitatory inputs in generating dendritic spikes allows the cells to respond with high time precision to specific input features (Losonczy & Magee, 2006; Poirazi et al., 2003b). Thus, a perturbation on the requirements for input synchrony would disrupt the coding of tuned temporal features leading to a less selective input-specific response in CA1 neurons.

Third, mechanisms that usually attenuate dendritic spikes are much less effective in epileptic animals. Normally, the ability to generate dendritic spikes is decreased by prior dendritic or somatic activity (Remy et al., 2009). This phenomenon relies on the rapid but long-lasting inactivation of dendritic sodium channels. I found that dendritic spike inactivation is occurring to a much lesser extent in epilepsy, suggesting that dendritic spikes can be generated at abnormal high frequency.

Fourth, dendritic spike strength is enhanced in epilepsy, resulting in a higher rate of rise during the initial phase of the dendritic spike. The initial phase of the dendritic spike in CA1 dendrites is generated by activation of transient Na^+ currents (Losonczy & Magee, 2006), suggesting an increased role of sodium channels in driving dendritic spikes in epileptic animals.

Previous studies on supralinear integration have demonstrated that the distribution of the maximum rate of rise of the initial phase of the dendritic spike is bimodal for large dendritic populations, with dendrites either generating weak or strong dendritic spikes (Losonczy et al., 2008; Remy et al., 2009). This is particularly relevant considering that strong spikes are much less affected by concurrently evoked inhibition (Müller et al., 2012), with a more prominent impact on the somatic output. Thus, the high fraction of dendrites generating strong dendritic spikes in epilepsy could render these spikes less sensitive to synaptic inhibition. It could thus contribute to the overall dendritic hyperexcitability in epilepsy, resulting in excitatory/inhibitory imbalance.

It should be noted that all these changes in dendritic integrative properties were observed only in 1st order but not in 2nd order dendrites. This is in line with plasticity observed during exposure to an enriched environment. Experience in such an environment led to a selective increase in the strength of dendritic spikes in 1st order dendrites. This, in turn, enhanced the propagation of distally evoked dendritic spikes into proximal dendrites (Makara et al., 2009). Thus, although we did not address this possibility directly, these results imply that propagation

of distally evoked dendritic spikes into proximal dendrites could be abnormally enhanced in chronic epilepsy.

In summary, these results show a dramatically augmented excitability of proximal dendrites in epilepsy, reflected in the abnormal prevalence and properties of dendritic spikes, as well as in the degraded mechanism that controls their sparse generation. As a consequence, it is likely that dendritic spikes can be widespread generated at abnormally high frequencies.

4.2 Mechanisms underlying aberrant dendritic integration in epilepsy

Intrinsic Na^+ voltage-dependent conductances exert robust control over dendritic excitability, and the currents carried by these channels are important in shaping the integrative properties of neurons. Many studies have demonstrated the presence of voltage-gated Na^+ channels in the entire somatodendritic axis of CA1 pyramidal neurons with homogeneous density within stratum radiatum (Magee & Johnston, 1995). Voltage-gated Na^+ channels located in dendrites allow action potentials initiated at the axonal segment to propagate back into the dendritic compartment (Stuart et al., 1997; Häusser et al., 2000; Frick et al., 2003). The action potential backpropagation can then sum with incoming synaptic activity (Stuart et al., 1997), increasing the calcium influx at the synaptic sites and thus driving the induction of associative synaptic plasticity (Magee & Johnston, 1997).

Furthermore, Na^+ channels in CA1 apical dendrites give rise to non-inactivating currents, termed persistent sodium currents (I_{NaP}), activated below the action potential threshold. These $I_{NaP,}$ already activated in the subthreshold voltage range, play an important role in amplifying distal EPSPs compensating for the electrotonic attenuation (Lipowsky et al., 1996).

In addition to I_{NaP} currents, Na^+ channels in CA1 dendrites drive fast Na^+ currents, generating dendritic spikes, a cornerstone of dendritic integration. Local dendritic spikes in apical dendrites of CA1 pyramidal neurons consist of a fast and slow phase. The fast phase is driven by transient Na^+ currents, which are indirectly responsible for the slow component through the activation of other conductances (Ca^{2+} and NMDARs). Blocking Na^+ channels prevents the initiation of dendritic spikes altogether (Gasparini et al., 2004; Losonczy & Magee, 2006). In the kainate model of epilepsy, I found changes in dendritic spikes consistent with an increase in dendritic Na^+ channels. Both a faster rate of rise, an increased propensity to generate strong spikes, and the reduced attenuation of repetitive dendritic spiking could plausibly be caused by a gain of Na^+ channel function.

My pharmacological experiments suggest that a blocker that acts primarily on $Na_v1.2$ and $Na_v1.6$ isoforms significantly inhibited somatic action potential generation but did not affect altered dendritic excitability. In contrast, a blocker that affects both $Nav1.1$ and $Na_v1.3$ channels reverts the changes in dendritic spikes but does not affect somatic action potential generation in epilepsy. Since $Nav1.1$ channels are not highly expressed in excitatory CA1 pyramidal neurons, these results provide the first evidence of a $Na_v1.3$ channel-dependent mechanism underlying a prominent change in hippocampal dendritic integration in chronic epilepsy.

Furthermore, in collaboration with Prof. Dr. Sandra Blaess, Institute of Reconstructive Neurobiology in Bonn, we have examined $Na_v1.3$ at the expression level using RNAscope experiments (Wang et al., 2011). This approach allowed us to specifically quantify $Na_v1.3$ mRNA in hippocampal neurons and revealed an increased expression of $Na_v1.3$ in epilepsy. This result supports the idea that $Na_v1.3$ channel up-regulation contributes to aberrant dendritic integration in epilepsy.

These findings are in line with previous studies which investigated $Na_v1.3$ regulation in chronic epilepsy. Several evidences have shown that $Nav1.3$ channels are increased in human epilepsy (Yu et al., 2012; Whitaker et al., 2001) and in experimental models (Xu et al., 2012; Guo et al., 2008), including the kainic acid model of chronic epilepsy (Tan et al., 2017; Lin et al., 2017; Li et al., 2015). Moreover, it has been shown that neurons expressing $Na_v1.3$ have a lower threshold and a higher frequency of firing (Cummins et al., 2001), suggesting their contribution to the development of epilepsy. In addition, changes in the functional and biophysical properties of $Na_v1.3$ lead to increased seizure susceptibility (Chen et al., 2000; Sun et al., 2007; Estation et al., 2010; Xiaoxue Xu et al., 2013).

Interestingly, Proparacaine (PPC), an old topical anesthetic for ophthalmic optometry that selectively antagonizes the $Na_v1.3$ isoform, has recently been used in epilepsy treatment. Strikingly, PPC exerted an anti-convulsive effect and reduced seizures in an animal model of TLE. In addition, PPC rescued impaired spatial recognition memory in epileptic animals (Taleb et al., 2021). Altogether, these results suggest that $Na_v1.3$ channels are up-regulated in chronic epilepsy and affect supralinear dendritic integration, promoting abnormal dendritic spiking in epilepsy.

Nevertheless, additional consideration has to be pointed regarding the specificity in the pharmacological intervention of ICA-121431used in this study to block $Na_v1.3$ channels.

ICA-121431 has a high affinity for $Na_v1.3$ but also for $Na_v1.1$ due to their shared domain 4 in the voltage-sensor region (IC50s <20 nM), much less potent inhibition of $Na_v1.2$ (IC50 240

nM), while the inhibition of $Na_v1.7$, $Na_v1.6$, $Na_v1.4$ is weak ($IC_{50}s$ >10 µM) (McCormarck et al., 2013).

It may be reasonable to wonder if $Na_v1.3$ is the only channel driving increased supralinear dendritic integration in epilepsy or if other channels such as $Na_v1.1$ and $Na_v1.2$ isoforms also play a role.

During my experiments, I used the Na^+ channel blocker and anticonvulsant Eslicarbazepine (S-Lic), which affects $Na_v1.2$ and 1.6 channels, but not $Na_v1.3$ or 1.1 channels (Holtkamp et al., 2018). As described previously, the $Na_v1.2/1.6$ blocker S-Lic significantly inhibited abnormal somatic action potential generation but did not alter dendritic spikes in control or epilepsy. In contrast, ICA-121431 does the converse and selectively affects dendritic spikes but not somatic firing. Thus, $Na_v1.2/1.6$ might be up-regulated as well in our experimental model of epilepsy, participating in abnormal somatic firing. However, these channels are unlikely to contribute to the enhanced dendritic integration due to S-Lic ineffectiveness on dendritic spiking. It is possible that part of the effects of ICA-121431 that we observed relies on the block of $Na_v1.1$ channels, which are also powerfully blocked by this compound.

Nevertheless, several lines of evidence argue against this idea. First, the $Na_v1.1$ channel is primarily expressed in interneurons, and even in epilepsy models, so far, no evidence of $Na_v1.1$ up-regulation in principal cells has been found. Secondly, an up-regulation of $Na_v1.3$ has been confirmed by us and other studies (Yu et al., 2012; Tan et al., 2017; Lin et al., 2017), rendering this the most likely hypothesis. Indeed, the $Na_v1.3$ channel isoform exhibits rapid repriming and recovery from the inactivation, as well as particularly slow closed-state inactivation (Cummins et al., 2001). Thus, a $Na_v1.3$ up-regulation may play an important role in boosting subthreshold inputs, and their properties are well suited to explain the abnormal repetitive generation of dendritic spikes and the loss of dendritic spike inactivation.

Despite the critical role of Na^+ channels in shaping the dendritic excitability, they are not the only active conductances involved in dendritic electrogenesis.

Indeed, additional voltage-gated ion channels prominently expressed in CA1 pyramidal cell dendrites include A-type K channels, HCN channels, and Ca^{2+} channels.

A-type K^+ channels limit the backpropagation of action potentials into the dendrites, reducing excitatory synaptic events (Hoffman et al., 1997). HCN channels are particularly relevant to attenuate repetitive excitatory synaptic input, modulating the temporal summation of EPSPs (Magee et al., 1999; Poolos et al., 2012). Ca^{2+} channels (mainly Cav3.2) are recruited by backpropagation of action potential into the dendrites (Stuart et al., 1997). In addition, they

are also known to drive complex spike firing (Golding et al., 1999) and to be activated during the slow phase of the dendritic Na$^+$ spike.

For all of these channels in CA1 dendrites, substantial differences in expression, protein levels, or functional properties have been described in epilepsy, resulting in enhanced intrinsic neuronal excitability (Bernard et al., 2004; Jung et al., 2007; Yaari et al., 2007; Becker et al., 2008).

Notably, due to the difficulty of obtaining patch-clamp recordings from small-caliber dendrites, all these pathological changes have been described in the main apical trunk. However, it is plausible that these additional mechanisms, increasing the main trunk's excitability, enable enhanced conduction of aberrant dendritic spikes to the soma.

4.3 Restoring degraded place coding in chronic epilepsy

The changes in dendritic spikes suggested that input feature detection of CA1 neurons is strongly degraded (Bittner et al., 2015). However, what do we know about the role of active dendrites in the context of a working brain? How can altered dendritic integration affect cognitive functions? And how to investigate this mechanism in vivo?

A prominent feature selectivity described in CA1 hippocampal neurons across different species is the spatial coding of place cells (Buzsáki & Moser, 2013; O'Keefe, 1971). Place cells within the CA1 show highly selective activity at distinct space locations (place fields) when an animal navigates its environment (O'Keefe & Nadel, 1978; Mizuseki et al., 2012) and are thought to form a spatial map.

These neurons receive spatial information from the entorhinal cortex and the hippocampus through inputs arriving on their dendrites. Accordingly, place cells provide an ideal substrate to study the relationship between dendritic integration and somatic output.

Multi-planar Ca^{2+} imaging from dendrites and somata of CA1 place cells showed that dendritic spikes often occur prior to somatic place field firing (Sheffield et al., 2017), and the prevalence of dendritic spikes predicts the spatial precision and stability of place fields. Indeed, it has been demonstrated how a higher prevalence of dendritic spikes across a place field (branch-spike prevalence) is strongly correlated with an increased spatial precision of place cells (Sheffield & Dombeck, 2015).

Because dendritic spikes have been proposed to drive place-specific firing in CA1 neurons, it is likely that a substantial decrease in the specificity of dendritic spikes and degraded input feature detection predict less spatial tuned responses. This hypothesis is also in line with

computational studies, where changes causing an increase in dendritic spike generation degrade place tuning of pyramidal neurons (Basak & Narayanan, 2018). Notably, the absence of dendritic spikes also impairs sharp spatial tuning, suggesting that the prevalence and properties of dendritic spikes have to be carefully tuned for optimal place coding (Basak & Narayanan, 2020).

I, therefore, examined the activity of CA1 neurons using 2-photon Ca^{2+} imaging in healthy and epileptic mice running on a linear track. CA1 neurons that exhibited significant place-related activity were found in both groups, although place-coding cells appeared to be less specific with a substantial broadening of place representations in epilepsy. These results were consistent with previous studies, which showed degraded place coding in different models of experimental epilepsy (Lenck-Santini & Holmes, 2008; Zhou et al., 2007; Shuman et al., 2020; Karnam et al., 2009).

Strikingly, epileptic animals following a systemic $Na_v1.3$ channels blocker treatment showed improved place coding, resulting in CA1 place cells with higher and precise spatial tuning.

Therefore, the convergent in-vitro and in-vivo data point to a role of $Na_v1.3$ channels in degrading the dendritic integration of spatial information in CA1 place cells.

Nevertheless, additional changes also influence the processing of CA1 neurons during navigation. Whereas I have focused on the role of excitatory input in dendritic spike generation, inhibitory circuits are also likely to play an important modulation in feature input integration, particularly in shaping place coding in CA1 pyramidal neurons.

Indeed, morphological (Bloss et al., 2016), computational (Gidon & Segev, 2012), and electrophysiological (Milstein et al., 2015; Lovett-Barron et al., 2012) studies suggested that synaptic inhibition influences spatiotemporal input summation. In particular, dendritically targeting interneurons are well suited to control the probability, the initiation and duration of dendritic spikes as well as the feature selectivity in hippocampal CA1 neurons (Müller et al., 2012; Royer et al., 2012; Palmer et al., 2012; Lovett-Barron et al., 2014). Thus, inhibitory mechanisms became particularly relevant in explaining the generation of place selectivity in hippocampal neurons (Burgess & O'Keefe, 2011).

In vivo experiments that combined electrophysiological recordings of CA1 pyramidal cells and optogenetically manipulation of GABAergic neurons revealed that inhibition selectively counters the influence of off-target excitatory inputs in CA1 pyramidal cells. Thus, inhibitory inputs, suppressing out-of-field AP firing that is mistuned in terms of location, expand the dynamic range and increase the signal-to-noise ratio in place cells (Grienberger et al., 2017). Furthermore, an inhibition that specifically targets pyramidal neuron dendrites is expected to

be especially effective in controlling active dendritic mechanisms that could lead to aberrant amplification and unwanted plasticity of off-target inputs (Milstein et al., 2015; Lovett-Barron et al., 2012). Together these findings indicate that local synaptic inhibition enhances the temporal coding of spatial location in CA1 place cells. Thus, perturbation in a well-balanced integration of excitatory and inhibitory input across place cells dendrites might contribute to degraded spatial coding.

Accordingly, inhibition became of particular interest within the investigation of mechanisms underlying degraded place coding in epilepsy.

Several morpho-functional alterations have been reported in human as well as experimental TLE, with changes in the amount and timing of inhibition, such as decreased release probability at inhibitory synapses targeting the CA1 apical dendrites (Cossart et al., 2001) and less effective feedback inhibition on CA1 neurons (Pothmann et al., 2019).

Moreover, hippocampal network reorganization in epilepsy models leads to altered inhibitory synchronization, and place cells cannot appropriately integrate the spatial information without timed excitation and inhibition (Shuman et al., 2020).

However, in different TLE models, it has been observed that interneuron loss occurs in the first 72 hours after the brain insult (Shetty et al., 2009; Dinocourt et al., 2003), long before instability of place representations which has been found after six weeks after epileptogenesis (Shuman et al., 2020). This suggests that changes in inhibitory mechanisms alone or interneuron loss per se cannot be the only factor underlying degraded spatial coding. Moreover, my results showed a higher propensity of CA1 pyramidal neurons to generate strong dendritic spikes that are known to be much less affected by concurrently evoked inhibition (Müller et al., 2012).

Nevertheless, changes in the timing of inhibition may potentially produce additive effects with the aberrant supralinear integration of excitatory inputs, converging in a remarkable impact on CA1 place coding,

4.4 Restoring degraded memory in chronic epilepsy

Cognitive symptoms observed in TLE patients include problems with spatial memory and executive function (Elger et al., 2004; Helmstaedter & Kockelmann, 2006; Cánovas et al., 2011; Amlerova et al., 2013).

These deficits have been largely explored in animal models of TLE through behavioral tasks, requiring spatial recognition and working memory. Generally, epileptic animals show retarded

acquisition and impaired retention of visual-spatial information in the Morris water maze test (Gröticke et al., 2008; Rattka et al., 2013), impaired spatial learning in the Barnes maze test (Van Den Herrewegen et al., 2019), and degraded information recall for object displacement during object location memory test (Kim et al., 2020).

Therefore, the question arises if the inhibition of $Na_v1.3$ channels, which normalizes dendritic excitability and place coding in epilepsy, may be exploited to revert epilepsy-associated behavioral deficit. To address this point, in collaboration with A. Haubrich, I used two types of memory tasks.

The OLM test relies on the animal's ability to recall the location of two objects they encountered in the past and preferentially explore the displaced one (Murai et al., 2007). The NOR test evaluates the differences in the exploration time of a novel versus a familiar object (Antunes & Biala, 2012).

The anatomical substrate for both types of memory tests is distinct. Lesions in the perirhinal or prefrontal cortex severely disrupt NOR (Norman & Eacott, 2004) but not OLM (Barker et al., 2007). In contrast, hippocampal damage does not affect object recognition memory but significantly impaired memory for an object's location. (Barker et al., 2011).

Indeed, in the OLM task, epileptic mice showed a performance deficit and did not discriminate the dislocated object. These results align with previous studies in experimental TLE (Pearson et al., 2014; Kim et al., 2020). Strikingly, this deficit was wholly rescued by $Na_v1.3$ blocker treatment.

In contrast, in the NOR task, a hippocampus-independent memory test (Winters et al., 2008), all groups showed a preference for the novel object relative to the familiar one. This suggests the absence of deleterious effect by $Na_v1.3$ blocker treatment in a non-hippocampal memory task.

In addition to impaired spatial learning, working memory deficits are well-described as pervasive comorbidities in TLE patients (Axmacher et al., 2009; López-Frutos et al., 2014; Zamarian et al., 2011) and in epilepsy animal models (Liu et al., 2020; Doucet et al., 2006).

Spatial working memory in animals can be measured through performance in the Y-maze spontaneous alternation task. This task not only recruits hippocampal-dependent processes but also involves the septum, basal forebrain, and prefrontal cortex (Biggan et al., 1991; Dean et al., 2009).

Therefore, I investigated if inhibition of $Na_v1.3$ channels affects performance in working memory using the Y maze spontaneous alternation test. Epileptic animals performed less

correct alternation during the test, but those receiving the $Na_v1.3$ channels blocker showed similar explorative behavior to the control group.

Together these behavioral experiments revealed how the pharmacological inhibition of $Na_v1.3$ channels restores impaired spatial memory as well as working memory in chronic epilepsy.

However, even if the $Na_v1.3$ up-regulation is a plausible explanation for altered dendritic spikes in epilepsy, the palliative effects of the $Na_v1.3$ blocker treatment in-vivo could be caused by a broader range of effects.

Therefore, the question of whether ICA-121431 blocks Nav1.3 channels de-novo expressed in GABAergic neurons or affects $Na_v1.3$ channels in other CNS regions is particularly pertinent.

In the first scenario, antagonizing the activity of the $Na_v1.3$ channel expressed in interneurons is expected to cause impaired GABAergic inhibition and then exert a proconvulsive effect due to E/I imbalance. Nevertheless, this idea is not easily reconciled with the observed substantial reduction of excitation and anticonvulsant actions of use-dependent Na^+ channel blockers in treating TLE. Although the systemic administration of these AEDs also implies a direct interaction with the Na^+ channel expressed in GABAergic neurons.

However, the role of interneurons is far from simply providing synaptic inhibition. Indeed, as previously mentioned, they synchronize neuronal ensembles with precisely timed signaling, and in epilepsy, changes in timing rather than in the amount of inhibition are relevant for spatial memory deficits (Shuman et al., 2020). This raises the possibility that blocking Na^+ channels in GABAergic neurons and then limiting their excitability in epilepsy, in which inhibition is uncoupled, might result in a protective mechanism that limits hippocampal rhythmopathy and then contributes to restoring place coding and spatial memory. Therefore, further experiments are necessary to address the effect of ICA-121431 at the network level and investigate possible interactions with the inhibitory circuits.

It should be noted that these considerations have pointed only to circuits inside the hippocampal CA1 region. This brings to light the second scenario in which the pharmacological treatment with ICA-121431 could exerts any effect on $Na_v1.3$ channels in other CNS areas.

Indeed, although the $Na_v1.3$ isoform in the hippocampus is strongly down-regulated starting from the postnatal stage (Beckh et al., 1989), neurons expressing this Na^+ channel have been described in the adult brain across the cerebral cortex, mesencephalic reticular formation,

mesencephalic trigeminal tract, vestibulospinal tract, spinal trigeminal tract, spinal cord, and motoneurons (Lindia et al., 2003).

Patch-clamp experiments have confirmed the expression of functional $Na_v1.3$ channels in the cardiac tissue, where $Na_v1.3$ channels expressed in ventricular myocytes cells participate in the coupling of cell depolarization to contraction (Maier et al., 2002). In the gastrointestinal epithelium, $Na_v1.3$ channels in enterochromaffin cells are important in regulating serotonin release (Strege et al., 2017).

Moreover, there is large evidence that sodium channels are expressed and participate in multiple functions in non-excitable cells (Black et al., 2013). For instance, $Na_v1.3$ channels have been found in astrocytes (Black et al., 1995; Youngsuk et al., 1994) and cardiac fibroblasts (Li et al., 2009).

When taking these possible roles of $Na_v1.3$ channels into account, it is difficult to foresee whether or not a systemic block of these channels to target a dysfunctional dendritic integration in epilepsy might leads to any central nervous system, cardiac, or immune system side effects.

Therefore, a beneficial therapeutic approach to modulate the up-regulation of Nav1.3 channels in epilepsy requires specific cell-type and region-specific characteristics.

4.5 Future strategy to treat cognitive comorbidities in chronic epilepsy

My work proposes a pharmacological approach to target $Na_v1.3$ channels that are up-regulated in chronic epilepsy, restoring aberrant dendritic integration, place coding, and spatial recognition memory. Together, these results contribute to understanding the biology underlying memory impairments, opening feasible ways to develop treatments to revert cognitive comorbidities in epilepsy.

An ideal pharmacological therapy, in particular when based on Na_v channel modulators, requires high target specificity. Indeed, in clinic, the absence of subtype selectivity can result in toxicities associated with unwanted interactions with off-target Na_v channels, for example, because of cardiac or nervous system toxicity (Bolognesi et al., 1997; Wolfe et al., 2011).

However, an impeccable pharmacological strategy is still difficult to obtain. Indeed, as a consequence of the high degree of structural similarity between individual Na^+ channel isoforms, truly selective antagonists for specific Na^+ channel subunits are extremely rare. After all, ICA-121431 inhibits $Na_v1.3$ as well as $Na_v1.1$ channels (McCormack et al., 2013; Tibery et al., 2019).

Ideally, combining Na$_v$1.3 selective antagonists with anticonvulsant drugs that inhibit other, non-Na$_v$1.3 Na$^+$ channel isoforms may improve traditional pharmacological therapies primarily targeting abnormal somatic action potential firing.

A promising candidate would be the combination of the anticonvulsants S-Lic which have proven efficacy against partial seizures affecting Na$_v$1.2 and 1.6 channels (Holtkamp et al., 2018), and Na$_v$1.3 channel inhibitors. Thus, commonly used AEDs drugs could be strengthened by associating selective Na$_v$1.3 channel modulators for highly specific treatment to improve cognition in epilepsy.

Nevertheless, despite their therapeutic potential in the treatment of epilepsy, Na$^+$ channel modulators are not always a suitable strategy. Indeed, nearly 30% of TLE patients are pharmacoresistant (Regesta & Tanganelli, 1999).

These observations point to a great need for newer therapeutic tools where the standard AEDs are not sufficient and possibly more specific strategies as an adjunct for cognitive enhancement. While pharmacologic treatments have been the only options for many years, recent research raises additional possibilities.

Na$_v$1.3 channels are encoded by the Scn3a gene. The mechanism for the up-regulation of Na$_v$1.3 has been identified as GAPDH mediated post-transcriptional regulation, where the methylation of a specific CpG (cytosine-guanine) site in the Scn3a promoter regulates the expression of this gene (Li et al.,2015). It has been demonstrated not only that the Scn3a mRNA level in epileptic mice was significantly increased but that this upregulation might result from reduced methylation of the CpG site. The anticonvulsant valproic acid, one of the most commonly used drugs for treating seizures, has been shown to epigenetically reduce Na$_v$1.3 expression, enhancing the methylation in the same CpG site from the Scn3a promoter (Tan et al., 2017).

The ketogenic diet represents a potential treatment option to leverage the up-regulation of Na$_v$1.3. Indeed, a high-fat and low-carbohydrate diet treatment is used to control therapy-refractory epilepsies in children (Lin et al.,2016). In these patients, the phosphorylation of GAPDH leads to upregulation of Scn3a, and administration of a ketogenic diet rescues the abnormal expressions of Scn3a, downregulating the GAPDH level.

In alternative to conventional antiepileptic drugs targeting specific proteins like voltage-gated ion channels, RNA-based treatment could potentially exploit an endogenous regulatory mechanism to leverage a pathological gene expression. This is possible thanks to the increased knowledge of the genetic basis of epilepsy and the enormous advances in genome-editing tools.

Strategies to directly modulate the expression of target genes involved in epilepsy, but also in the treatment of other CNS diseases, have been recently proposed with antisense oligonucleotides (ASO) (Bennett, 2019), ribonucleic acid interference (RNAi) (Rinaldi & Wood, 2018; Setten et al., 2019) and with clustered regularly interspaced short palindromic repeats gene editing (CRISPR gene editing) (Doudna, 2020).

ASO therapy is used to alter or inhibit mRNA expression through a variety of mechanisms, including ribonuclease decay of the pre-mRNA, direct steric blockage, and modulation through splicing site binding on pre-mRNA (Bennett & Swayze, 2010; Chan et al., 2006). Notably, the ASO strategy showed promising results in treating different developmental epileptic encephalopathies in animal models, where the therapy was successfully used to reduce seizure onset and lethality in mouse models of Scn8a, Scn2a encephalopathy, and Dravet syndrome. In the first case, ASO was used to target and reduce the mutated pathogenic Scn28 transcript, which leads to a gain-of-function mutation of sodium channel $Na_v1.6$ (Lenk et al., 2020). In the second case, ASOs were explicitly designed to down-regulate Scn2a gene expression in a mouse model of human Scn2a early seizure onset encephalopathy, preventing premature death, suppressing spontaneous seizures, and reverting abnormal neuronal excitability (Li et al., 2020). In the third case, ASO therapy was used to successfully increase the expression of Scn1a transcript in the Dravet syndrome model, suffering from mutations in the Scn1A gene, which result in haploinsufficiency of the sodium channel $Na_v1.1$ (Han et al., 2020). Thus, ASO therapy showed encouraging proof-of-principle results.

RNAi, or Post-Transcriptional gene silencing, is a different gene-editing tool to be taken into consideration. RNAi is based on the suppression of gene expression through translational or transcriptional repression by activating ribonucleases which, along with other enzymes and complexes, coordinately degrade the RNA. RNAi represents another potential tool to target and silencing the pathological Scn3a expression inhibiting the up-regulation of $Na_v1.3$ channels. Recently, an RNAi-based gene therapy approach was used in an animal model of severe childhood epilepsy, where a single treatment eliminated ataxia and decreased lethal seizures (Aimiuwu et al., 2020).

CRISPR-Cas9 is the most revolutionary gene-editing tool which has been awarded a Nobel prize for Chemistry in 2020. It is considered faster, cheaper, and more accurate than previous techniques and has a wide range of potential applications. Indeed, the recent event of the CRISPR/Cas9 gene-editing system (Knott & Doudna, 2018; Zhang et al., 2019), together with the optimization of gene therapy approaches (Doudna, 2020), has become increasingly prominent in the field of neurological diseases treatment and particularly in TLE.

CRISPR/Cas9 can be customized to modulate the endogenous expression of genes by directly targeting their promoters. Indeed, through an approach known as CRISPR activation (CRISPRa), it is possible to increase the expression of specific genes, while via CRISPR interference (CRISPRi), it is possible to silence a gene through transcriptional suppression (Qi et al., 2013). Therefore, CRISPRi is a promising tunable tool candidate to target Scn3a genes and revert increased levels of $Na_v1.3$ channels in chronic epilepsy.

Recent experiments provided the first proof of principle for a CRISPR-based therapy in the kainate mouse model of acquired epilepsy (Colasante & Qiu et al., 2020).

CRISPRa was used to increase the expression of Kcna1 genes encoding the Kv1.1 channel, which is important for the regulation of action potentials firing and synaptic transmission in excitatory neurons. Thus, it was possible to decrease spontaneous seizures and even rescue cognitive impairments. In a different study, the CRISPR/dCas9 system was successfully used to enhances the transcription of Scn1a in a model of Dravet syndrome and significantly rescue epileptic and behavioral phenotypes (Yamagata et al., 2020).

Along with this evidence, genome-editing strategies, like ASO, RNAi, CRISPR/Cas9, have proven efficacy in treating epilepsy in experimental models. Thus, these novel therapeutic approaches offer the capability for cell-type and region-specific modulation of the expression of specific ion channels. This opens the avenue that expression of Nav1.3 channels, underlying degraded dendritic integration, could be one day leveraged for highly specific treatment to improve cognition in epilepsy.

Conclusion

This study provides the first description of altered dendritic integration via dendritic spikes in chronic temporal lobe epilepsy. It is also the first evidence of pathological dendritic spikes in a neurological disorder.

This aberrant dendritic phenotype is likely relevant for degraded spatial coding and memory, uncovering a potential mechanism underlying cognitive impairments in epilepsy.

I have identified the mechanism for this change, which relies on $Na_v1.3$ sodium channels, a channel normally only highly expressed in early development but up-regulated in epilepsy.

Strikingly, this abnormality can be pharmacologically targeted, and doing this significantly improves both spatial codes in-vivo in the hippocampus and impaired spatial memory.

This is relevant because, in contrast to the successful development of numerous anti-seizure drugs, treatments for cognitive comorbidities are very limited, primarily due to an insufficient understanding of the mechanisms of impaired cognition.

Bibliography

Abbott LF., 1999. Lapicque's introduction of the integrate-and-fire model neuron (1907). Brain Res Bull. 50(5-6):303-4.

Aimiuwu OV, Fowler AM, Sah M, Teoh JJ, Kanber A, Pyne NK, Petri S, Rosenthal-Weiss C, Yang M, Harper SQ, Frankel WN., 2020. RNAi-Based Gene Therapy Rescues Developmental and Epileptic Encephalopathy in a Genetic Mouse Model. Mol Ther. 28(7):1706-1716.

Alonso-Nanclares L, Kastanauskaite A, Rodriguez JR, Gonzalez-Soriano J, Defelipe J., 2011. A stereological study of synapse number in the epileptic human hippocampus. Front Neuroanat. 24;5:8.

Amaral DG, Witter MP., 1989. The three-dimensional organization of the hippocampal formation: a review of anatomical data. Neuroscience. 31(3):571-91.

Amaral DG., 1993. Emerging principles of intrinsic hippocampal organization. Curr Opin Neurobiol. 3(2):225-9.

Amaral DG. and Lavenex P., 2007. Hippocampal neuroanatomy. In: Andersen, P., Morris, R., Amaral, D., Bliss, T., and O'Keefe, J. (Eds.), The hippocampus book. New York: Oxford University Press, 37–117.

Amaral DG, Scharfman HE, Lavenex P., 2007. The dentate gyrus: fundamental neuroanatomical organization. Prog Brain Res. 163:3-22.

Amlerova J, Laczo J, Vlcek K, Javurkova A, Andel R, Marusic P., 2013 Risk factors for spatial memory impairment in patients with temporal lobe epilepsy. Epilepsy Behav. 26(1):57-60.

Andersen, P., Bliss, T. V., and Skrede, K. K., 1971. Lamellar organization of hippocampal pathways. Exp. Brain Res. 13, 222–238.

Ang CW, Carlson GC, Coulter DA., 2006. Massive and specific dysregulation of direct cortical input to the hippocampus in temporal lobe epilepsy. J Neurosci. 15;26(46):11850-6.

Anthony JC, Eaton WW, Henderson AS., 1995. Looking to the future in psychiatric epidemiology. Epidemiol Rev. 17(1):240-2.

Antunes M, Biala G., 2012. The novel object recognition memory: neurobiology, test procedure, and its modifications. Cogn Process. 13(2):93-110.

Ariav G., Polsky A., Schiller J., 2003. Submillisecond precision of the input output transformation function mediated by fast sodium dendritic spikes in basal dendrites of CA1 pyramidal neurons. J Neurosci. (21):7750–7758.

Axmacher N, Elger CE, Fell J., 2009. Working memory-related hippocampal deactivation interferes with long-term memory formation. J Neurosci. 29(4):1052-960.

Azouz R., Jensen MS., Yaari Y., 1996. Ionic basis of spike after-depolarization and burst generation in adult rat hippocampal CA1 pyramidal cells. J Physiol. 1;492:211-23.

Banerjee PN, Filippi D, Allen Hauser W., 2009. The descriptive epidemiology of epilepsy-a review. Epilepsy Res. 85(1):31-45.

Bannister NJ, Larkman AU., 1995a. Dendritic morphology of CA1 pyramidal neurones from the rat hippocampus: I. Branching patterns. J Comp Neurol. 11;360(1):150-60.

Bannister NJ, Larkman AU., 1995b. Dendritic morphology of CA1 pyramidal neurones from the rat hippocampus: II. Spine distributions. J Comp Neurol. 11;360(1):161-71.

Barbarosie M, Louvel J, Kurcewicz I, Avoli M., 2000. CA3-released entorhinal seizures disclose dentate gyrus epileptogenicity and unmask a temporoammonic pathway. J Neurophysiol. 83(3):1115-24.

Barker GR, Warburton EC., 2011. When is the hippocampus involved in recognition memory? J Neurosci. 31(29):10721-31.

Barker GR, Bird F, Alexander V, Warburton EC., 2007. Recognition memory for objects, place, and temporal order: a disconnection analysis of the role of the medial prefrontal cortex and perirhinal cortex. J Neurosci. 27(11):2948-57.

Barry J.M., B. Rivard, S.E. Fox, A.A. Fenton, T.C. Sacktor, R.U. Muller, 2012. Inhibition of Protein Kinase M Disrupts the Stable Spatial Discharge of Hippocampal Place Cells in a Familiar Environment, Journal of Neuroscience. 32 13753–13762.

Bartsch T, Döhring J, Rohr A, Jansen O, Deuschl G., 2011. CA1 neurons in the human hippocampus are critical for autobiographical memory, mental time travel, and autonoetic consciousness. Proc. Natl. Acad. Sc.i USA. 18;108(42):17562-7.

Basak R, Narayanan R., 2018. Spatially dispersed synapses yield sharply-tuned place cell responses through dendritic spike initiation. J Physiol. 596(17):4173-4205.

Basak R, Narayanan R., 2020. Robust emergence of sharply tuned place-cell responses in hippocampal neurons with structural and biophysical heterogeneities. Brain Struct Funct. 225(2):567-590.

Bear MF, Abraham WC., 1996. Long-term depression in hippocampus. Annu Rev Neurosci. 19:437-62.

Beck, H., Elger, C. E., 2008. Epilepsy research: a window onto function to and dysfunction of the human brain. Dialogues Clin Neurosci 10, 7–15.

Beck H, Yaari Y., 2008. Plasticity of intrinsic neuronal properties in CNS disorders. Nat Rev Neuros. 9(5):357-69.

Beck H, Goussakov IV, Lie A, Helmstaedter C, Elger CE., 2000. Synaptic plasticity in the human dentate gyrus. J Neurosci. 15;20(18):7080-6.

Becker AJ, Pitsch J, Sochivko D, Opitz T, Staniek M, Chen CC, Campbell KP, Schoch S, Yaari Y, Beck H., 2008. Transcriptional upregulation of Cav3.2 mediates epileptogenesis in the pilocarpine model of epilepsy. J Neurosci. 3;28(49):13341-53.

Beckh S, Noda M, Lübbert H, Numa S., 1989. Differential regulation of three sodium channel messenger RNAs in the rat central nervous system during development. EMBO J. 1;8(12):3611-6.

Bedner P, Dupper A, Hüttmann K, Müller J, Herde MK, Dublin P, Deshpande T, Schramm J, Häussler U, Haas CA, Henneberger C, Theis M, Steinhäuser C., 2015. Astrocyte uncoupling as a cause of human temporal lobe epilepsy. Brain. 138(Pt 5):1208-22.

Benini R, Avoli M., 2005. Rat subicular networks gate hippocampal output activity in an in vitro model of limbic seizures. J Physiol. 1;566(Pt 3):885-900.

Bennett CF, Swayze EE., 2010. RNA targeting therapeutics: molecular mechanisms of antisense oligonucleotides as a therapeutic platform. Annu Rev Pharmacol Toxicol. 50:259-93.

Bennett CF., 2019. Therapeutic Antisense Oligonucleotides Are Coming of Age. Annu Rev Med. 70:307-321.

Bernard C, Anderson A, Becker A, Poolos NP, Beck H, Johnston D., 2004. Acquired dendritic channelopathy in temporal lobe epilepsy. Science. 23;305(5683):532-5.

Biggan SL, Beninger RJ, Cockhill J, Jhamandas K, Boegman RJ., 1991. Quisqualate lesions of rat NBM: selective effects on working memory in a double Y-maze. Brain Res Bull. 26(4):613-6.

Bird CM, Burgess N., 2008. The hippocampus and memory: insights from spatial processing. Nat Rev Neurosci. 9(3):182-94.

Bittner KC, Grienberger C, Vaidya SP, Milstein AD, Macklin JJ, Suh J, Tonegawa S, Magee JC. 2015. Conjunctive input processing drives feature selectivity in hippocampal CA1 neurons. Nat Neurosci. 18(8):1133-42.

Bittner KC, Milstein AD, Grienberger C, Romani S, Magee JC., 2017. Behavioral time scale synaptic plasticity underlies CA1 place fields. Science. 357(6355):1033-1036.

Black JA, Westenbroek R, Minturn JE, Ransom BR, Catterall WA, Waxman SG., 1995. Isoform-specific expression of sodium channels in astrocytes in vitro: immunocytochemical observations. Glia. 14(2):133-44.

Black JA, Waxman SG., 2013. Noncanonical roles of voltage-gated sodium channels. Neuron. 80(2):280-91.

Bliss TV, Collingridge GL., 1993. A synaptic model of memory: long-term potentiation in the hippocampus. Nature. 361(6407):31-9.

Bloss EB, Cembrowski MS, Karsh B, Colonell J, Fetter RD, Spruston N., 2016. Structured Dendritic Inhibition Supports Branch-Selective Integration in CA1 Pyramidal Cells. Neuron. 89(5):1016-30.

Blumcke, I., Becker, A. J., Klein, C., Scheiwe, C., Lie, A. A., Beck, H., Waha, A., Friedl, Kuhn, R., Emson, P., Elger, C., Wiestler, O. D., 2000. Temporal lobe epilepsy associated up-regulation of metabotropic glutamate receptors: correlated changes in mGluR1 mRNA and protein expression in experimental animals and human patients. J Neuropathol Exp Neurol 59, 1–10.

Blümcke and Wiestler, 2002 Ammon's Horn Sclerosis: A Maldevelopmental Disorder Associated with Temporal Lobe Epilepsy. Brain Pathol. 12(2):199-211.

Blümcke I, Pauli E, Clusmann H, Schramm J, Becker A, Elger C, Merschhemke M, Meencke HJ, Lehmann T, Von Deimling A, Scheiwe C, Zentner J, Volk B, Romstöck J, Stefan H, Hildebrandt M, 2007. A new clinico-pathological classification system for mesial temporal sclerosis. Acta Neuropathol. 113(3):235-44.

Blümcke I, Coras R, Miyata H, Özkara C, 2012. Defining clinico-neuropathological subtypes of mesial temporal lobe epilepsy with hippocampal sclerosis. In: Brain Pathology. 22(3):402-11.

Blümcke I., Thom, M., Aronica, E., Armstrong, D. D., Bartolomei, F., Bernasconi, A., Bernasconi, N., Bien, C. G., Cendes, F., Coras, R., Cross, J. H., Jacques, T. S., Oz, B., Ozkara, Perucca, E., Sisodiya, S., Wiebe, S., and Spreafico, R., 2013. International consensus classification of hippocampal sclerosis in temporal lobe epilepsy: a task force report from the ILAE commission on diagnostic methods. Epilepsia 54, 1315–1329.

Bohbot VD, Iaria G, Petrides M., 2004. Hippocampal function and spatial memory: evidence from functional neuroimaging in healthy participants and performance of patients with medial temporal lobe resections. Neuropsychology. (3):418-25.

Bolognesi R, Tsialtas D, Vasini P, Conti M, Manca C., 1997. Abnormal ventricular repolarization mimicking myocardial infarction after heterocyclic antidepressant overdose. Am J Cardiol. 79(2):242-5.

Bonansco C., M. Fuenzalida, 2016. Plasticity of Hippocampal Excitatory-Inhibitory Balance: Missing the Synaptic Control in the Epileptic Brain, Neural Plasticity. 1– 13.

Bonthius DJ, McKim R, Koele L, Harb H, Karacay B, Mahoney J, Pantazis NJ., 2004. Use of frozen sections to determine neuronal number in the murine hippocampus and neocortex using the optical disector and optical fractionator. Brain Res Brain Res Protoc. 14(1):45-57.

Bragin A, Engel J Jr, Wilson CL, Fried I, Mathern GW., 1999. Hippocampal and entorhinal cortex high-frequency oscillations (100--500 Hz) in human epileptic brain and in kainic acid-treated rats with chronic seizures. Epilepsia. 40(2):127-37.

Bragin A, Engel J Jr, Wilson CL, Vizentin E, Mathern GW., 1999. Electrophysiologic analysis of a chronic seizure model after unilateral hippocampal KA injection. Epilepsia. 40(9):1210-21.

Bratz E., 1899. Ammonshornbefunde der epileptischen. Arch Psychiatr Nervenkr. 31:820-836.

Brooks-Kayal AR, Bath KG, Berg AT, Galanopoulou AS, Holmes GL, Jensen FE, Kanner AM, O'Brien TJ, Whittemore VH, Winawer MR, Patel M, Scharfman HE., 2013. Issues related to symptomatic and disease-modifying treatments affecting cognitive and neuropsychiatric comorbidities of epilepsy. Epilepsia. 4(0 4):44-60.

Brown FC, Hirsch LJ, Spencer DD., 2015. Spatial memory for asymmetrical dot locations predicts lateralization among patients with presurgical mesial temporal lobe epilepsy. Epilepsy Behav. 52(Pt A):19-24.

Bui AD, Nguyen TM, Limouse C, Kim HK, Szabo GG, Felong S, Maroso M, Soltesz I., 2018. Dentate gyrus mossy cells control spontaneous convulsive seizures and spatial memory. Science. 16;359(6377):787-790.

Burgess N, O'Keefe J., 2011. Models of place and grid cell firing and theta rhythmicity. Curr Opin Neurobiol. 21(5):734-44.

Butler C.R., A.Z. Zeman, 2008. Recent insights into the impairment of memory in epilepsy: transient epileptic amnesia, accelerated long-term forgetting and remote memory impairment, Brain. 131 2243–2263.

Buzsáki G, Leung LW, Vanderwolf CH., 1983. Cellular bases of hippocampal EEG in the behaving rat. Brain Res. 287(2):139-71.

Buzsáki G., 1989. Two-stage model of memory trace formation: a role for "noisy" brain states. Neuroscience. (3):551-70.

Buzsáki G., 2002. Theta oscillations in the hippocampus. Neuron. 31;33(3):325-40.

Buzsáki G., 2010. Neural syntax: cell assemblies, synapsembles, and readers. Neuron. 68(3):362-85.

Buzsáki G, Moser EI., 2013. Memory, navigation and theta rhythm in the hippocampal-entorhinal system. Nat Neurosci. 16(2):130-8.

Cánovas R, León I, Serrano P, Roldán MD, Cimadevilla JM., 2011. Spatial navigation impairment in patients with refractory temporal lobe epilepsy: Evidence from a new virtual reality-based task. Epilepsy Behav. 22:364–9.

Catterall WA., 2000. From ionic currents to molecular mechanisms: the structure and function of voltage-gated sodium channels. Neuron. 26(1):13-25.

Catterall WA., 2012. Voltage-gated sodium channels at 60: structure, function and pathophysiology. J Physiol. 1;590(11):2577-89.

Cavazos JE, Zhang P, Qazi R, Sutula TP., 2003. Ultrastructural features of sprouted mossy fiber synapses in kindled and kainic acid-treated rats. J Comp Neurol. 458(3):272-92.

Cendes, F., Sakamoto, A. C., Spreafico, R., Bingaman, W., Becker, A. J., 2014. Epilepsies associated with hippocampal sclerosis. Acta Neuropathol 128, 21–37.

Chan JH, Lim S, Wong WS., 2006. Antisense oligonucleotides: from design to therapeutic application. Clin Exp Pharmacol Physiol. 33(5-6):533-40.

Cheah CS, Westenbroek RE, Roden WH, Kalume F, Oakley JC, Jansen LA, Catterall WA., 2013. Correlations in timing of sodium channel expression, epilepsy, and sudden death in Dravet syndrome. Channels. 7(6):468-72.

Chen C, Westenbroek RE, Xu X, Edwards CA, Sorenson DR, Chen Y, McEwen DP, O'Malley HA, Bharucha V, Meadows LS, Knudsen GA, Vilaythong A, Noebels JL, Saunders TL, Scheuer T, Shrager P, Catterall WA, Isom LL., 2004. Mice lacking sodium channel beta1 subunits display defects in neuronal excitability, sodium channel expression, and nodal architecture. J Neurosci. 24(16):4030-42.

Chen Y. H., Dale, T. J., Romanos, M. A., Whitaker, W. R. J., Xie, X. M., Clare, J. J., 2000. Cloning, distribution and functional analysis of the type III sodium channel from human brain. Eur. J. Neurosci. 12, 4281–4289.

Chen S, Su H, Yue C, Remy S, Royeck M, Sochivko D, Opitz T, Beck H, Yaari Y., 2011. An increase in persistent sodium current contributes to intrinsic neuronal bursting after status epilepticus. J Neurophysiol. 105:117–129.

Cheung M., A.S. Chan, Y. Chan, J.M.K. Lam, W. Lam, 2006. Effects of Illness Duration on Memory Processing of Patients with Temporal Lobe Epilepsy, Epilepsia. 47 1320–1328.

Chevaleyre V, Siegelbaum SA., 2010. Strong CA2 pyramidal neuron synapses define a powerful disynaptic cortico-hippocampal loop. Neuron. 66(4):560-72.

Chiu YC, Algase D, Whall A, Liang J, Liu HC, Lin KN, Wang PN, 2004. Getting lost: directed attention and executive functions in early Alzheimer's disease patients. Dementia and Geriatric Cognit. Disord.. 17 (3): 174–80.

Cohen JD, Bolstad M, Lee AK., 2017. Experience-dependent shaping of hippocampal CA1 intracellular activity in novel and familiar environments. Elife. 6:e23040.

Colbert CM, Magee JC, Hoffman DA, Johnston D., 1997. Slow recovery from inactivation of Na+ channels underlies the activity-dependent attenuation of dendritic action potentials in hippocampal CA1 pyramidal neurons. J Neurosci. 1;17(17):6512-21.

Collingridge GL, Kehl SJ, McLennan H., 1983. Excitatory amino acids in synaptic transmission in the Schaffer collateral-commissural pathway of the rat hippocampus. J Physiol. 334:33-46.

Cossart R, Dinocourt C, Hirsch JC, Merchan-Perez A, De Felipe J, Ben-Ari Y, Esclapez M, Bernard C., 2001. Dendritic but not somatic GABAergic inhibition is decreased in experimental epilepsy. Nat Neurosci. 4(1):52-62.

Cummins TR, Aglieco F, Renganathan M, Herzog RI, Dib-Hajj SD, Waxman SG., 2001. Nav1.3 sodium channels: rapid repriming and slow closed-state inactivation display quantitative differences after expression in a mammalian cell line and in spinal sensory neurons. J Neurosci. 21(16):5952-61.

Curia, G., Lucchi, C., Vinet, J., Gualtieri, F., Marinelli, C., Torsello, A., Costantino, L., and Biagini, G. 2014. Pathophysiogenesis of mesial temporal lobe epilepsy: is prevention of damage antiepileptogenic? Curr Med Chem. 21, 663–688.

Dana H, Chen TW, Hu A, Shields BC, Guo C, Looger LL, Kim DS, Svoboda K., 2014. Thy1-GCaMP6 transgenic mice for neuronal population imaging in vivo. PLoS One. 24;9(9):e108697.

Danielson NB, Kaifosh P, Zaremba JD, Lovett-Barron M, Tsai J, Denny CA, Balough EM, Goldberg AR, Drew LJ, Hen R, Losonczy A, Kheirbek MA., 2016. Distinct Contribution of Adult-Born Hippocampal Granule Cells to Context Encoding. Neuron. 6;90(1):101-12.

Danielson NB, Zaremba JD, Kaifosh P, Bowler J, Ladow M, Losonczy A., 2016. Sublayer-Specific Coding Dynamics during Spatial Navigation and Learning in Hippocampal Area CA1. Neuron. 3;91(3):652-65.

Davidson M, Dorris L, O'Regan M, Zuberi SM., 2017. Memory consolidation and accelerated forgetting in children with idiopathic generalized epilepsy. Epilepsy Behav. 11:394–4

Davies JA., 1995. Mechanisms of action of antiepileptic drugs. Seizure. 4(4):267-71.

Davies KG, Hermann BP, Dohan FC, Foley KT, Bush AJ, Wyler AR, 1996. Relationship of hippocampal sclerosis to duration and age of onset of epilepsy, and childhood febrile seizures in temporal lobectomy patients. Epilepsy Res. 24(2):119-26.

Dean O, Bush AI, Berk M, Copolov DL, van den Buuse M., 2009. Glutathione depletion in the brain disrupts short-term spatial memory in the Y-maze in rats and mice. Behav Brain Res. 198(1):258-62.

Devinsky O, Vezzani A, O'Brien TJ, Jette N, Scheffer IE, de Curtis M, Perucca P., 2018. Epilepsy. Nat Rev Dis Primers. 4:18024

Dinocourt C, Petanjek Z, Freund TF, Ben-Ari Y, Esclapez M., 2003. Loss of interneurons innervating pyramidal cell dendrites and axon initial segments in the CA1 region of the hippocampus following pilocarpine-induced seizures. J Comp Neurol. 459(4):407-25.

Dodrill CB., 2002. Progressive cognitive decline in adolescents and adults with epilepsy. Prog Brain Res. 135:399-407.

Doudna JA., 2020. The promise and challenge of therapeutic genome editing. Nature. 578(7794):229-236.

Duarte IC, Ferreira C, Marques J, Castelo-Branco M., 2014. Anterior/posterior competitive deactivation/activation dichotomy in the human hippocampus as revealed by a 3D navigation task. PLoS One. 27;9(1):e86213.

Dudman JT, Tsay D, Siegelbaum SA., 2007. A role for synaptic inputs at distal dendrites: instructive signals for hippocampal long-term plasticity. Neuron. 56(5):866-79.

Dyhrfjeld-Johnsen J, Morgan RJ, Soltesz I., 2009. Double Trouble? Potential for Hyperexcitability Following Both Channelopathic up- and Downregulation of I(h) in Epilepsy. Front Neurosci. 1;3(1):25-33.

Ego-Stengel V, Wilson MA., 2010. Disruption of ripple-associated hippocampal activity during rest impairs spatial learning in the rat. Hippocampus. 20(1):1-10.

Ekstrom AD, Kahana MJ, Caplan JB, Fields TA, Isham EA, Newman EL, Fried I., 2003. Cellular networks underlying human spatial navigation. Nature. 11;425(6954):184-8.

Elger, C. E., Helmstaedter, C., Kurthen, M., 2004. Chronic epilepsy and cognition. Lancet Neurol 3, 663–672.

Elmslie F, Gardiner M., 1995. Genetics of the epilepsies. Curr Opin Neurol. 8(2):126-9.

Engel, J., 1996. Introduction to temporal lobe epilepsy. Epilepsy Res 26, 141–150.

Engel, J., 2001a. A proposed diagnostic scheme for people with epileptic seizures and with epilepsy: report of the ILAE Task Force on Classification and Terminology. Epilepsia 42, 796–803.

Engel, J., 2001b. Mesial temporal lobe epilepsy: what have we learned? Neuroscientist 7, 340–352.

Engel, J., 2006. Report of the ILAE classification core group. Epilepsia 47, 1558–1568.

Engel, J., Pedley, T. A., 2008. Introduction: What is Epilepsy? In: Engel, J. and Pedley, T. A. (eds) Epilepsy: A comprehensive textbook. Lippincott Williams & Wilkins, Philadelphia, p. 1-8.

Ewell LA, Fischer KB, Leibold C, Leutgeb S, Leutgeb JK., 2019. The impact of pathological high-frequency oscillations on hippocampal network activity in rats with chronic epilepsy. Elife. 22;8:e42148.

Fisher RS, Van Emde Boas W, Blume W, Elger C, Genton P, Lee P, Engel J (2005) Epileptic seizures and epilepsy: Definitions proposed by the International League Against Epilepsy (ILAE) and the International Bureau for Epilepsy (IBE). Epilepsia.

Fisher RS, Acevedo C, Arzimanoglou A, Bogacz A, Cross JH, Elger CE, Engel J, Forsgren L, French JA, Glynn M, Hesdorffer DC, Lee BI, Mathern GW, Moshé SL, Perucca E, Scheffer IE, Tomson T, Watanabe M, Wiebe S (2014) ILAE Official Report: A practical clinical definition of epilepsy. Epilepsia.

Fisher RS, Cross JH, French JA, Higurashi N, Hirsch E, Jansen FE, Lagae L, Moshé SL, Peltola J, Roulet Perez E, Scheffer IE, Zuberi SM (2018) Operational classification of seizure types by the International League Against Epilepsy: position paper of the ILAE Commission for Classification and Terminology. Zeitschrift fur Epileptol.

Fleidervish IA, Gutnick MJ., 1996. Kinetics of slow inactivation of persistent sodium current in layer V neurons of mouse neocortical slices. J Neurophysiol. 76(3):2125-30.

Frick A, Magee J, Koester HJ, Migliore M, Johnston D., 2003. Normalization of Ca^{2+} signals by small oblique dendrites of CA1 pyramidal neurons. *J Neurosci*. 23(8):3243-3250.

Fyhn M, Molden S, Witter MP, Moser EI, Moser MB., 2004. Spatial representation in the entorhinal cortex. Science. 305(5688):1258-64.

Gasparini S, Migliore M, Magee JC., 2004. On the initiation and propagation of dendritic spikes in CA1 pyramidal neurons. J Neurosci. 8;24(49):11046-56.

Gastaldi M, Bartolomei F, Massacrier A, Planells R, Robaglia-Schlupp A, Cau P., 1997. Increase in mRNAs encoding neonatal II and III sodium channel alpha-isoforms during kainate-induced seizures in adult rat hippocampus. Brain Res Mol Brain Res. 44(2):179-90.

George MS, Abbott LF, Siegelbaum SA., 2009. HCN hyperpolarization-activated cation channels inhibit EPSPs by interactions with M-type K(+) channels. Nat Neurosci. 12(5):577-84.

Gidon A, Segev I., 2012. Principles governing the operation of synaptic inhibition in dendrites. Neuron. 75(2):330-41.

Girardeau G, Inema I, Buzsáki G., 2017. Reactivations of emotional memory in the hippocampus-amygdala system during sleep. Nat Neurosci. 20(11):1634-1642.

Girardeau G, Benchenane K, Wiener SI, Buzsáki G, Zugaro MB., 2009. Selective suppression of hippocampal ripples impairs spatial memory. Nat Neurosci. 12(10):1222-3.

Girardi-Schappo M, Fadaie F, Lee HM, Caldairou B, Sziklas V, Crane J, Bernhardt BC, Bernasconi A, Bernasconi N., 2021. Altered communication dynamics reflect cognitive deficits in temporal lobe epilepsy. Epilepsia. 62(4):1022-1033.

Goldin, A. L., 2001. Resurgence of sodium channel research. Annu Rev Physiol. 63, 871–894.

Golding NL, Spruston N., 1998. Dendritic sodium spikes are variable triggers of axonal action potentials in hippocampal CA1 pyramidal neurons. Neuron. 21(5):1189-200.

Golding NL, Jung HY, Mickus T, Spruston N., 1999. Dendritic calcium spike initiation and repolarization are controlled by distinct potassium channel subtypes in CA1 pyramidal neurons. J Neurosci. 19(20):8789-98.

Golding NL, Staff NP, Spruston N., 2002. Dendritic spikes as a mechanism for cooperative long-term potentiation. Nature. 18;418(6895):326-31.

Gómez González JF, Mel BW, Poirazi P. 2011. Distinguishing Linear vs. Non-Linear Integration in CA1 Radial Oblique Dendrites: It's about Time. Front Comput Neurosci. 14;5:44.

Gothard KM, Skaggs WE, Moore KM, McNaughton BL., 1996a. Binding of hippocampal CA1 neural activity to multiple reference frames in a landmark-based navigation task. J Neurosci. 15;16(2):823-35.

Gothard KM, Skaggs WE, McNaughton BL., 1996b. Dynamics of mismatch correction in the hippocampal ensemble code for space: interaction between path integration and environmental cues. J Neurosci. (24):8027-40.

Govindarajan A, Kelleher RJ, Tonegawa S., 2006. A clustered plasticity model of long-term memory engrams. Nat Rev Neurosci. 7(7):575-83.

Greenberg DS, Kerr JN., 2009. Automated correction of fast motion artifacts for two-photon imaging of awake animals. J Neurosci Methods. 15;176(1):1-15.

Grewe P, Lahr D, Kohsik A, Dyck E, Markowitsch HJ, Bien CG, Botsch M, Piefke M., 2014. Real-life memory and spatial navigation in patients with focal epilepsy: ecological validity of a virtual reality supermarket task. Epilepsy Behav. 31:57-66.

Grienberger C, Chen X, Konnerth A., 2014. NMDA receptor-dependent multidendrite Ca(2+) spikes required for hippocampal burst firing in vivo. Neuron. 81(6):1274-1281.

Gröticke I, Hoffmann K, Löscher W., 2008. Behavioral alterations in a mouse model of temporal lobe epilepsy induced by intrahippocampal injection of kainate. Exp Neurol. 213:71–83.

Guerreiro CA. Epilepsy: Is there hope? Indian J Med Res. 144(5):657-660.

Gulledge AT, Kampa BM, Stuart GJ., 2005. Synaptic integration in dendritic trees. J Neurobiol. 64(1):75-90.

Guo F, Yu N, Cai JQ, Quinn T, Zong ZH, Zeng YJ, Hao LY., 2008. Voltage-gated sodium channel Nav1.1, Nav1.3 and beta1 subunit were up-regulated in the hippocampus of spontaneously epileptic rat. Brain Res. 75(1):179-87.

Gupta AS, van der Meer MA, Touretzky DS, Redish AD., 2012. Segmentation of spatial experience by hippocampal θ sequences. Nat Neurosci. 15(7):1032-9.

Halford JJ, Edwards JC., 2020. Seizure freedom as an outcome in epilepsy treatment clinical trials. Acta Neurol Scand. 142(2):91-107.

Hamilton SE, Loose MD, Qi M, Levey AI, Hille B, McKnight GS, Idzerda RL, Nathanson NM., 1997. Disruption of the m1 receptor gene ablates muscarinic receptor-dependent M current regulation and seizure activity in mice. Proc Natl Acad Sci U S A. 94(24):13311-6.

Han Z, Chen C, Christiansen A, Ji S, Lin Q, Anumonwo C, Liu C, Leiser SC, Meena, Aznarez I, Liau G, Isom LL., 2020. Antisense oligonucleotides increase Scn1a expression and reduce seizures and SUDEP incidence in a mouse model of Dravet syndrome. Sci Transl Med. 12(558):eaaz6100.

Hartley T, Lever C., 2014. Know your limits: the role of boundaries in the development of spatial representation. Neuron. 2;82(1):1-3

Hashemi P, Fahanik Babaei J, Vazifekhah S, Nikbakht F., 2019. Evaluation of the neuroprotective, anticonvulsant, and cognition-improvement effects of apigenin in temporal lobe epilepsy: Involvement of the mitochondrial apoptotic pathway. Iran J Basic Med Sci. 22(7):752-758.

Häusser, M., Spruston, N., and Stuart, G. J., 2000. Diversity and dynamics of dendritic signaling. Science, 290(5492):739–744.

Häusser M, Mel B., 2003. Dendrites: bug or feature? Curr Opin Neurobiol. 13(3):372-83.

Helmstaedter C. and Witt J.A., 2012. Clinical neuropsychology in epilepsy: theoretical and practical issues. Handbook of clinical neurology. 107:437-459.

Helmstaedter C, Kockelmann E., 2006. Cognitive outcomes in patients with chronic temporal lobe epilepsy. Epilepsia. 47 Suppl 2:96-8.

Helmstaedter C, Elger CE., 2009. Chronic temporal lobe epilepsy: a neurodevelopmental or progressively dementing disease? Brain. 132(Pt 10):2822-30.

Helmstaedter C., 2002. Effects of chronic epilepsy on declarative memory systems. Prog Brain Res. 135:439-53.

Helmstaedter C, Kurthen M., 2001. Memory and epilepsy: characteristics, course, and influence of drugs and surgery. Curr Opin Neurol. 14(2):211-6.

Hermann BP, Seidenberg M, Schoenfeld J, Davies K., 1997. Neuropsychological characteristics of the syndrome of mesial temporal lobe epilepsy. Arch Neurol. 54(4):369-76.

Hermann B, Meador KJ, Gaillard WD, Cramer JA., 2010. Cognition across the lifespan: antiepileptic drugs, epilepsy, or both? Epilepsy Behav. 17:1–5.

Hill DN, Varga Z, Jia H, Sakmann B, Konnerth A., 2013. Multibranch activity in basal and tuft dendrites during firing of layer 5 cortical neurons in vivo. Proc Natl Acad Sci USA. 13;110(33):13618-23.

Hille B., 1971. The permeability of the sodium channel to organic cations in myelinated nerve. J Gen Physiol. 58(6):599-619.

Hille B., 1972. Ionic permeability changes in active axon membranes. Arch Intern Med. 129(2):293-8.

Hitti FL, Siegelbaum SA., 2014. The hippocampal CA2 region is essential for social memory. Nature. 508(7494):88-92.

Hoffman DA, Magee JC, Colbert CM, Johnston D., 1997. K^+ channel regulation of signal propagation in dendrites of hippocampal pyramidal neurons. Nature. 26;387(6636):869-75.

Holthoff K., 2004. Regenerative dendritic spikes and synaptic plasticity. Cur Neurov Res. 1(4):381-7.

Holtkamp D, Opitz T, Hebeisen S, Soares-da-Silva P, Beck H., 2018. Effects of eslicarbazepine on slow inactivation processes of sodium channels in dentate gyrus granule cells. Epilepsia. 59(8):1492-1506.

Hötting K, Katz-Biletzky T, Malina T, Lindenau M, Bengner T., 2010. Long-term versus short-term memory deficits for faces in temporal lobe and generalized epilepsy patients. J Int Neuropsychol Soc. (3):574-8.

Hoppe C, Elger CE, Helmstaedter C., 2007. Long-term memory impairment in patients with focal epilepsy. Epilepsia. 48 Suppl 9:26-9.

Horak PC, Meisenhelter S, Song Y, Testorf ME, Kahana MJ, Viles WD, et al., 2017. Interictal epileptiform discharges impair word recall in multiple brain areas. Epilepsia. 58:373–80.

Hort J, Laczó J, Vyhnálek M, Bojar M, Bures J, Vlcek K., 2007. Spatial navigation deficit in amnestic mild cognitive impairment. Proc Natl Acad Sci U S A. 104(10):4042-7.

Ikegaya Y, Saito H, Abe K., 1994. Attenuated hippocampal long-term potentiation in basolateral amygdala-lesioned rats. Brain Res. 5;656(1):157-64.

Iaria G, Petrides M, Dagher A, Pike B, Bohbot VD., 2003. Cognitive strategies dependent on the hippocampus and caudate nucleus in human navigation: variability and change with practice. J Neurosci. 23(13):5945-52.

Jacobs J, Levan P, Châtillon CE, Olivier A, Dubeau F, Gotman J., 2009. High frequency oscillations in intracranial EEGs mark epileptogenicity rather than lesion type. Brain. 132(Pt 4):1022-37.

Jensen MS, Azouz R, Yaari Y., 1994. Variant firing patterns in rat hippocampal pyramidal cells modulated by extracellular potassium. J Neurophysiol. 71(3):831-9.

Jensen MS, Azouz R, Yaari Y., 1996. Spike after-depolarization and burst generation in adult rat hippocampal CA1 pyramidal cells. J Physiol. 1;492:199-210.

Jodie Wilcox, Mike Kerr, 2006. Epilepsy in people with learning disabilities. Volume 5, Issue 10, Pages 372-377.

Johnston D, Magee JC, Colbert CM, Cristie BR., 1996. Active properties of neuronal dendrites. Annu Rev Neurosci. 19:165-86.

Johnson, M. R., Sander, J. W., 2001. The clinical impact of epilepsy genetics. J Neurol Neuros Psych 70, 428–430.

Jung HY, Mickus T, Spruston N., 1997. Prolonged sodium channel inactivation contributes to dendritic action potential attenuation in hippocampal pyramidal neurons. J Neurosci. 1;17(17):6639-46.

Kalitzin S, Petkov G, Suffczynski P, Grigorovsky V, Bardakjian BL, Lopes da Silva F, Carlen PL., 2019. Epilepsy as a manifestation of a multistate network of oscillatory systems. Neurobiol Dis. 130:104488.

Kamondi A, Acsády L, Buzsáki G., 1998. Dendritic spikes are enhanced by cooperative network activity in the intact hippocampus. J Neurosci. 15;18(10):3919-28.

Kampa BM, Letzkus JJ, Stuart GJ., 2006. Requirement of dendritic calcium spikes for induction of spike-timing-dependent synaptic plasticity. J Physiol. 1;574(Pt 1):283-90.

Karnam HB, Zhou JL, Huang LT, Zhao Q, Shatskikh T, Holmes GL., 2009. Early life seizures cause long-standing impairment of the hippocampal map. Exp Neurol. 217(2):378-87.

Kasperaviciute, D., Catarino, C. B., Matarin, M., Leu, C., Novy, J., Tostevin, A., Leal, B., Hessel, E. V. S., Hallmann, K., Hildebrand, M. S., Dahl, H.-H. M., Ryten, M., Trabzuni, D., Ramasamy, A., Alhusaini, S., Doherty, C. P., Dorn, Sisodiya, S. M., 2013. Epilepsy, hippocampal sclerosis and febrile seizures linked by common genetic variation around SCN1A. Brain. 136, 3140–3150.

Katz Y, Menon V, Nicholson DA, Geinisman Y, Kath WL, Spruston N., 2009. Synapse distribution suggests a two-stage model of dendritic integration in CA1 pyramidal neurons. Neuron. 30;63(2):171-7.

Kelly T, Beck H., 2017. Functional properties of granule cells with hilar basal dendrites in the epileptic dentate gyrus. Epilepsia. 58(1):160-171.

Kerr, M. P., 2012. The impact of epilepsy on patients' lives. Acta Neurol Scand Suppl (194):1-9.

Kim HK, Gschwind T, Nguyen TM, Bui AD, Felong S, Ampig K, Suh D, Ciernia AV, Wood MA, Soltesz I., 2020. Optogenetic intervention of seizures improves spatial memory in a mouse model of chronic temporal lobe epilepsy. Epilepsia. 61(3):561-571.

Kim TH, Reid CA, Petrou S., 2015. Oxcarbazepine and its active metabolite, (S)-licarbazepine, exacerbate seizures in a mouse model of genetic generalized epilepsy. Epilepsia. 56(1):e6-9.

Klausberger T, Magill PJ, Márton LF, Roberts JD, Cobden PM, Buzsáki G, Somogyi P., 2003. Brain-state- and cell-type-specific firing of hippocampal interneurons in vivo. Nature. 421(6925):844-8.

Knierim JJ, Lee I, Hargreaves EL., 2006. Hippocampal place cells: parallel input streams, subregional processing, and implications for episodic memory. Hippocampus. 16(9):755-64.

Knott GJ, Doudna JA. CRISPR-Cas guides the future of genetic engineering. Science. 2018 361(6405):866-869.

Zhang, F., 2019. Development of CRISPR-Cas systems for genome editing and beyond. Quar. Rev. Bioph.. 52, 6.

Koch, 1999. Biophysics of computation: Information processing in single neurons. Oxford University Press.

Kohara K, Pignatelli M, Rivest AJ, Jung HY, Kitamura T, Suh J, Frank D, Kajikawa K, Mise N, Obata Y, Wickersham IR, Tonegawa S., 2014. Cell type-specific genetic and optogenetic tools reveal hippocampal CA2 circuits. Nat Neurosci. 17(2):269-79.

Kraeuter AK, Guest PC, Sarnyai Z., 2019. The Y-Maze for Assessment of Spatial Working and Reference Memory in Mice. Methods Mol Biol. 1916:105-111.

Kubie JL, Levy ERJ, Fenton AA., 2020. Is hippocampal remapping the physiological basis for context? Hippocampus. 30(8):851-864.

Kuwabara, T., Hasegawa, D., Kobayashi, M., Fujita, M., and Orima, H., 2010. Clinical magnetic resonance volumetry of the hippocampus in 58 epileptic dogs. Vet Radiol Ultrasound 51, 485–490.

Larkum ME, Zhu JJ, Sakmann B., 2001. Dendritic mechanisms underlying the coupling of the dendritic with the axonal action potential initiation zone of adult rat layer 5 pyramidal neurons. J Physiol. 1;533(Pt 2):447-66.

Larkum ME, Nevian T., 2008. Synaptic clustering by dendritic signalling mechanisms. Curr Opin Neurobiol. 18(3):321-31.

Larkum, M. E., Nevian, T., Sandler, M., Polsky, A., and Schiller, J., 2009. Synaptic integration in tuft dendrites of layer 5 pyramidal neurons: a new unifying principle. Science, 325(5941):756–760.

Lavenex P, Banta Lavenex P, Amaral DG., 2007. Postnatal development of the primate hippocampal formation. Dev Neurosci. 29(1-2):179-92.

Lee D, Lin BJ, Lee AK., 2012. Hippocampal place fields emerge upon single -cell manipulation of excitability during behavior. Science. 337(6096):849-53.

LeGates TA, Kvarta MD, Tooley JR, Francis TC, Lobo MK, Creed MC, Thompson SM., 2018. Reward behaviour is regulated by the strength of hippocampus-nucleus accumbens synapses. Nature. 564(7735):258-262.

Lenk GM, Jafar-Nejad P, Hill SF, Huffman LD, Smolen CE, Wagnon JL, Petit H, Yu W, Ziobro J, Bhatia K, Parent J, Giger RJ, Rigo F, Meisler MH., 2020. Scn8a Antisense Oligonucleotide Is Protective in Mouse Models of SCN8A Encephalopathy and Dravet Syndrome. Ann Neurol. 87(3):339-346.

Lenck-Santini, P. P. & Scott, R. C., 2015. Mechanisms responsible for cognitive impairment in epilepsy. Cold Spring Harb. Perspect. Med. 5, pii: a022772.

Lenck-Santini, P. P. & Holmes, G. L., 2008. Altered phase precession and compression of temporal sequences by place cells in epileptic rats. J. Neurosci. 28, 5053–5062.

Lévesque M, Salami P, Shiri Z, Avoli M., 2018. Interictal oscillations and focal epileptic disorders. Eur J Neurosci. 48(8):2915-2927.

Lévesque M, Avoli M., 2013. The kainic acid model of temporal lobe epilepsy. Neurosci Biobehav Rev. 37(10 Pt 2):2887-99.

Li GR, Sun HY, Chen JB, Zhou Y, Tse HF, Lau CP., 2009. Characterization of multiple ion channels in cultured human cardiac fibroblasts. PLoS One. 4(10):e7307.

Li HJ, Wan RP, Tang LJ, Liu SJ, Zhao QH, Gao MM, Yi YH, Liao WP, Sun XF, Long YS., 2015. Alteration of Scn3a expression is mediated via CpG methylation and MBD2 in mouse hippocampus during postnatal development and seizure condition. Biochim Biophys Acta. 1849(1):1-9.

Li XG, Somogyi P, Ylinen A, Buzsáki G., 1994. The hippocampal CA3 network: an in vivo intracellular labeling study. J Comp Neurol. 8;339(2):181-208.

Lin GW, Lu P, Zeng T, Tang HL, Chen YH, Liu SJ, Gao MM, Zhao QH, Yi YH, Long YS., 2017. GAPDH-mediated posttranscriptional regulations of sodium channel Scn1a and Scn3a genes under seizure and ketogenic diet conditions. Neuropharmacology. 113(Pt A):480-489.

Lindia JA, Abbadie C., 2003. Distribution of the voltage gated sodium channel Na(v)1.3-like immunoreactivity in the adult rat central nervous system. Brain Res. 960(1-2):132-41.

Lipowsky R, Gillessen T, Alzheimer C., 1996. Dendritic Na$^+$ channels amplify EPSPs in hippocampal CA1 pyramidal cells. J Neurophysiol. 76(4):2181-91.

Liu C, Wen Y, Huang H, Lin W, Huang M, Lin R, Ma Y., 2019. Over-expression of 5-HT6 Receptor and Activated Jab-1/p-c-Jun Play Important Roles in Pilocarpine-Induced Seizures and Learning-Memory Impairment. J Mol Neurosci. 67(3):388-399.

Liu X, Muller RU, Huang LT, Kubie JL, Rotenberg A, Rivard B, Cilio MR, Holmes GL., 2003. Seizure-induced changes in place cell physiology: relationship to spatial memory. J Neurosci. 17;23(37):11505-15.

Liu Y, Duan Y, Du D, Chen F., 2020. Rescuing Kv10.2 protein changes cognitive and emotional function in kainic acid-induced status epilepticus rats. Epilepsy Behav. 106:106894.

López-Frutos JM, Poch C, García-Morales I, Ruiz-Vargas JM, Campo P., 2014. Working memory retrieval differences between medial temporal lobe epilepsy patients and controls: a three memory layer approach. Brain Cogn. 84(1):90-6.

Lorente de Nò, R., 1934. Studies on the Structure of the Cerebral Cortex II. Continuation of the Study of the Ammonic System. Journal für Psychologie und Neurologie. 46, 113-177.

Losonczy A., Magee J. C., 2006. Integrative properties of radial oblique dendrites in hippocampal CA1 pyramidal neurons. Neuron. 50, 291–307.

Losonczy A, Makara JK, Magee JC., 2008. Compartmentalized dendritic plasticity and input feature storage in neurons. Nature. 27;452(7186):436-41.

Lovett-Barron M, Turi GF, Kaifosh P, Lee PH, Bolze F, Sun XH, Nicoud JF, Zemelman BV, Sternson SM, Losonczy A., 2012. Regulation of neuronal input transformations by tunable dendritic inhibition. Nat Neurosci. 15(3):423-30, S1-3.

Lovett-Barron M, Kaifosh P, Kheirbek MA, Danielson N, Zaremba JD, Reardon TR, Turi GF, Hen R, Zemelman BV, Losonczy A., 2014. Dendritic inhibition in the hippocampus supports fear learning. Science. 343(6173):857-63.

Lugo JN, Barnwell LF, Ren Y, Lee WL, Johnston LD, Kim R, Hrachovy RA, Sweatt JD, Anderson AE., 2008. Altered phosphorylation and localization of the A-type channel, Kv4.2 in status epilepticus. J Neurochem. 106:1929–1940.

Lunko O, Isaev D, Maximyuk O, Ivanchick G, Sydorenko V, Krishtal O, Isaeva E., 2014. Persistent sodium current properties in hippocampal CA1 pyramidal neurons of young and adult rats. Neurosci Lett. 559:30-3.

Macdonald RL, Kelly KM., 1995. Antiepileptic drug mechanisms of action. Epilepsia. 36 Suppl 2:S2-12.

Magee JC, Johnston D., 1995. Synaptic activation of voltage-gated channels in the dendrites of hippocampal pyramidal neurons. Science. 14;268(5208):301-4.

Magee JC, Johnston D., 1995. Characterization of single voltage-gated Na^+ and Ca^{2+} channels in apical dendrites of rat CA1 pyramidal neurons. *J Physiol.* 487:67–90.

Magee JC, Johnston D., 1997. A synaptically controlled, associative signal for Hebbian plasticity in hippocampal neurons. Science 275, 209–213.

Magee JC., 1998. Dendritic hyperpolarization-activated currents modify the integrative properties of hippocampal CA1 pyramidal neurons. J Neurosci. 1;18(19):7613-24.

Magee JC., 1999. Dendritic Ih normalizes temporal summation in hippocampal CA1 neurons. Nat Neurosci. 2(9):848.

Magee JC., 2000. Dendritic integration of excitatory synaptic input. Nat Rev Neurosci. 1(3):181-90.

Maglóczky Z., 2010. Sprouting in human temporal lobe epilepsy: excitatory pathways and axons of interneurons. Epilepsy Res. 89(1):52-9.

Maier SK, Westenbroek RE, Schenkman KA, Feigl EO, Scheuer T, Catterall WA., 2002. An unexpected role for brain-type sodium channels in coupling of cell surface depolarization to contraction in the heart. Proc Natl Acad Sci USA. 99(6):4073-8.

Makara JK, Losonczy A, Wen Q, Magee JC., 2009. Experience-dependent compartmentalized dendritic plasticity in rat hippocampal CA1 pyramidal neurons. Nat Neurosci. 12(12):1485-7.

Malenka RC, Kauer JA, Perkel DJ, Mauk MD, Kelly PT, Nicoll RA, Waxham MN., 1989. An essential role for postsynaptic calmodulin and protein kinase activity in long-term potentiation. Nature. 340(6234):554-7.

Malinow R, Schulman H, Tsien RW., 1989. Inhibition of postsynaptic PKC or CaMKII blocks induction but not expression of LTP. Science. 245(4920):862-6.

Maren S, Fanselow MS., 1995. Synaptic plasticity in the basolateral amygdala induced by hippocampal formation stimulation in vivo. J Neurosci. 15(11):7548-64.

Margerison and Corsellis, 1966. Epilepsy and the temporal lobes. A clinical, electroencephalographic and neuropathological study of the brain in epilepsy, with particular reference to the temporal lobes. Brain 89(3):499-530.

Marr D., 1971. Simple memory: a theory for archicortex. Philos Trans R Soc Lond B Biol Sci. 1;262(841):23-81.

Marcelin B, Chauvière L, Becker A, Migliore M, Esclapez M, Bernard C., 2009. h channel-dependent deficit of theta oscillation resonance and phase shift in temporal lobe epilepsy. Neurobiol Dis33(3):436-47.

Martin SJ, Morris RG., 2002. New life in an old idea: the synaptic plasticity and memory hypothesis revisited. Hippocampus. 12(5):609-36.

Mathern, G. W., Babb, T. L., Vickrey, B. G., Melendez, M., Pretorius, J. K., 1995. The clinical-pathogenic mechanisms of hippocampal neuron loss and surgical outcomes in temporal lobe epilepsy. Brain 118, 105–118.

McAuley JW, Elliott JO, Patankar S, Hart S, Long L, Moore JL, et al., 2010. Comparing patients' and practitioners' views on epilepsy concerns: a call to address memory concerns. Epilepsy Behav. 19: 580–3

McCormack K, Santos S, Chapman ML, Krafte DS, Marron BE, West CW, Krambis MJ, Antonio BM, Zellmer SG, Printzenhoff D, Padilla KM, Lin Z, Wagoner PK, Swain NA, Stupple PA, de Groot M, Butt RP, Castle NA., 2103. Voltage sensor interaction site for selective small molecule inhibitors of voltage-gated sodium channels. Proc Natl Acad Sci USA. 16;110(29):E2724-32.

McNamara JO, Huang YZ, Leonard AS (October 2006). Molecular signaling mechanisms underlying epileptogenesis. Sci. STKE. (356): re12.

Mel BW., 1993. Synaptic integration in an excitable dendritic tree. J Neurophysiol. 70(3):1086-101. Shepherd GM, Brayton RK., 1987. Logic operations are properties of computer-simulated interactions between excitable dendritic spines. Neuroscience. 21(1):151-65.

Meador KJ, Loring DW, Abney OL, Allen ME, Moore EE, Zamrini EY, et al., 1993. Effects of carbamazepine and phenytoin on EEG and memory in healthy adults. Epilepsia. 34:153–7.

Meador KJ, Loring DW, Moore E, Thompson WO, Nichols ME, Oberzan R, et al., 1995. Comparative cognitive effects of phenobarbital, phenytoin, and valproate in healthy adults. Neurology. 45: 1494–9.

Meador KJ., 2002. Cognitive outcomes and predictive factors in epilepsy. Neurology. 58(8 Suppl 5):S21-6.

Meador KJ., 2006. Cognitive and memory effects of the new antiepileptic drugs. Epilepsy Res. 68(1):63-7.

Mel BW, Ruderman DL, Archie KA., 1998. Translation-invariant orientation tuning in visual "complex" cells could derive from intradendritic computations. J Neurosci. 1;18(11):4325-34.

Melody Li, Nikola Jancovski, Paymaan Jafar-Nejad, Lisseth Estefania Burbano, Ben Rollo, Kay Richards, Lisa Drew, Alicia Sedo, Svenja Pachernegg, Armand Soriano, Linghan Jia, Todd Blackburn, Blaine Roberts, Alex Nemiroff, Kelley Dalby, Snezana Maljevic, Christopher Reid, Frank Rigo, Steven Petrou., 2020. Antisense oligonucleotide therapy for SCN2A gain-of-function epilepsy. bioRxiv 2020.09.09.289900.

Migliore, M. and Shepherd, G. M., 2002. Emerging rules for the distributions of active dendritic conductances. Nat Rev Neurosci, 3(5):362–370.

Milojkovic BA, Radojicic MS, Goldman-Rakic PS, Antic SD., 2004. Burst generation in rat pyramidal neurones by regenerative potentials elicited in a restricted part of the basilar dendritic tree. J Physiol. 1;558:193-211.

Milstein AD, Bloss EB, Apostolides PF, Vaidya SP, Dilly GA, Zemelman BV, Magee JC., 2015. Inhibitory Gating of Input Comparison in the CA1 Microcircuit. Neuron. 87(6):1274-1289.

Mizuseki K, Royer S, Diba K, Buzsáki G., 2012. Activity dynamics and behavioral correlates of CA3 and CA1 hippocampal pyramidal neurons. Hippocampus. 22(8):1659-80.

Morris R., Garrud P, Rawlins JN, O'Keefe J, 1982. Place navigation impaired in rats with hippocampal lesions". Nature. 297 (5868): 681–83.

Morris R., 2007. The Hippocampus Book. 591–617.

Moscovitch M, Cabeza R, Winocur G, Nadel L., 2016. Episodic Memory and Beyond: The Hippocampus and Neocortex in Transformation. Annu Rev Psychol. 67:105-34.

Moser EI, Kropff E, Moser MB., 2008. Place cells, grid cells, and the brain's spatial representation system. Annu Rev Neurosci. 31:69-89.

Müller C, Beck H, Coulter D, Remy S., 2012. Inhibitory control of linear and supralinear dendritic excitation in CA1 pyramidal neurons. Neuron. 6;75(5):851-64.

Muller RU, Kubie JL., 1987. The effects of changes in the environment on the spatial firing of hippocampal complex-spike cells. J Neurosci. 7(7):1951-68.

Muller RU, Kubie JL., 1989. The firing of hippocampal place cells predicts the future position of freely moving rats. J Neurosci. 9(12):4101-10.

Murai T, Okuda S, Tanaka T, Ohta H., 2007. Characteristics of object location memory in mice: Behavioral and pharmacological studies. Physiol Behav. 30;90(1):116-24.

Nair S, Szaflarski JP., 2020. Neuroimaging of memory in frontal lobe epilepsy. Epilepsy Behav. 103(Pt A):106857.

Neveu D, Zucker RS., 1996. Postsynaptic levels of Ca2+ i needed to trigger LTD and LTP. Neuron. 16(3):619-29.

Norman G, Eacott MJ., 2004. Impaired object recognition with increasing levels of feature ambiguity in rats with perirhinal cortex lesions. Behav Brain Res. 148(1-2):79-91.

O'Keefe, J., Dostrovsky, J. & J. O'Keefe, J. D., 1971. The hippocampus as a spatial map. Preliminary evidence from unit activity in the freely-moving rat. Brain Research. 34, 171–175.

O'Keefe, J., 1976. Place units in the hippocampus of the freely moving rat. Experimental Neurology 51, 78–109.

O'Keefe J, Nadel L, 1978. The Hippocampus as a Cognitive Map. Oxford University Press. 263–267.

O'Keefe J, Burgess N., 1996. Geometric determinants of the place fields of hippocampal neurons. Nature. 30;381(6581):425-8.

Oh Y, Black JA, Waxman SG., 1994. The expression of rat brain voltage-sensitive Na+ channel mRNAs in astrocytes. Brain Res Mol Brain Res. 23(1-2):57-65.

Orman R, Von Gizycki H, Lytton WW, Stewart M., 2008. Local axon collaterals of area CA1 support spread of epileptiform discharges within CA1, but propagation is unidirectional. Hippocampus. 18(10):1021-33.

Pack AM., 2019. Epilepsy Overview and Revised Classification of Seizures and Epilepsies. Continuum (Minneap Minn). 25(2):306-321.

Palmer L, Murayama M, Larkum M., 2012. Inhibitory Regulation of Dendritic Activity in vivo. Front Neural Circuits. 6:26.

Pathak, H. R., Weissinger, F., Terunuma, M., Carlson, G. C., Hsu, F.-C., Moss, S. J., Coulter, D. A., 2007. Disrupted dentate granule cell chloride regulation enhances synaptic excitability during development of temporal lobe epilepsy. J Neurosci 27, 14012–14022.

Pearson JN, Schulz KM, Patel M., 2014. Specific alterations in the performance of learning and memory tasks in models of chemoconvulsant-induced status epilepticus. Epilepsy Res. 108(6):1032-40.

Pnevmatikakis EA, Soudry D, Gao Y, Machado TA, Merel J, Pfau D, Reardon T, Mu Y, Lacefield C, Yang W, Ahrens M, Bruno R, Jessell TM, Peterka DS, Yuste R, Paninski L., 2016. Simultaneous Denoising, Deconvolution, and Demixing of Calcium Imaging Data. Neuron. 20;89(2):285-99.

Pyapali GK, Sik A, Penttonen M, Buzsaki G, Turner DA., 1998. Dendritic properties of hippocampal CA1 pyramidal neurons in the rat: intracellular staining in vivo and in vitro. J Comp Neurol. 16;391(3):335-52.

Poirazi P, Mel BW., 2001. Impact of active dendrites and structural plasticity on the memory capacity of neural tissue. Neuron. 29(3):779-96.

Poirazi P, Brannon T, Mel BW., 2003a. Arithmetic of subthreshold synaptic summation in a model CA1 pyramidal cell. Neuron. 27;37(6):977-87.

Poirazi P, Brannon T, Mel BW., 2003b. Pyramidal neuron as two-layer neural network. Neuron. 27;37(6):989-99.

Polli, R. S., Malheiros, J. M., Santos, R. dos, Hamani, C., Longo, B. M., Tann´us, A., Mello, L. E., and Covolan, L., 2014. Changes in hippocampal volume are correlated with cell loss but not with seizure frequency in two chronic models of temporal lobe epilepsy. Front Neurol 5:111, 1–11.

Polsky A, Mel BW, Schiller J., 2004. Computational subunits in thin dendrites of pyramidal cells. Nat Neurosci. 7(6):621-7.

Poolos NP., 2012. Hyperpolarization-Activated Cyclic Nucleotide-Gated (HCN) Ion Channelopathy in Epilepsy. Jasper's Basic Mechanisms of the Epilepsies.

Pothmann L, Klos C, Braganza O, Schmidt S, Horno O, Memmesheimer RM, Beck H., 2019. Altered Dynamics of Canonical Feedback Inhibition Predicts Increased Burst Transmission in Chronic Epilepsy. J Neurosci. 6;39(45):8998-9012.

Ptácek LJ., 1997. Channelopathies: ion channel disorders of muscle as a paradigm for paroxysmal disorders of the nervous system. Neuromuscul Disord. 7(4):250-5.

Pulliainen V, Kuikka P, Jokelainen M., 2000. Motor and cognitive functions in newly diagnosed adult seizure patients before antiepileptic medication. Acta Neurol Scand. 101(2):73-8.

Qi LS, Larson MH, Gilbert LA, Doudna JA, Weissman JS, Arkin AP, Lim WA., 2013. Repurposing CRISPR as an RNA-guided platform for sequence-specific control of gene expression. Cell. 152(5):1173-83.

Ragsdale, D. S. and Avoli, M., 1998. Sodium channels as molecular targets for antiepileptic drugs. Brain Res. Rev. 26, 16–28.

Rall W., 1967. Distinguishing theoretical synaptic potentials computed for different soma-dendritic distributions of synaptic input. J Neurophysiol. 30(5):1138-68.

Rall W, Rinzel J., 1973. Branch input resistance and steady attenuation for input to one branch of a dendritic neuron model. Biophys J. 13(7):648-87.

Ramón y Cajal S., 1893. Los Ganglios y Plexos Nerviosos del Intestino de los Mamíferos y Pequeñas Adiciones a Nuestros Trabajos Sobre la Médula y Gran Simpatico General.

Rattka M, Brandt C, Löscher W., 2013. The intrahippocampal kainate model of temporal lobe epilepsy revisited: epileptogenesis, behavioral and cognitive alterations, pharmacological response, and hippoccampal damage in epileptic rats. Epilepsy Res. 103:135–52.

Regesta G, Tanganelli P., 1999. Clinical aspects and biological bases of drug-resistant epilepsies. Epilepsy Res. 34(2-3):109-22.

Remy S, Spruston N., 2007. Dendritic spikes induce single-burst long-term potentiation. Proc Natl Acad Sci USA. 23;104(43):17192-7.

Remy S., Csicsvari J., Beck H., 2009. Activity-dependent control of neuronal output by local and global dendritic spike attenuation. Neuron, 61, 906-16.

Rinaldi C, Wood MJA., 2018. Antisense oligonucleotides: the next frontier for treatment of neurological disorders. Nat Rev Neurol. 14(1):9-21.

Rosas K, Parrón I, Serrano P, Cimadevilla JM., 2013. Spatial recognition memory in a virtual reality task is altered in refractory temporal lobe epilepsy. Epilepsy Behav. 28(2):227-31.

Royeck M, Kelly T, Opitz T, Otte DM, Rennhack A, Woitecki A, Pitsch J, Becker A, Schoch S, Kaupp UB, Yaari Y, Zimmer A, Beck H., 2015. Downregulation of Spermine Augments Dendritic Persistent Sodium Currents and Synaptic Integration after Status Epilepticus. J Neurosci. 18;35(46):15240-53.

Royer S, Zemelman BV, Losonczy A, Kim J, Chance F, Magee JC, Buzsáki G., 2012. Control of timing, rate and bursts of hippocampal place cells by dendritic and somatic inhibition. Nat Neurosci. 25;15(5):769-75.

Rugg MD, Vilberg KL., 2013. Brain networks underlying episodic memory retrieval. Curr Opin Neurobiol. 23(2):255-60.

Rzezak P, Lima EM, Gargaro AC, Coimbra E, de Vincentiis S, Velasco TR, Leite JP, Busatto GF, Valente KD., 2017. Everyday memory impairment in patients with temporal lobe epilepsy caused by hippocampal sclerosis. Epilepsy Behav. 69:31-36.

Sanabria ER, Su H, Yaari Y., 2001. Initiation of network bursts by Ca2+-dependent intrinsic bursting in the rat pilocarpine model of temporal lobe epilepsy. J Physiol. 1;532(Pt 1):205-16.

Sari P, Kerr DS., 2001. Domoic acid-induced hippocampal CA1 hyperexcitability independent of region CA3 activity. Epilepsy Res. 47(1-2):65-76.

Sarkisian MR., 2001. Overview of the Current Animal Models for Human Seizure and Epileptic Disorders. Epilepsy Behav. (3):201-216.

Sato, C., Ueno, Y., Asai, K., Takahashi, K., Sato, M., Engel, A., and Fujiyoshi, Y., 2001. The voltage-sensitive sodium channel is a bell-shaped molecule with several cavities. Nature. 409,1047–1051.

Scheffer IE, Berkovic S, Capovilla G, Connolly MB, French J, Guilhoto L, Hirsch E, Jain S, Mathern GW, Moshé SL, Nordli DR, Perucca E, Tomson T, Wiebe S, Zhang Literature 70 YH, Zuberi SM, 2018. ILAE classification of the epilepsies. Zeitschrift fur Epileptol.

Schiller J, Schiller Y, Stuart G, Sakmann B., 1997. Calcium action potentials restricted to distal apical dendrites of rat neocortical pyramidal neurons. J Physiol. 15;505:605-16.

Schiller, J., Schiller, Y. & Clapham, D. E., 1998. NMDA receptors amplify calcium influx into dendritic spines during associative pre- and postsynaptic activation. Nature Neurosci. 1, 114–118.

Schiller J., Major, G., Koester, H. J., and Schiller, Y., 2000. NMDA spikes in basal dendrites of cortical pyramidal neurons. Nature, 404(6775):285–289.

Schmied, O., Scharf, G., Hilbe, M., Michal, U., Tomsa, K., and Steffen, F., 2008. Magnetic resonance imaging of feline hippocampal necrosis. Vet Radiol Ultrasound 49, 343–349.

Scoville, W. B. & Milner, B., 1957. J Neurol Neurosurg Psychiatry. 20(1):11-21.

Sendrowski, K., Sobaniec, W., 2013. Hippocampus, hippocampal sclerosis and epilepsy. Pharm. Rep 65, 555–565.

Setten RL, Rossi JJ, Han SP., 2019. The current state and future directions of RNAi-based therapeutics. Nat Rev Drug Discov. 18(6):421-446.

Shah MM, Anderson AE, Leung V, Lin X, Johnston D., 2004. Seizure-induced plasticity of h channels in entorhinal cortical layer III pyramidal neurons. Neuron. 28;44(3):495-508.

Sheffield ME, Dombeck DA., 2015. Calcium transient prevalence across the dendritic arbour predicts place field properties. Nature. 8;517(7533):200-4.

Sheffield ME, Adoff MD, Dombeck DA., 2017. Increased Prevalence of Calcium Transients across the Dendritic Arbor during Place Field Formation. Neuron. 11;96(2):490-504.e5.

Sheffield ME, Dombeck DA., 2019. Dendritic mechanisms of hippocampal place field formation. Curr Opin Neurobiol. 54:1-11.

Shetty AK, Hattiangady B, Rao MS., 2009. Vulnerability of hippocampal GABA-ergic interneurons to kainate-induced excitotoxic injury during old age. J Cell Mol Med. 13(8B):2408-23.

Shneker, B. F., Fountain, N. B., 2003. Epilepsy. Dis Mon 49, 426–478.

Shuman T, Aharoni D, Cai DJ, Lee CR, Chavlis S, Page-Harley L, Vetere LM, Feng Y, Yang CY, Mollinedo-Gajate I, Chen L, Pennington ZT, Taxidis J, Flores SE, Cheng K, Javaherian M, Kaba CC, Rao N, La-Vu M, Pandi I, Shtrahman M, Bakhurin KI, Masmanidis SC, Khakh BS, Poirazi P, Silva AJ, Golshani P., 2020. Breakdown of spatial coding and interneuron synchronization in epileptic mice. Nat Neurosci. 23(2):229-238.

Sidhu MK, Stretton J, Winston GP, Symms M, Thompson PJ, Koepp MJ, et al., 2015. Factors affecting reorganization of memory encoding networks in temporal lobe epilepsy. Epilepsy Res. 110:1–9.

Sillanpää, M., 2004. Learning disability: occurrence and long-term consequences in childhood-onset epilepsy. Epilepsy Behav. (6):937-44.

Singh B, Ogiwara I, Kaneda M, Tokonami N, Mazaki E, Baba K, Matsuda K, Inoue Y, Yamakawa K., 2006. A Kv4.2 truncation mutation in a patient with temporal lobe epilepsy. Neurobiol Dis. 24:245–253.

Sjöström PJ, Nelson SB., 2002. Spike timing, calcium signals and synaptic plasticity. Curr Opin Neurobiol. 12(3):305-14.

Sjöström PJ, Rancz EA, Roth A, Häusser M., 2008. Dendritic excitability and synaptic plasticity. Physiol Rev. 88(2):769-840

Sjulson L, Peyrache A, Cumpelik A, Cassataro D, Buzsáki G., 2018. Cocaine Place Conditioning Strengthens Location-Specific Hippocampal Coupling to the Nucleus Accumbens. Neuron. 6;98(5):926-934.e5.
.

Sloviter, R. 2005. The neurobiology of temporal lobe epilepsy: too much information, not enough knowledge". Comptes Rendus Biologies. 328(2):143-53.

Spruston N., 2008. Pyramidal neurons: dendritic structure and synaptic integration. Nat Rev Neuros. 9(3):206-21.

Squire LR, Stark CE, Clark RE., 2004. The medial temporal lobe. Annu Rev Neurosci. 27:279-306.

Steward O, Scoville SA., 1976. Cells of origin of entorhinal cortical afferents to the hippocampus and fascia dentata of the rat. J Comp Neurol. 1;169(3):347-70.

Strege PR, Knutson K, Eggers SJ, Li JH, Wang F, Linden D, Szurszewski JH, Milescu L, Leiter AB, Farrugia G, Beyder A., 2017. Sodium channel NaV1.3 is important for enterochromaffin cell excitability and serotonin release. Sci Rep. 7(1):15650.

Stuart G, Spruston N, Sakmann B, Häusser M., 1997. Action potential initiation and backpropagation in neurons of the mammalian CNS. Trends Neurosci. 20(3):125-31.

Stuart, G., Spruston, N., and Häusser, M., 2008. Dendrites. Oxford University Press. pp. 351-399.

Stuart GJ, Spruston N., 2015. Dendritic integration: 60 years of progress. Nat Neurosci. 18(12):1713-21.

Su H, Sochivko D, Becker A, Chen J, Jiang Y, Yaari Y, Beck H., 2002. Upregulation of a T-type Ca^{2+} channel causes a long-lasting modification of neuronal firing mode after status epilepticus. J Neurosci. 1;22(9):3645-55.

Subramaniam SR, Khoo CS, Raymond AA, Che Din N, Syed Zakaria SZ, Tan HJ., 2020. Prevalence and factors of verbal learning and memory dysfunction in patients with epilepsy. A single centre study. J Clin Neur. 73:31-36.

Sutherland RJ, Kolb B, Whishaw IQ, 1982. Spatial mapping: definitive disruption by hippocampal or medial frontal cortical damage in the rat. Neuroscience Letters. 31(3): 271–6.

Sutula T, Cascino G, Cavazos J, Parada I, Ramirez L., 1989. Mossy fiber synaptic reorganization in the epileptic human temporal lobe. Ann Neurol. (3):321-30.

Suzuki WA, Miller EK, Desimone R., 1997. Object and place memory in the macaque entorhinal cortex. J Neurophysiol. 78(2):1062-81.

Taleb A, Zhou YP, Meng LT, Zhu MY, Zhang Q, Naveed M, Li LD, Wang P, Zhou QG, Meng F, Han F., 2021. New application of an old drug proparacaine in treating epilepsy via liposomal hydrogel formulation. Pharmacol Res. 169:105636.

Tamás G, Szabadics J, Somogyi P., 2002. Cell type- and subcellular position-dependent summation of unitary postsynaptic potentials in neocortical neurons. J Neurosci. 1;22(3):740-7.

Tai C, Kuzmiski JB, MacVicar BA., 2006. Muscarinic enhancement of R-type calcium currents in hippocampal CA1 pyramidal neurons. J Neurosci. 26(23):6249-58.

Tan NN, Tang HL, Lin GW, Chen YH, Lu P, Li HJ, Gao MM, Zhao QH, Yi YH, Liao WP, Long YS., 2017. Epigenetic Downregulation of Scn3a Expression by Valproate: a Possible Role in Its Anticonvulsant Activity. Mol Neurobiol. 54(4):2831-2842.

Tang YP, Shimizu E, Dube GR, Rampon C, Kerchner GA, Zhuo M, Liu G, Tsien JZ., 1999. Genetic enhancement of learning and memory in mice. Nature. 401(6748):63-9.

Tassi L., A. Meroni, F. Deleo, F. Villani, R. Mai, G.L. Russo, N. Colombo, G. Avanzini, C. Falcone, M. Bramerio, A. Citterio, R. Garbelli, R. Spreafico, 2009. Temporal lobe epilepsy: neuropathological and clinical correlations in 243 surgically treated patients, Epileptic Disorders. 281–292.

Taylor DC, 1989. The Neuropathology of Temporal Lobe Epilepsy. By C. J. Bruton. Pp. 158; Oxford University Press: Oxford.

Thijs, R. D., Surges, R., O'Brien, T. J., & Sander, J. W. (2019). Epilepsy in adults. Lancet, 393(10172), 689–701.

Tibery DV, Campos LA, Mourão CBF, Peigneur S, E Carvalho AC, Tytgat J, Schwartz EF., 2019. Electrophysiological characterization of Tityus obscurus β toxin 1 (To1) on Na+-channel isoforms. Biochim Biophys Acta Biomembr. 1861(1):142-150.

Tramoni E, Felician O, Barbeau EJ, Guedj E, Guye M, Bartolomei F, Ceccaldi M., 2011. Long-term consolidation of declarative memory: insight from temporal lobe epilepsy. Brain. 134(Pt 3):816-31.

Vacher H, Mohapatra DP, Trimmer JS., 2008. Localization and targeting of voltage-dependent ion channels in mammalian central neurons. Physiol Rev. 88(4):1407-47.

Valero M, Averkin RG, Fernandez-Lamo I, Aguilar J, Lopez-Pigozzi D, Brotons-Mas JR, Cid E, Tamas G, Menendez de la Prida L., 2017. Mechanisms for Selective Single-Cell Reactivation during Offline Sharp-Wave Ripples and Their Distortion by Fast Ripples. Neuron. 21;94(6):1234-1247.e7.

Van Den Herrewegen Y, Denewet L, Buckinx A, Albertini G, Van Eeckhaut A, Smolders I, et al., 2019. The Barnes maze task reveals specific impairment of spatial learning strategy in the intrahippocampal kainic acid model for temporal lobe epilepsy. Neurochem Res. 44:600–8.

Van Geldorp B, Bouman Z, Hendriks MP, Kessels RP., 2014. Different types of working memory binding in epilepsy patients with unilateral anterior temporal lobectomy. Brain Cogn. 85:231-8.

Van Strien NM, Cappaert NL, Witter MP., 2009. The anatomy of memory: an interactive overview of the parahippocampal-hippocampal network. Nat Rev Neurosci. 10(4):272-82.

Varga C, Golshani P, Soltesz I., 2012. Frequency-invariant temporal ordering of interneuronal discharges during hippocampal oscillations in awake mice. Proc Natl Acad Sci U S A. 109(40):E2726-34.

Vazdarjanova A, McGaugh JL., 1999. Basolateral amygdala is involved in modulating consolidation of memory for classical fear conditioning. J Neurosci. 1;19(15):6615-22.

Wagner, E., Rosati, M., Molin, J., Foitzik, U., Wahle, A. M., Fischer, A., Matiasek, L. A., Reese, S., Flegel, T., and Matiasek, K., 2014. Hippocampal sclerosis in feline epilepsy. Brain Pathol 24, 607–619.

Wang C, Chen X, Lee H, Deshmukh SS, Yoganarasimha D, Savelli F, Knierim JJ., 2018. Egocentric coding of external items in the lateral entorhinal cortex. Science. 362(6417):945-949.

Wang F, Flanagan J, Su N, Wang LC, Bui S, Nielson A, Wu X, Vo HT, Ma XJ, Luo Y., 2012. RNAscope: a novel in situ RNA analysis platform for formalin-fixed, paraffin-embedded tissues. J Mol Diagn. 14(1):22-9.

Wang J, Ou SW, Wang YJ., 2017. Distribution and function of voltage-gated sodium channels in the nervous system. Channels (Austin). 2;11(6):534-554.

Ward AA Jr., 1961. The epileptic neurone. Epilepsia. 2:70-80.

Weniger G, Ruhleder M, Wolf S, Lange C, Irle E., 2009. Egocentric memory impaired and allocentric memory intact as assessed by virtual reality in subjects with unilateral parietal cortex lesions. Neuropsyc.. 47(1):59-69.

Whatley, A.D., et al., 2010. Examining the relationships of depressive symptoms, stigma, social support and regimen-specific support on quality of life in adult patients with epilepsy. Health Educ Res. (4):575-84.

Whitaker WR, Clare JJ, Powell AJ, Chen YH, Faull RL, Emson PC., 2000. Distribution of voltage-gated sodium channel alpha-subunit and beta-subunit mRNAs in human hippocampal formation, cortex, and cerebellum. J Comp Neurol. 19;422(1):123-39.

Whitaker WR, Faull RL, Dragunow M, Mee EW, Emson PC, Clare JJ., 2001. Changes in the mRNAs encoding voltage-gated sodium channel types II and III in human epileptic hippocampus. Neuroscience. 106(2):275-85.

Wieser, 2004. ILAE Commission Report. Mesial temporal lobe epilepsy with hippocampal sclerosis. Epilepsia. 45, 695–714.

Wilkinson H, Holdstock JS, Baker G, Herbert A, Clague F, Downes JJ., 2012. Long-term accelerated forgetting of verbal and non-verbal information in temporal lobe epilepsy. Cortex. 48:317–32.

Williams J., 2003 Learning and behavior in children with epilepsy. Epilepsy Behav. (2):107-11.

Wilson DE, Whitney DE, Scholl B, Fitzpatrick D., 2016. Orientation selectivity and the functional clustering of synaptic inputs in primary visual cortex. Nat Neurosci. 19(8):1003-9.

Winnubst J, Lohmann C. Synaptic clustering during development and learning: the why, when, and how. Front Mol Neurosci. 2012 May 31;5:70.

Winters BD, Saksida LM, Bussey TJ., 2008. Object recognition memory: neurobiological mechanisms of encoding, consolidation and retrieval. Neurosci Biobehav Rev. 32(5):1055-70.

Witter MP, Griffioen AW, Jorritsma-Byham B, Krijnen JL., 1988. Entorhinal projections to the hippocampal CA1 region in the rat: an underestimated pathway. Neurosci Lett. 29;85(2):193-8.

Witter, M. P., Groenewegen, H. J., da Silva, F. H. L., Lohman, A. H., 1989. Functional organization of the extrinsic and intrinsic circuitry of the parahippocampal region. Prog Neurobiol 33, 161–253.

Witter MP, Amaral DG., 1991. Entorhinal cortex of the monkey: V. Projections to the dentate gyrus, hippocampus, and subicular complex. J Comp Neurol. 15;307(3):437-59.

Witter, M. P., 1993. Organization of the entorhinal-hippocampal system: A review of current anatomical data. Hippocampus 3, 33–44.

Wolfe JW, Butterworth JF., 2011. Local anesthetic systemic toxicity: update on mechanisms and treatment. Curr Opin Anaesthesiol. 24(5):561-6.

Wozny C, Gabriel S, Jandova K, Schulze K, Heinemann U, Behr J., 2005. Entorhinal cortex entrains epileptiform activity in CA1 in pilocarpine-treated rats. Neurobiol Dis. 19(3):451-60.

Xu X, Guo F, Lv X, Feng R, Min D, Ma L, Liu Y, Zhao J, Wang L, Chen T, Shaw C, Hao L, Cai J., 2013. Abnormal changes in voltage-gated sodium channels Na(V)1.1, Na(V)1.2, Na(V)1.3, Na(V)1.6 and in

calmodulin/calmodulin-dependent protein kinase II, within the brains of spontaneously epileptic rats and tremor rats. Brain Res Bull. 96:1-9.

Yaari Y, Yue C, Su H., 2007. Recruitment of apical dendritic T-type Ca2+ channels by backpropagating spikes underlies de novo intrinsic bursting in hippocampal epileptogenesis. J Physiol. 15;580(Pt. 2):435-50.

Yamagata T, Raveau M, Kobayashi K, Miyamoto H, Tatsukawa T, Ogiwara I, Itohara S, Hensch TK, Yamakawa K., 2020. CRISPR/dCas9-based Scn1a gene activation in inhibitory neurons ameliorates epileptic and behavioral phenotypes of Dravet syndrome model mice. Neurobiol Dis. 141:104954.

Yu S, Li S, Shu H, Zhang C, He J, Fan X, Yang H., 2012. Upregulated expression of voltage-gated sodium channel Nav1.3 in cortical lesions of patients with focal cortical dysplasia type IIb. Neuroreport. 23(7):407-11.

Yuste R., 2011. Dendritic spines and distributed circuits. Neuron. 8;71(5):772-81.

Yuste R, Denk W., 1995. Dendritic spines as basic functional units of neuronal integration. Nat. 375(6533):682-4.

Zamarian L, Trinka E, Bonatti E, Kuchukhidze G, Bodner T, Benke T, Koppelstaetter F, Delazer M., 2011. Executive functions in chronic mesial temporal lobe epilepsy. Epilepsy Res Treat. 2011:596174.

Zhou, JL, Shatskikh, T. N., Liu, X. & Holmes, G. L., 2007. Impaired single cell firing and long-term potentiation parallels memory impairment following recurrent seizures. Eur. J. Neurosci. 25, 3667–3677.

Zhou JL, Lenck-Santini PP, Holmes GL., 2007. Postictal single-cell firing patterns in the hippocampus. Epilepsia. 48(4):713-9.

Žiburkus J., J.R. Cressman, S.J. Schiff, 2013. Seizures as imbalanced up states: excitatory and inhibitory conductances during seizure-like events, Journal of Neurophysiology. 109 1296–1306.

Zola-Morgan S, Squire LR, Amaral DG., 1986a. Human amnesia and the medial temporal region: enduring memory impairment following a bilateral lesion limited to field CA1 of the hippocampus. J Neuro. 6(10):2950-67.

Zola-Morgan S, Squire LR., 1986b. Memory impairment in monkeys following lesions limited to the hippocampus. Behav Neurosci. 100(2):155-60.

Acknowledgments

The main purpose of writing an acknowledgment page is to offer a thankful note to those who provided support to you during the study. Typically starting with the most important person, the principal supervisor, then mentioning any major advisors overseeing your project, the lab mates who contributed to your Ph.D., and finally, your family and friends. At least according to what is reported on "10 Helpful ideas for writing a masterpiece thesis acknowledgment".

Well, I not only consider it as a page saying thank you to your doctors after a lifesaving surgery but also as a memorandum for the me of tomorrow, so that I will never forget the beautiful people who accompanied the years of my doctorate.

First and foremost, I would like to express my sincere thanks to Prof. Dr. Heinz Beck. His passion for science and plentiful experience have encouraged me in all the time of my academic journey and daily life. I am very grateful to him for the opportunity to experience one of the most challenging and exciting adventures of my life, conducting a Ph.D. thesis in his lab, and for his teachings to trust my ideas and abilities (in science and life). I could always knock on his office door while bringing some authentic Caffe espresso and ask him for advice, receiving all the times support and care. Thanks for turning on the light on my mind. Thanks for the trust you put in me.

I would like to express my gratitude to Prof. Dr. Walter Witke, who agreed on co-supervising this thesis, who represents the Faculty of Math and Natural Sciences.

I am very thankful to Dr. Tony Kelly for his assistance at every stage of my research project and his unwavering support. I can always count on him for anything, sometimes even neuroscience.

Special thanks to Prof. Dr. Laura Ewell, an extraordinary young brain whose experience, advice, and insightful suggestions meant a lot to me. She is truly inspiring, and it will be an enormous honor to start a new adventure in conducting a Post Doc in her lab.

Thanks to Prof. Dr. Christian Henneberger and Prof. Dr. Sandra Blaess, without your essential contribution, this entire project not have been possible.

Thanks to Martin Pofahl, Negar Nikbakht, Andre Haubrich, Ushna Sameen Islam, Maryam Pasdarnavab, Fateme Kamali, Kirsten Bohmbach, and Kurtulus Gölcük for their contribution to my thesis project. Thanks to Dr. Thoralf Opitz, which was never tired of answering each of my thousands of questions.

My entire Ph.D. and this work would not have been possible due to the ever-present help by Margit Reitze, Sabrina Walch, Nicole Schönfelder, and Lea Keller. Whether in the technical or organizational area, you have always been a great support. You are the lab foundation.

Thanks to Martin Pofahl, Negar Nikbakht, and Pedro Royero, my soul-lab-mates. Thanks for being not just colleagues but great friends who shared the joys and difficulties of our lab journeys and for all the good times in the lab and outside in the real open world. I am really grateful for our friendship.

Thanks to Andre Haubrich, Fabian Distler, Michela Barboni, Oliver Braganza. I am happy to call them friends. Thanks for sharing some funny scientific discussions, gossip, humor, and psychotherapy lab group sessions.

Nevertheless, none of this could have happened, including my survival during all this long time in a foreign country, without Kristian Reichelt. He was there during meiner Tage der Schwarzen Pest. He was there during meiner Renaissance. He is indeed a truly Deutscher Bruder. Danke mein Genosse.

Most importantly, Nicole thank you, for being the fig.1 of my main life project.

I also thank Milan Pabst, you have been an inspiration to many people, including me.

I am also profoundly grateful to Dr. Giuseppe Talani. I blame him for my insane love of neuroscience. That is all because of him. Thanks.

To my family for supporting all the chapters of my life, even those with bad and inconclusive experimental results.

A mia madre e mio padre. Tutto questo è solo grazie ai vostri sacrifici e amore. Senza il vostro sostegno e i vostri insegnamenti non sarei quello che sono. A voi va il merito di chi sono e di chi un domani saro. Grazie.

Statement

I hereby certify that the work presented here was accomplished by myself and without the use of illegitimate means or support, and that no sources ant tools were used other than those cited.

Bonn, September 10, 2021